Evolution Equations on Gabor Transforms and their Applications

Remco Duits and Hartmut Führ and Bart Janssen and
Mark Bruurmijn and Luc Florack and Hans van Assen

Remco Duits, Department of Mathematics and Computer Science & Department of Biomedical Engineering, Eindhoven University of Technology, 5600 MB Eindhoven, The Netherlands,
R.Duits@tue.nl
Hartmut Führ, Lehrstuhl A für Mathematik, RWTH Aachen University, 52056 Aachen, Germany,
fuehr@MathA.rwth-aachen.de
Bart Janssen, Department of Mathematics and Computer Science, Eindhoven University of Technology, 5600 MB Eindhoven, The Netherlands,
B.J.Janssen@tue.nl
Mark Bruurmijn, Department of Biomedical Engineering, Eindhoven University of Technology, 5600 MB Eindhoven, The Netherlands, L.C.M.Bruurmijn@alumnus.tue.nl
Luc Florack, Department of Mathematics and Computer Science & Department of Biomedical Engineering, Eindhoven University of Technology, 5600 MB Eindhoven, The Netherlands,
L.M.J.Florack@tue.nl
Hans van Assen, Department of Electrical Engineering, Eindhoven University of Technology, 5600 MB Eindhoven, The Netherlands, H.C.v.Assen@tue.nl

Abstract

We introduce a systematic approach to the design, implementation and analysis of left-invariant evolution schemes acting on Gabor transform, primarily for applications in signal and image analysis. Within this approach we relate operators on signals to operators on Gabor transforms. In order to obtain a translation and modulation invariant operator on the space of signals, the corresponding operator on the reproducing kernel space of Gabor transforms must be left invariant, i.e. it should commute with the left regular action of the reduced Heisenberg group H_r. By using the left-invariant vector fields on H_r in the generators of our evolution equations on Gabor transforms, we naturally employ the essential group structure on the domain of a Gabor transform. Here we distinguish between two tasks. Firstly, we consider non-linear adaptive left-invariant convection (reassignment) to sharpen Gabor transforms, while maintaining the original signal. Secondly, we consider signal enhancement via left-invariant diffusion on the corresponding Gabor transform. We provide numerical experiments and analytical evidence for our methods and we consider an explicit medical imaging application.

Keywords: Evolution equations, Heisenberg group, Differential reassignment, Left-invariant vector fields, Diffusion on Lie groups, Gabor transforms, Medical imaging 35R03, 22E25, 35Q68

1. Introduction

The Gabor transform of a signal $f \in \mathbb{L}_2(\mathbb{R}^d)$ is a function $\mathcal{G}_\psi[f] : \mathbb{R}^d \times \mathbb{R}^d \to \mathbb{C}$ that can be roughly understood as a musical score of f, with $\mathcal{G}_\psi[f](p,q)$ describing the contribution of frequency q to the behaviour of f near p [40, 43]. This interpretation is necessarily of limited precision, due to the various uncertainty principles, but it has nonetheless turned out to be a very rich source of mathematical theory as well as practical signal processing algorithms.

The use of a window function for the Gabor transform results in a smooth, and to some extent blurred, time-frequency representation. For purposes of signal analysis, say for the extraction of instantaneous frequencies, various authors tried to improve the resolution of the Gabor transform, literally in order to sharpen the time-frequency picture of the signal; this type of procedure is often called "reassignment" in the literature. For instance, Kodera et al. [50] studied techniques for the enhancement of the spectrogram, i.e. the squared modulus of the short-time Fourier transform. Since the phase of the Gabor transform is neglected, the original signal is not easily recovered from the reassigned spectrogram. Since then, various authors developed reassignment methods that were intended to allow (approximate) signal recovery [3, 14, 19, 18]. We claim

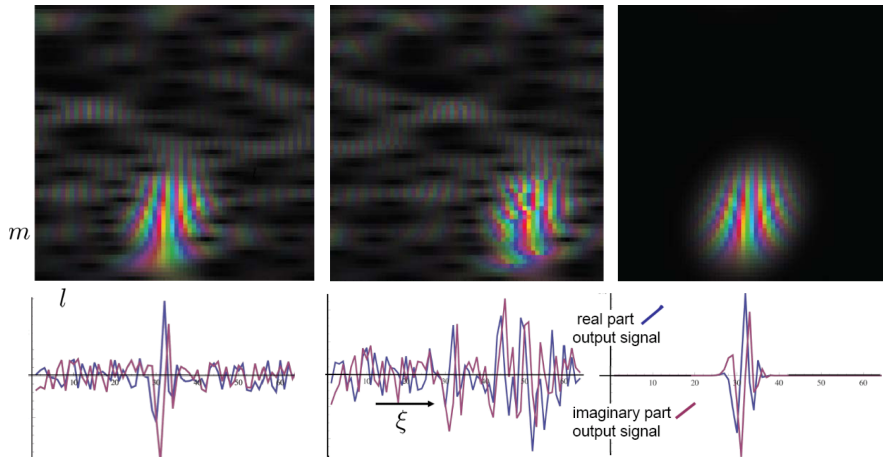

Figure 1: Top row from left to right, (1) the Gabor transform of original signal f, (2) processed Gabor transform $\Phi_t(\mathcal{W}_\psi f)$ where Φ_t denotes a phase invariant shift (for more elaborate adaptive convection/reassignment operators see Section 6 where we operationalize the theory in [19]) using a discrete Heisenberg group, where l represents discrete spatial shift and m denotes discrete local frequency, (3) processed Gabor transform $\Phi_t(\mathcal{W}_\psi f)$ where Φ_t denotes a *phase covariant* diffusion operator on Gabor transforms with stopping time $t > 0$. For details on phase covariant diffusions on Gabor transforms, see [29, ch:7] and [47, ch:6]. Note that phase-covariance is preferable over phase invariance. For example, restoration of the old phase in the phase invariant shift creates noisy artificial patterns (middle image) in the phase of the transported strong responses in the Gabor domain. Bottom row, from left to right: (1) Original complex-valued signal f, (2) output signal $\Upsilon_\psi f = \mathcal{W}_\psi^* \Phi_t \mathcal{W}_\psi f$ where Φ_t denotes a *phase-invariant* spatial shift (due to phase invariance the output signal looks bad and clearly phase invariant spatial shifts in the Gabor domain do not correspond to spatial shifts in the signal domain), (3) Output signal $\Upsilon_\psi f = \mathcal{W}_\psi^* \Phi_t \mathcal{W}_\psi f$ where Φ_t denotes *phase-covariant* adaptive diffusion in the Gabor domain with stopping time $t > 0$.

that a proper treatment of phase may be understood as *phase-covariance*, rather than *phase-invariance*, as advocated previously. An illustration of this claim is contained in Figure 1.

We adapt the group theoretical approach developed for the Euclidean motion groups in the recent works [22, 38, 25, 26, 31, 24, 27, 57, 58], thus illustrating the scope of the methods devised for general Lie groups in [23] in signal and image processing. Reassignment will be seen to be a special case of left-invariant convection. A useful source of ideas specific to Gabor analysis and reassignment was the paper [19].

1.1. Structure of the article

This article provides a systematic approach to the design, implementation and analysis of left-invariant evolution schemes acting on Gabor transform, primarily for applications in signal and image analysis. The article is structured as follows:

- **Introduction and preliminaries:** Sections 1, 2. In Section 2 we consider time-frequency analysis and its inherent connection to the Heisenberg group, and subsequently we introduce relevant structures on the Heisenberg group.
- **Evolution equations on the Heisenberg group and on related manifolds:** Sections 3, 4 and 5. In Section 3 we set up the left-invariant evolution equations on Gabor transforms. We explain the rationale behind these convection-diffusion schemes, and we comment on their interpretation in differential-geometric terms. Sections 4 and 5 are concerned with a transfer of the schemes from the full Heisenberg group to phase space, resulting in a dimension reduction that is beneficial for implementation.
- **Convection:** In Section 6 we consider convection (reassignment) as an important special case. For a suitable choice of Gaussian window, it is possible to exploit Cauchy-Riemann equations for the analysis of the algorithms, and for the design of more efficient alternatives. For example, in Section 6 we deduce from these Cauchy-Riemann relations that differential reassignment according to Daudet et al. [19], boils down to a convection system on Gabor transforms that is equivalent to erosion on the modulus, while preserving the phase.

- **Discretization and Implementation:** Sections 7 and 8. In order to derive various suitable algorithms for differential reassignment and diffusion we consider discrete Gabor transforms in Section 7. As these Gabor transforms are defined on discrete Heisenberg groups, we need left-invariant shift operators for the generators in our left-invariant evolutions on discrete Heisenberg groups. These discrete left-invariant shifts are derived in Section 8. They are crucial in the algorithms for left-invariant evolutions on Gabor transforms, as straightforward finite difference approximations of the continuous framework produce considerable errors due to phase oscillations in the Gabor domain.
- **Implementation and analysis of reassignment:** Sections 9 and 10. In Section 9 we employ the results from the previous Sections in four algorithms for discrete differential reassignment. We compare these four numerical algorithms by applying them to reassignment of a chirp signal. We provide evidence that it actually works as reassignment (via numerical experiments, subsection 9.1) and indeed yields a concentration about the expected curve in the time-frequency plane (Section 10). We show this by deriving the corresponding analytic solutions of reassigned Gabor transforms of arbitrary chirp signals in Section 10.
- **Diffusion:** In Section 11 we consider signal enhancement via left-invariant diffusion on Gabor transforms. Here we do not apply thresholds on Gabor coefficients. Instead we use both spatial and frequency context of Gabor-atoms in locally adaptive flows in the Gabor domain. We include a basic experiment of enhancement of a noisy 1D-chirp signal. This experiments is intended as a preliminary feasibility study to show possible benefits for various imaging- and signal applications. The benefits are comparable to our directly related[1] previous works on enhancement of (multiply crossing) elongated structures in 2D- and 3D medical images via nonlinear adaptive evolutions on invertible orientation scores and/or diffusion-weighted MRI images, [22, 38, 25, 26, 31, 24, 27, 57, 58].
- **2D Imaging Applications:** In Section 12 we investigate extensions of our algorithms to left-invariant evolutions on Gabor transforms of 2-dimensional greyscale images. We carry out experiments of differential reassignment and texture enhancement on basic images. Finally, we consider a cardiac imaging application where cardiac wall deformations can be directly computed from a robust frequency field estimates obtained using Gabor transforms of MRI-tagging images. Our approach by Gabor transforms is inspired by [2], and it is relatively simple compared to existing approaches on cardiac deformation (or strain/velocity) estimations, cf. [30, 37, 62, 63].

2. Gabor transforms and the reduced Heisenberg group

Throughout the paper, we fix integers $d \in \mathbb{N}$ and $n \in \mathbb{Z} \setminus \{0\}$. The continuous Gabor-transform $\mathcal{G}_\psi[f] : \mathbb{R}^d \times \mathbb{R}^d \to \mathbb{C}$ of a square integrable signal $f : \mathbb{R}^d \to \mathbb{C}$ is commonly defined as

$$\mathcal{G}_\psi[f](p,q) = \int_{\mathbb{R}^d} f(\xi)\overline{\psi(\xi - p)}e^{-2\pi n i\,(\xi-p)\cdot q}\,\mathrm{d}\xi\ , \tag{1}$$

where $\psi \in \mathbb{L}_2(\mathbb{R}^d)$ is a suitable window function. For window functions centered around zero both in space and frequency, the Gabor coefficient $\mathcal{G}_\psi[f](p,q)$ expresses the contribution of the frequency nq to the behaviour of f near p.

This interpretation is suggested by the Parseval formula associated to the Gabor transform, which reads

$$\int_{\mathbb{R}^d}\int_{\mathbb{R}^d} |\mathcal{G}_\psi[f](p,q)|^2\,\mathrm{d}p\,\mathrm{d}q = C_\psi \int_{\mathbb{R}^d} |f(p)|^2\,\mathrm{d}p, \quad \text{where } C_\psi = \frac{1}{n}\|\psi\|^2_{\mathbb{L}_2(\mathbb{R}^d)} \tag{2}$$

for all $f, \psi \in \mathbb{L}_2(\mathbb{R}^d)$. This property can be rephrased as an inversion formula:

$$f(\xi) = \frac{1}{C_\psi}\int_{\mathbb{R}^d}\int_{\mathbb{R}^d} \mathcal{G}_\psi[f](p,q)\, e^{i2\pi n(\xi-p)\cdot q}\psi(\xi-p)\,\mathrm{d}p\mathrm{d}q\ , \tag{3}$$

[1] Replace the Heisenberg group and the Schrödinger representation with the special Euclidean motion group and its left-regular representation on $\mathbb{L}_2(\mathbb{R}^d)$, $d = 2, 3$.

to be read in the weak sense. The inversion formula is commonly understood as the decomposition of f into building blocks, indexed by a time and a frequency parameter; most applications of Gabor analysis are based on this (heuristic) interpretation[2]. For many such applications, the phase of the Gabor transform is of secondary importance (see, e.g., the characterization of function spaces via Gabor coefficient decay [42]). However, since the Gabor transform uses highly oscillatory complex-valued functions, its phase information is often crucial, a fact that has been specifically acknowledged in the context of reassignment for Gabor transforms [19].

For this aspect of Gabor transform, as for many others[3], the group-theoretic viewpoint becomes particularly beneficial, cf. [33]. The underlying group is the *reduced Heisenberg group* H_r. As a set, $H_r = \mathbb{R}^{2d} \times \mathbb{R}/\mathbb{Z}$, with the group product

$$(p, q, s + \mathbb{Z})(p', q', s' + \mathbb{Z}) = (p + p', q + q', s + s' + \frac{1}{2}(q \cdot p' - p \cdot q') + \mathbb{Z}) \ .$$

This makes H_r a connected (nonabelian) nilpotent Lie group that arises as a quotient group

$$H_r = H(2d + 1)/(\{0\} \times \{0\} \times \mathbb{Z})$$

of the well-known simpy connected $2d + 1$-dimensional Heisenberg group $H(2d + 1)$. The Lie algebra is spanned by vectors $A_1, \ldots, A_{2d+1}$ with Lie brackets $[A_i, A_{i+d}] = -A_{2d+1}$, and all other brackets vanishing.

H_r acts on $\mathbb{L}_2(\mathbb{R}^d)$ via the *Schrödinger representations* $\mathcal{U} : H_r \to \mathcal{B}(\mathbb{L}_2(\mathbb{R}^d))$,

$$\mathcal{U}_{g=(p,q,s+\mathbb{Z})}\psi(\xi) = e^{2\pi i n(s+q\xi-\frac{p\cdot q}{2})}\psi(\xi - p), \qquad \psi \in \mathbb{L}_2(\mathbb{R}^d). \tag{4}$$

The associated matrix coefficients are defined as

$$\mathcal{W}_\psi f(p, q, s + \mathbb{Z}) = (\mathcal{U}_{(p,q,s+\mathbb{Z})}\psi, f)_{\mathbb{L}_2(\mathbb{R}^d)}, \tag{5}$$

where we assume linearity of the inner-product in the second entry. In the following, we will often omit the superscript n from $\mathcal{U}$, implicitly assuming that we use the same choice of n as in the definition of $\mathcal{G}_\psi$. Then a simple comparison of (5) with (1) reveals that

$$\mathcal{G}_\psi[f](p, q) = \mathcal{W}_\psi f(p, q, s = -\frac{p \cdot q}{2}). \tag{6}$$

Since $\mathcal{W}_\psi f(p, q, s + \mathbb{Z}) = e^{2\pi i n s}\mathcal{W}_\psi f(p, q, 0 + \mathbb{Z})$, the phase variable s does not affect the modulus, and (2) can be rephrased as

$$\int_0^1 \int_{\mathbb{R}^d} \int_{\mathbb{R}^d} |\mathcal{W}_\psi[f](p, q, s + \mathbb{Z})|^2 \, \mathrm{d}p \, \mathrm{d}q \mathrm{d}s = C_\psi \int_{\mathbb{R}^d} |f(p)|^2 \, \mathrm{d}p. \tag{7}$$

Just as before, this induces a weak-sense inversion formula, which reads

$$f = \frac{1}{C_\psi} \int_0^1 \int_{\mathbb{R}^d} \int_{\mathbb{R}^d} \mathcal{W}_\psi[f](p, q, s + \mathbb{Z}) \, \mathcal{U}_{(p,q,s+\mathbb{Z})}\psi \, \mathrm{d}p \, \mathrm{d}q \mathrm{d}s \ .$$

As a byproduct of (7), we note that the Schrödinger representation is irreducible. Furthermore, the orthogonal projection $\mathbb{P}_\psi$ of $\mathbb{L}_2(H_r)$ onto the range $\mathfrak{R}(\mathcal{W}_\psi)$ turns out to be right convolution with a suitable (reproducing) kernel function,

$$(\mathbb{P}_\psi U)(h) = U * K(h) = \int_{H_r} U(g) K(g^{-1}h) dg \ , \tag{8}$$

[2]Under some conditions on the window function ψ the corresponding Riemannian sums converge to f in the modulation spaces and in Wiener amalgam norms, hence also in the $\mathbb{L}_p$-sense, for details see cf. [65].

[3]Regarding the phase factor that arises in the composition of time frequency shifts and the H_r group-structure in the Gabor domain we quote "*This phase factor is absolutely essential for a deeper understanding of the mathematical structure of time frequency shifts, and it is the very reason for a non-commutative group in the analysis.*" from [42, Ch:9].

with dg denoting the left Haar measure (which is just the Lebesgue measure on $\mathbb{R}^{2d} \times \mathbb{R}/\mathbb{Z}$) and

$$K(p,q,s) = \frac{1}{C_\psi} \mathcal{W}_\psi \psi(p,q,s) = \frac{1}{C_\psi} (U_{(p,q,s)}\psi, \psi). \tag{9}$$

The chief reason for choosing the somewhat more redundant function $\mathcal{W}_\psi f$ over $\mathcal{G}_\psi[f]$ is that $\mathcal{W}_\psi$ translates time-frequency shifts acting on the signal f to shifts in the argument. If $\mathcal{L}$ and $\mathcal{R}$ denote the left and right regular representation, i.e., for all $g, h \in H_r$ and $F \in \mathbb{L}_2(H_r)$,

$$(\mathcal{L}_g F)(h) = F(g^{-1}h) \ , \ (\mathcal{R}_g F)(h) = F(hg) \ ,$$

then $\mathcal{W}_\psi$ intertwines $\mathcal{U}$ and $\mathcal{L}$,

$$\mathcal{W}_\psi \circ \mathcal{U}_g = \mathcal{L}_g \circ \mathcal{W}_\psi \ . \tag{10}$$

Thus the group parameter s in H_r keeps track of the phase shifts induced by the noncommutativity of time-frequency shifts. By contrast, applying *right shifts* on the Gabor transform corresponds to changing the window:

$$\mathcal{R}_g(\mathcal{W}_\psi(h)) = (\mathcal{U}_{hg}\psi, f) = \mathcal{W}_{\mathcal{U}_g\psi} f(h) \ . \tag{11}$$

3. Left Invariant Evolutions on Gabor Transforms

We relate operators $\Phi : \mathfrak{R}(\mathcal{W}_\psi) \to \mathbb{L}_2(H_r)$ on Gabor transforms, which actually use and change the relevant phase information of a Gabor transform, in a well-posed manner to operators $\Upsilon_\psi : \mathbb{L}_2(\mathbb{R}^d) \to \mathbb{L}_2(\mathbb{R}^d)$ on signals via

$$\begin{aligned} &(\Upsilon_\psi f)(\xi) = (\mathcal{W}_\psi^* \circ \Phi \circ \mathcal{W}_\psi f)(\xi) \\ &= \tfrac{1}{C_\psi} \int\limits_{[0,1]} \int\limits_{\mathbb{R}^d} \int\limits_{\mathbb{R}^d} (\Phi(\mathcal{W}_\psi f))(p,q,s)\, e^{i2\pi n[(\xi,q)+s-(1/2)p\cdot q]} \psi(\xi - p)\, \mathrm{d}p\, \mathrm{d}q\, \mathrm{d}s. \end{aligned} \tag{12}$$

Our aim is to design operators Υ_ψ that address signal processing problems such as denoising or detection.

3.1. Design principles

We now formulate a few desirable properties of Υ_ψ, and sufficient conditions for Φ to guarantee that Υ_ψ meets these requirements.

1. *Covariance with respect to time-frequency-shifts:* The operator Υ_ψ should commute with time-frequency shifts;

   $$\Upsilon_\psi \circ \mathcal{U}_g = \mathcal{U}_g \circ \Upsilon_\psi$$

   for all $g \in H(2d+1)$. This requires a proper treatment of the phase.
   One easy way of guaranteeing covariance of Υ_ψ is to ensure left invariance of Φ:

   $$\Phi \circ \mathcal{L}_g = \mathcal{L}_g \circ \Phi \tag{13}$$

   for all $g \in H(2d+1)$. If Φ commutes with $\mathcal{L}_g$, for all $g \in H_r$, it follows from (10) that

   $$\Upsilon_\psi \circ \mathcal{U}_g = \mathcal{W}_\psi^* \circ \Phi \circ \mathcal{W}_\psi \circ \mathcal{U}_g = \mathcal{W}_\psi^* \circ \Phi \circ \mathcal{L}_g \circ \mathcal{W}_\psi = \mathcal{U}_g \circ \Upsilon_\psi \ .$$

   Generally speaking, left invariance of Φ is not a *necessary* condition for invariance of Υ_ψ: Note that $\mathcal{W}_\psi^* = \mathcal{W}_\psi^* \circ \mathbb{P}_\psi$. Thus if Φ is left-invariant, and $A : \mathbb{L}_2(H_r) \to \mathfrak{R}(\mathcal{W}_\psi)^\perp$ an arbitrary operator, then $\Phi + A$ cannot be expected to be left-invariant, but the resulting operator on the signal side will be the same as for Φ, thus covariant with respect to time-frequency shifts.
   The authors of [19] studied reassignment procedures that leave the phase invariant, whereas we shall put emphasis on phase-covariance. Note however that the two properties are not mutually exclusive; convection along equiphase lines fulfills both. (See also the discussion in subsection 3.4.)

2. *Covariance with respect to rotation and translations :*

$$\Upsilon_\psi \circ \mathcal{U}_g^{SE(d)} = \mathcal{U}_g^{SE(d)} \circ \Upsilon_\psi \tag{14}$$

for all $g = (x, R) \in SE(d) = \mathbb{R}^d \rtimes SO(d)$ with unitary representation $\mathcal{U}^{SE(d)} : SE(d) \to B(\mathbb{L}_2(\mathbb{R}^2))$ given by $(\mathcal{U}_{(x,R)}^{SE(d)} f)(\xi) = f(R^{-1}(\xi - x))$, for almost every $(x, R) \in SE(d)$. Furthermore, we introduce the representation $\mathcal{V}_{(x,R)}^{SE(d)} : SE(d) \to \mathbb{L}_2(H(2d+1))$ by

$$(\mathcal{V}_{(x,R)}^{SE(d)} U)(p, q, s) = U(R^{-1}(p - x), R^{-1}q, s + \frac{x \cdot q}{2}),$$

for almost every $(p, q, s) \in H(2d + 1)$ and all $U \in \mathbb{L}_2(H(2d + 1))$. Rigid body motions on signals and Gabor transforms relate via

$$\begin{aligned}
&(\mathcal{W}_\psi \mathcal{U}_{(\mathbf{x},R)}^{SE(d)} f)(p, q, s) = \int_{\mathbb{R}^d} f(R^{-1}(\xi - x)) e^{-2\pi i n(s + q\cdot\xi - \frac{1}{2}p\cdot q)} \, \overline{\psi(\xi - p)} \, \mathrm{d}\xi \\
&= \int_{\mathbb{R}^d} f(\xi') \, e^{-2\pi i n(s + \frac{x\cdot q}{2} + R^{-1}q\cdot\xi' - \frac{1}{2}(R^{-1}(p-x)\cdot R^{-1}q))} \, \overline{\psi(R\xi' + x - p)} \, \mathrm{d}\xi' \\
&= (\mathcal{W}_{\mathcal{U}_{(0,R^{-1})}^{SE(d)}\psi} f)(R^{-1}(p - x), R^{-1}q, s + \tfrac{x\cdot q}{2}) = (\mathcal{V}_{(x,R)}^{SE(d)} \mathcal{W}_{\mathcal{U}_{(0,R^{-1})}^{SE(d)}\psi} f)(p, q, s),
\end{aligned} \tag{15}$$

for all $f \in \mathbb{L}_2(\mathbb{R}^d)$ and for all $(x, R) \in SE(d)$ and for all $(p, q, s) \in H(2d + 1)$ and therefore we require the kernel to be isotropic (besides $\Phi \circ \mathcal{L}_{(x,0,0)} = \mathcal{L}_{(x,0,0)} \circ \Phi$ included in Eq. (13)) and we require

$$\Phi \circ \mathcal{V}_{(0,R)}^{SE(d)} = \mathcal{V}_{(0,R)}^{SE(d)} \circ \Phi \tag{16}$$

for all $R \in SO(d)$.

3. *Nonlinearity:* The requirement that Υ_ψ commute with $\mathcal{U}$ immediately rules out linear operators Φ. Recall that $\mathcal{U}$ is irreducible, and by Schur's lemma [20], any linear intertwining operator is a scalar multiple of the identity operator.
4. By contrast to left invariance, right invariance of Φ is undesirable. By a similar argument as for left-invariance, it would provide that $\Upsilon_\psi = \Upsilon_{\mathcal{U}_g\psi}$, where we recall Eq. (11).

We stress that one cannot expect that the processed Gabor transform $\Phi(\mathcal{W}_\psi f)$ is again the Gabor transform of a function constructed by the same kernel ψ, i.e. we do not expect that $\Phi(\mathfrak{R}(\mathcal{W}_\psi)) \subset \mathfrak{R}(\mathcal{W}_\psi)$.

3.2. Invariant differential operators on H_r

The basic building blocks for the evolution equations are the left-invariant differential operators on H_r of degree one. These operators are conveniently obtained by differentiating the *right* regular representation, restricted to one-parameter subgroups through the generators $\{A_1, \ldots, A_{2d+1}\} = \{\partial_{p_1}, \ldots, \partial_{p_d}, \partial_{q_1}, \ldots, \partial_{q_d}, \partial_s\} \subset T_e(H_r)$,

$$\mathrm{d}\mathcal{R}(A_i)U(g) = \lim_{\epsilon\to 0} \frac{U(g e^{\epsilon A_i}) - U(g)}{\epsilon} \text{ for all } g \in H_r \text{ and smooth } U \in \mathcal{C}^\infty(H_r), \tag{17}$$

The resulting differential operators $\{\mathrm{d}\mathcal{R}(A_1), \ldots, \mathrm{d}\mathcal{R}(A_{2d+1})\} =: \{\mathcal{A}_1, \ldots, \mathcal{A}_{2d+1}\}$ denote the left-invariant vector fields on H_r, and brief computation of (17) yields:

$$\mathcal{A}_i = \partial_{p_i} + \frac{q_i}{2}\partial_s, \quad \mathcal{A}_{d+i} = \partial_{q_i} - \frac{p_i}{2}\partial_s, \quad \mathcal{A}_{2d+1} = \partial_s, \qquad \text{for } i = 1, \ldots, d. \tag{18}$$

The differential operators obey the same commutation relations as their Lie algebra counterparts $A_1, \ldots, A_{2d+1}$

$$[\mathcal{A}_i, \mathcal{A}_{d+i}] := \mathcal{A}_i\mathcal{A}_{d+i} - \mathcal{A}_{d+i}\mathcal{A}_i = -\mathcal{A}_{2d+1}, \tag{19}$$

and all other commutators are zero.

3.3. Setting up the equations

For the effective operator Φ, we will choose left-invariant evolution operators with stopping time $t > 0$. To stress the dependence on the stopping time we shall write Φ_t rather than Φ. Typically, such operators are defined by $\Phi_t(\mathcal{W}_\psi f)(p,q,s) = W(p,q,s,t)$ where W is the solution of

$$\boxed{\begin{cases} \partial_t W(p,q,s,t) &= Q(|\mathcal{W}_\psi f|, \mathcal{A}_1, \dots, \mathcal{A}_{2d}) W(p,q,s,t), \\ W(p,q,s,0) &= \mathcal{W}_\psi f(p,q,s). \end{cases}} \tag{20}$$

where we note that the left-invariant vector fields $\{\mathcal{A}_i\}_{i=1}^{2d+1}$ on H_r are given by Eq. (18) and with left-invariant quadratic differential form

$$Q(|\mathcal{W}_\psi f|, \mathcal{A}_1, \dots, \mathcal{A}_{2d}) = -\sum_{i=1}^{2d} a_i(|\mathcal{W}_\psi f|)(p,q)\mathcal{A}_i + \sum_{i=1}^{2d}\sum_{j=1}^{2d} \mathcal{A}_i \; D_{ij}(|\mathcal{W}_\psi f|)(p,q) \; \mathcal{A}_j. \tag{21}$$

Here $a_i(|\mathcal{W}_\psi f|)$ and $D_{ij}(|\mathcal{W}_\psi f|)$ are functions such that $(p,q) \mapsto a_i(|\mathcal{W}_\psi f|)(p,q) \in \mathbb{R}$ and $(p,q) \mapsto D_{ij}(|\mathcal{W}_\psi f|)(p,q) \in \mathbb{R}$ are smooth and either $D = 0$ (pure convection) or $D^T = D > 0$ holds pointwise (with $D = [D_{ij}]$) for all $i = 1, \dots, 2d$, $j = 1, \dots 2d$. Moreover, in order to guarantee left-invariance, the mappings $a_i : \mathcal{W}_\psi f \mapsto a_i(|\mathcal{W}_\psi f|)$ need to fulfill the covariance relation

$$a_i(|\mathcal{L}_h \mathcal{W}_\psi f|)(g) = a_i(|\mathcal{W}_\psi f|)(p - p', q - q'), \tag{22}$$

for all $f \in \mathbb{L}_2(\mathbb{R}^d)$, and all $g = (p,q,s+\mathbb{Z}), h = (p',q',s'+\mathbb{Z}) \in H_r$.

For $a_1 = \ldots = a_{2d+1} = 0$, the equation is a diffusion equation, whereas if $D = 0$, the equation describes a convection. We note that existence, uniqueness and square-integrability of the solutions (and thus well-definedness of Υ_ψ) are issues that will have to be decided separately for each particular choice of $a := (a_1, \dots, a_{2d})^T$ and D. In general existence and uniqueness are guaranteed, provided that the convection vector and the diffusion-matrix are smoothly depending on the initial condition, see Appendix B. Furthermore, continuity of the effective non-linear operator Υ_ψ is a difficult and relevant issue, that is beyond the scope of this article.

Occasionally, we shall consider the case where the convection vector $(a_i)_{i=1}^{2d}$ and the diffusion-matrix D are updated with the absolute value of the current solution $|W(\cdot,t)|$ at time $t > 0$, rather than having them prescribed by the modulus of the initial condition $|W(\cdot,0)| = |\mathcal{W}_\psi f| = |\mathcal{G}_\psi f|$ at time $t = 0$, i.e.

$$\begin{array}{lll} a_i(|W(\cdot,0)|) & \text{is sometimes replaced by} & a_i(|W(\cdot,t)|) \text{ and/or} \\ D_{ij}(|W(\cdot,0)|) & \text{is sometimes replaced by} & D_{ij}(|W(\cdot,t)|) \end{array}$$

In the case of such a replacement the PDE gets non-linear, and unique (weak) solutions are not a priori guaranteed. For example in the cases of differential re-assignment we shall consider in Section 6, we will restrict ourselves to *viscosity solutions* of the corresponding Hamilton-Jacobi evolution systems, [32, 54].

In order to guarantee rotation covariance we set column vector $a := (a^1, \dots, a^{2d})^T$ and $D = [D_{ij}]$ with row-index i and column-index j and we require

$$\begin{array}{l} (a(\mathcal{V}^{SE(d)}_{(\mathbf{0},R)} W(\cdot,t)))(g) = \mathbf{R}\,(a(W(\cdot,t)))(\mathbf{R}^{-1}g)\;, \\ (D(\mathcal{V}^{SE(d)}_{(\mathbf{0},R)} W(\cdot,t)))(g) = \mathbf{R}^{-1}\,(D(W(\cdot,t)))(\mathbf{R}^{-1}g)\,\mathbf{R}\;, \\ \text{with } \mathbf{R}^{-1}g = \mathbf{R}^{-1}(p,q,s) = (R^{-1}p, R^{-1}q, s), \end{array} \tag{23}$$

for all $\mathbf{R} = R \otimes R \in SO(2d)$, $R \in SO(d)$, $g = (p,q,s) \in H_r$, $U \in \mathbb{L}_2(H_r)$, where we recall (15).

This definition of Φ_t, for each $t > 0$ fixed, satisfies the criteria we set up above:

1. Since the evolution equation is left-invariant (and provided uniqueness of the solutions), it follows that Φ_t is left-invariant. Thus the associated Υ_ψ is invariant under time-frequency shifts.
2. The rotated left-invariant gradient transforms as follows

$$\left(\underline{\mathcal{A}}_g \mathcal{V}^{SE(d)}_{(\mathbf{0},R)} W(\cdot,t)\right)(g) = \mathbf{R}\;\left(\underline{\mathcal{A}}_{\mathbf{R}^{-1}g} W(\cdot,t)\right)(\mathbf{R}^{-1}g), \text{ with } \underline{\mathcal{A}} = (\mathcal{A}_1, \dots, \mathcal{A}_{2d})^T.$$

Thereby (the generator of) our diffusion operator Φ_t is rotation covariant, i.e.

$$Q(|W(\cdot,t)|,\underline{\mathcal{A}}) \circ \mathcal{V}^{SE(d)}_{(\mathbf{0},R)} = \mathcal{V}^{SE(d)}_{(\mathbf{0},R)} \circ Q(|W(\cdot,t)|,\underline{\mathcal{A}}) \text{ for all } R \in SO(d),$$

if Eq. (23) and Eq. (22) hold. For example, if $a = 0$ and D would be constant, then by Eq. (23) and Schur's lemma one has $D = \text{diag}\{D^{11},\dots,D^{11},D^{d+1,d+1},\dots,D^{d+1,d+1}\}$ yielding the Kohn's Laplacian $\Delta_K = D_{11}\sum_{i=1}^{d}\mathcal{A}_i^2 + D_{d+1,d+1}\sum_{i=d+1}^{2d}\mathcal{A}_i^2$, cf. [41], and indeed $\Delta_K \circ \mathcal{V}^{SE(d)}_{(\mathbf{0},R)} = \mathcal{V}^{SE(d)}_{(\mathbf{0},R)} \circ \Delta_K$.

3. In order to ensure non-linearity, not all of the functions a_i, D_{ij} should be constant, i.e. the schemes should be *adaptive convection* and/or *adaptive diffusion*, via adaptive choices of convection vectors $(a_1,\dots,a_{2d})^T$ and/or conductivity matrix D. We will use ideas similar to our previous work on adaptive diffusions on invertible orientation scores [39], [25], [24], [26]. We use the absolute value of the (evolving) Gabor transform to adapt the diffusion and convection in order to avoid oscillations.
4. The two-sided invariant differential operators of degree one correspond to the center of the Lie algebra, which is precisely the span of A_{2d+1}. Both in the cases of diffusion and convection, we consistently removed the $\mathcal{A}_{2d+1} = \partial_s$-direction, and we removed the s-dependence in the coefficients $a_i(|\mathcal{W}_\psi f|)(p,q)$, $D_{ij}(|\mathcal{W}_\psi f|)(p,q)$ of the generator $Q(|\mathcal{W}_\psi f|,\mathcal{A}_1,\dots,\mathcal{A}_{2d})$ by taking the absolute value $|\mathcal{W}_\psi f|$, which is independent of s. A more complete discussion of the role of the s-variable is contained in the following subsection.

3.4. Convection and Diffusion along Horizontal Curves

So far our motivation for (20) has been group theoretical. There is one issue we did not address yet, namely the omission of $\partial_s = \mathcal{A}_{2d+1}$ in (20). Here we first motivate this omission and then consider the differential geometrical consequence that (adaptive) convection and diffusion takes place along so-called horizontal curves.

The reason for the removal of the $\mathcal{A}_{2d+1}$ direction in our diffusions and convections is simply that this direction leads to a scalar multiplication operator mapping the space of Gabor transform to itself, since $\partial_s \mathcal{W}_\psi f = -2\pi i n\, \mathcal{W}_\psi f$. Moreover, we adaptively steer the convections and diffusions by the modulus of a Gabor transform $|\mathcal{W}_\psi f(p,q,s)| = |\mathcal{G}_\psi f(p,q)|$, which is independent of s, and clearly a vector field $(p,q,s) \mapsto F(p,q)\partial_s$ is left-invariant iff F is constant. Consequently it does not make sense to include the separate ∂_s in our convection-diffusion equations, as it can only yield a scalar multiplication. Indeed, for all constant $\alpha > 0, \beta \in \mathbb{R}$ we have

$$[\partial_s, Q(|\mathcal{W}_\psi f|,\mathcal{A}_1,\dots,\mathcal{A}_{2d})] = 0 \text{ and } \partial_s \mathcal{W}_\psi f = -2\pi i n\, \mathcal{W}_\psi f \Rightarrow$$
$$e^{t\left((\alpha\partial_s^2+\beta\partial_s)+Q(|\mathcal{W}_\psi f|,\mathcal{A}_1,\dots,\mathcal{A}_{2d})\right)} = e^{-t\alpha(2\pi n)^2 - t\beta 2\pi i n}\, e^{tQ(|\mathcal{W}_\psi f|,\mathcal{A}_1,\dots,\mathcal{A}_{2d})}.$$

In other words ∂_s is a redundant direction in each tangent space $T_g(H_r)$, $g \in H_r$. This however does not imply that it is a redundant direction in the group manifold H_r itself, since clearly the s-axis represents the relevant phase and stores the non-commutative nature between position and frequency, [29, ch:1].

The omission of the redundant direction ∂_s in the *tangent bundle* $T(H_r)$ has an important differential geometrical consequence as we will see next.

Theorem 1. *Let $f \in \mathbb{L}_2(\mathbb{R}^d)$ be a signal and $\mathcal{W}_\psi f$ be its Gabor transform associated to the Schwartz function ψ. If we just consider convection and no diffusion (i.e. $D = 0$) then the solution of (20) is given by*

$$W(g,t) = \mathcal{W}_\psi f(\gamma_f^g(t)) \ , \qquad g = (p,q,s) \in H_r,$$

where the characteristic curve $t \mapsto \gamma_f^{g_0}(t) = (p(t),q(t),s(t))$ for each $g_0 = (p_0,q_0,s_0) \in H_r$ is given by the unique solution of the following ODE:

$$\begin{cases} \dot{p}(t) = -(a^1(|\mathcal{W}_\psi f|)(p(t),q(t)),\dots,a^d(|\mathcal{W}_\psi f|)(p(t),q(t)))^T, & p(0) = p_0, \\ \dot{q}(t) = -(a^{d+1}(|\mathcal{W}_\psi f|)(p(t),q(t)),\dots,a^{2d}(|\mathcal{W}_\psi f|)(p(t),q(t)))^T, & q(0) = q_0, \\ \dot{s}(t) = \frac{q(t)}{2}\cdot\dot{p}(t) - \frac{p(t)}{2}\cdot\dot{q}(t), & s(0) = s_0, \end{cases}$$

Consequently, the operator $\mathcal{W}_\psi f \mapsto W(\cdot,t)$ is phase covariant (the phase moves along with the characteristic curves of transport):

$$arg\{W(g,t)\} = arg\{\mathcal{W}_\psi f\}(\gamma_f^g) \text{ for all } t > 0. \tag{24}$$

Proof See Appendix A.

3.5. Additional Remarks Concerning the Omission of ∂_s from the Tangent Bundle $T(H_r)$

The removal of the ∂_s direction from the tangent space does not imply that one can ignore the s-axis in the domain of a (processed) Gabor transform. The domain of a (processed) Gabor transform $\Phi_t(\mathcal{W}_\psi f)$ should *not*[4] be considered as $\mathbb{R}^{2d} \equiv H_r/\Theta$. Simply, because $[\partial_p, \partial_q] = 0$ whereas we should have (19).

The omission of the redundant direction ∂_s in $T(H_r)$ has an important geometrical consequence. Similarly as for our framework of linear evolutions on orientation scores, cf. [26, 39], this means that we enforce *horizontal* diffusion and convection. In other words, the generator of our evolutions will only include derivations within the horizontal part of the Lie algebra spanned by $\{\mathcal{A}_1, \dots \mathcal{A}_{2d}\}$. On the Lie group H_r this means that transport and diffusion only takes place along so-called *horizontal curves* in H_r which are curves $t \mapsto (p(t), q(t), s(t)) \in H_r$, with $s(t) \in (0, 1)$, along which

$$s(t) = \frac{1}{2} \int_0^t \sum_{i=1}^d q_i(\tau) p_i'(\tau) - p_i(\tau) q_i'(\tau) \mathrm{d}\tau \ , \tag{25}$$

see Theorem 1. For $d = 1$ this gives a nice geometric interpretation to the phase variable $s(t)$, as by the Stokes theorem it represents the net surface area between a straight line connection between $(p(0), q(0), s(0))$ and $(p(t), q(t), s(t))$ and the actual horizontal curve connection $[0, t] \ni \tau \mapsto (p(\tau), q(\tau), s(\tau))$. For example, horizontal diffusion with diagonal D is the forward Kolmogorov equation [15] of Brownian motion $t \mapsto (P(t), Q(t))$ in position and frequency and Eq. (25) associates a random variable $S(t)$. This random variable measures the net surface area enclosed by a random walk departing from the unity element and a straight-line connection from the endpoint $(p(t), q(t), s(t))$ to the origin $(p(0), q(0), s(0)))$. This provides us with a clear probabilistic interpretation of the implicit smoothing in the phase direction due to the commutator $[\mathcal{A}_2, \mathcal{A}_1] = \mathcal{A}_3 = \partial_s$, cf. [41, 29, 25].

In order to explain why the omission of the redundant direction ∂_s from the tangent bundle $T(H_r)$ implies a restriction to horizontal curves satisfying Eq. (25), we consider the dual frame associated to our frame of reference $\{\mathcal{A}_1, \dots, \mathcal{A}_{2d+1}\}$. We will denote this dual frame by $\{\mathrm{d}\mathcal{A}^1, \dots, \mathrm{d}\mathcal{A}^{2d+1}\}$, where in this particular case 'd' stands for 'dual' and not[5] for 'exterior derivative'. The dual frame is uniquely determined by

$$\langle \mathrm{d}\mathcal{A}^i, \mathcal{A}_j \rangle = \delta^i_j,$$

which holds for $i, j = 1, 2, 3$ and where δ^i_j denotes the Kronecker delta. A brief computation yields

$$\begin{array}{l} \mathrm{d}\mathcal{A}^i\big|_{g=(p,q,s)} = \mathrm{d}p^i \ , \ \ \mathrm{d}\mathcal{A}^{d+i}\big|_{g=(p,q,s)} = \mathrm{d}q^i \ , \quad i = 1, \dots, d \\ \mathrm{d}\mathcal{A}^{2d+1}\big|_{g=(p,q,s)} = \mathrm{d}s + \frac{1}{2}(p \cdot \mathrm{d}q - q \cdot \mathrm{d}p). \end{array} \tag{26}$$

Consequently a smooth curve $t \mapsto \gamma(t) = (p(t), q(t), s(t))$ is horizontal iff

$$\langle \mathrm{d}\mathcal{A}^{2d+1}\big|_{\gamma(s)}, \gamma'(s) \rangle = 0 \Leftrightarrow s'(t) = \frac{1}{2}(q(t) \cdot p'(t) - p(t) \cdot q'(t)).$$

Finally, we note that the transport in Theorem 1 indeed takes place along horizontal (characteristic) curves. Even for the (degenerate) diffusion case with $D = D^T = [D_{ij}]_{i,j=1,\dots,d} > 0$, the omission of the $2d{+}1^{\text{th}}$ direction $\partial_s = \mathcal{A}_{2d+1}$ implies that diffusion takes place along horizontal curves. Moreover, the omission does not affect the smoothness and uniqueness of the solutions of (20), since the initial condition is infinitely differentiable (if ψ is a Schwartz function) and the Hörmander condition [44], [23] is by (19) still satisfied.

[4] As we explain in [29, App. B and App. C] the Gabor domain is a principal fiber bundle $P_T = (H_r, \mathbb{T}, \pi, \mathcal{R})$ equipped with the Cartan connection form $\omega_g(X_g) = \langle \mathrm{d}s + \frac{1}{2}(p\mathrm{d}q - q\mathrm{d}p), X_g \rangle$, or equivalently, it is a contact manifold, cf. [11, p.6], [29, App. B, def. B.14] , $(H_r, \mathrm{d}\mathcal{A}^{2d+1})$).

[5] Exterior derivatives must be taken from volume forms, e.g. if we take the exterior derivatives of the dual forms themselves we find Cartan's structural formula $\mathrm{d}(\mathrm{d}\mathcal{A}^{\mathrm{k}}) = \sum_{\mathrm{i,j}} \mathrm{c}^{\mathrm{k}}_{\mathrm{ij}} \mathrm{d}\mathcal{A}^{\mathrm{j}} \wedge \mathrm{d}\mathcal{A}^{\mathrm{k}}$ with structure constants c^k_{ij} given by $[\mathcal{A}_i, \mathcal{A}_j] = \sum_k c^k_{ij} \mathcal{A}_k$.

4. Towards Phase Space and Back

As pointed out in the introduction it is very important to keep track of the phase variable $s > 0$. The first concern that arises here is whether this results in slower algorithms. In this section we will show that this is not the case. As we will explain next, one can use an invertible mapping $\mathcal{S}$ from the space $\mathcal{H}_n$ of Gabor transforms to phase space (the space of Gabor transforms restricted to the plane $s = \frac{pq}{2}$). As a result we can map our diffusions on $\mathcal{H}_n \subset \mathbb{L}_2(\mathbb{R}^2 \times [0,1])$ uniquely to diffusions on $\mathbb{L}_2(\mathbb{R}^2)$ simply by conjugation with $\mathcal{S}$. From a geometrical point of view it is easier to consider the diffusions on $\mathcal{H}_n \subset \mathbb{L}_2(\mathbb{R}^{2d} \times [0,1])$ than on $\mathbb{L}_2(\mathbb{R}^{2d})$, whereas all our numerical PDE-algorithms take place in phase space in order to gain speed.

Definition 2. *Let $\mathcal{H}_n$ denote the space of all complex-valued functions F on H_r such that $F(p,q,s+\mathbb{Z}) = e^{-2\pi i n s} F(p,q,0)$ and $F(\cdot,\cdot,s+\mathbb{Z}) \in \mathbb{L}_2(\mathbb{R}^{2d})$ for all $s \in \mathbb{R}$. Clearly $\mathcal{W}_\psi f \in \mathcal{H}_n$ for all $f, \psi \in \mathcal{H}_n$.*

In fact $\mathcal{H}_n$ is the closure of the space $\{\mathcal{W}_\psi f \mid \psi, f \in \mathbb{L}_2(\mathbb{R}^d)\}$ in $\mathbb{L}_2(H_r)$. The space $\mathcal{H}_n$ is bi-invariant, since:

$$\mathcal{W}_\psi \circ \mathcal{U}_g = \mathcal{L}_g \circ \mathcal{W}_\psi \text{ and } \mathcal{W}_{\mathcal{U}_g \psi} = \mathcal{R}_g \circ \mathcal{W}_\psi, \tag{27}$$

where $\mathcal{R}$ denotes the right regular representation on $\mathbb{L}_2(H_r)$ and $\mathcal{L}$ denotes the left regular representation of H_r on $\mathbb{L}_2(H_r)$. We can identify $\mathcal{H}_n$ with $\mathbb{L}_2(\mathbb{R}^{2d})$ by means of the following operator $\mathcal{S} : \mathcal{H}_n \to \mathbb{L}_2(\mathbb{R}^{2d})$ given by

$$(\mathcal{S}F)(p,q) = F(p,q,\frac{p\cdot q}{2} + \mathbb{Z}) = e^{i\pi n p\cdot q} F(p,q,0+\mathbb{Z}). \tag{28}$$

Clearly, this operator is invertible and its inverse is given by

$$(\mathcal{S}^{-1}F)(p,q,s+\mathbb{Z}) = e^{-2\pi i s n} e^{-i\pi n p\cdot q} F(p,q) \tag{29}$$

The operator $\mathcal{S}$ simply corresponds to taking the section $s(p,q) = -\frac{p\cdot q}{2}$ in the left cosets H_r/Θ where $\Theta = \{(0,0,s+\mathbb{Z}) \mid s \in \mathbb{R}\}$ of H_r. Furthermore we recall the common Gabor transform $\mathcal{G}_\psi$ given by (1) and its relation (6) to the full Gabor transform, which we can now write as

$$\mathcal{G}_\psi = \mathcal{S} \circ \mathcal{W}_\psi.$$

Theorem 3. *Let the operator Φ map the closure $\mathcal{H}_n$, $n \in \mathbb{Z}$, of the space of Gabor transforms into itself, i.e. $\Phi : \mathcal{H}_n \to \mathcal{H}_n$. Define the left and right-regular representations of H_r on $\mathcal{H}_n$ by restriction*

$$\mathcal{R}_g^{(n)} = \mathcal{R}_g|_{\mathcal{H}_n} \text{ and } \mathcal{L}_g^{(n)} = \mathcal{L}_g|_{\mathcal{H}_n} \qquad \text{for all } g \in H_r. \tag{30}$$

Define the corresponding left and right-regular representations of H_r on phase space by

$$\tilde{\mathcal{R}}_g^{(n)} := \mathcal{S} \circ \mathcal{R}_g^{(n)} \circ \mathcal{S}^{-1}, \quad \tilde{\mathcal{L}}_g^{(n)} := \mathcal{S} \circ \mathcal{L}_g^{(n)} \circ \mathcal{S}^{-1}.$$

Let $\tilde{\Phi} := \mathcal{S} \circ \Phi \circ \mathcal{S}^{-1}$ be the corresponding operator on $\mathbb{L}_2(\mathbb{R}^{2d})$ and

$$\Upsilon_\psi = (\mathcal{W}_\psi)^* \circ \Phi \circ \mathcal{W}_\psi = (\mathcal{S}\mathcal{W}_\psi)^{-1} \circ \tilde{\Phi} \circ \mathcal{S}\mathcal{W}_\psi = (\mathcal{G}_\psi)^* \circ \tilde{\Phi} \circ \mathcal{G}_\psi.$$

Then one has the following correspondence:

$$\Upsilon_\psi \circ \mathcal{U} = \mathcal{U} \circ \Upsilon_\psi \Leftarrow \Phi \circ \mathcal{L} = \mathcal{L} \circ \Phi \Leftrightarrow \tilde{\Phi} \circ \tilde{\mathcal{L}}^{(n)} = \tilde{\mathcal{L}}^{(n)} \circ \tilde{\Phi}. \tag{31}$$

If moreover $\Phi(\mathfrak{R}(\mathcal{W}_\psi)) \subset \mathfrak{R}(\mathcal{W}_\psi)$ then the left implication may be replaced by an equivalence. If Φ does not satisfy this property then one may replace $\Phi \to \mathcal{W}_\psi \mathcal{W}_\psi^* \Phi$ in (31) to obtain full equivalence in Eq. (31).

Proof For details see our technical report [29, Thm 2.2].

Remark 4. *With respect to the final remark in the above theorem we note that $\mathcal{W}_\psi : \mathbb{L}_2(\mathbb{R}^d) \to \mathbb{L}_2(H_r)$ is an isometry (and not a unitary map) and $\mathbb{P}_\psi = \mathcal{W}_\psi \mathcal{W}_\psi^*$ is the orthogonal projection onto the (closed) range $\mathfrak{R}(\mathcal{W}_\psi)$ (recall Eq. (8)) and thereby $\Upsilon_\psi = \mathcal{W}_\psi^* \Phi \mathcal{W}_\psi = (\mathcal{W}_\psi^* \mathcal{W}_\psi) \circ (\mathcal{W}_\psi^* \Phi \mathcal{W}_\psi) = \mathcal{W}_\psi^* (\mathbb{P}_\psi \Phi) \mathcal{W}_\psi$*

$$\Upsilon_\psi \circ \mathcal{U} = \mathcal{U} \circ \Upsilon_\psi \Leftrightarrow \mathbb{P}_\psi \Phi \circ \mathcal{L} = \mathcal{L} \circ \mathbb{P}_\psi \Phi.$$

This statement follows by applying the result in [22, Thm 21] to operator $\mathbb{P}_\psi \Phi$ which maps $\mathfrak{R}(\mathcal{W}_\psi)$ (i.e. the unique reproducing kernel space induced by $(g,h) \mapsto K(h^{-1}g)$ given in Eq. (9)), into itself.

5. Left-invariant Evolutions on Phase Space

For the next three chapters, for the sake of simplicity, we fix $d = 1$ and we consider left-invariant evolutions on Gabor transforms of 1D-signals. We will return to the case $d = 2$ in Section 12 where the rotation-covariance (2nd design principle in Subsection 3.1) comes into play.

We want to apply Theorem 3 to our left-invariant evolutions (20) to obtain the left-invariant diffusions on phase space (where we reduce 1 dimension in the domain). To this end we first compute the left-invariant vector fields $\{\tilde{\mathcal{A}}_i\} := \{\mathcal{S}\mathcal{A}_i\mathcal{S}^{-1}\}_{i=1}^3$ on phase space. The left-invariant vector fields on phase space are

$$\begin{array}{l} \tilde{\mathcal{A}}_1 U(p,q) = \mathcal{S}\mathcal{A}_1\mathcal{S}^{-1}U(p,q) = ((\partial_p - 2n\pi i q)U)(p,q), \\ \tilde{\mathcal{A}}_2 U(p,q) = \mathcal{S}\mathcal{A}_2\mathcal{S}^{-1}U(p,q) = (\partial_q U)(p,q), \\ \tilde{\mathcal{A}}_3 U(p,q) = \mathcal{S}\mathcal{A}_3\mathcal{S}^{-1}U(p,q) = -2in\pi U(p,q)\ , \end{array} \tag{32}$$

for all $(p,q) \in \mathbb{R}^2$ and all (locally defined) smooth functions $U : \mathbb{R}^2 \to \mathbb{C}$.

Now that we have computed the left-invariant vector fields on phase space, we can express our left-invariant evolution equations (20) on phase space

$$\boxed{\begin{cases} \partial_t \tilde{W}(p,q,t) & = \tilde{Q}(|\mathcal{G}_\psi f|, \tilde{\mathcal{A}}_1, \tilde{\mathcal{A}}_2)\tilde{W}(p,q,t), \\ \tilde{W}(p,q,0) & = \mathcal{G}_\psi f(p,q). \end{cases}} \tag{33}$$

with left-invariant quadratic differential form

$$\tilde{Q}(|\mathcal{G}_\psi f|, \tilde{\mathcal{A}}_1, \tilde{\mathcal{A}}_2) = -\sum_{i=1}^{2} a_i(|\mathcal{G}_\psi f|)(p,q)\tilde{\mathcal{A}}_i + \sum_{i=1}^{2}\sum_{j=1}^{2} \tilde{\mathcal{A}}_i\ D_{ij}(|\mathcal{G}_\psi f|)(p,q)\ \tilde{\mathcal{A}}_j. \tag{34}$$

Similar to the group case, the a_i and D_{ij} are functions such that $(p,q) \mapsto a_i(|\mathcal{G}_\psi f|)(p,q) \in \mathbb{R}$ and $(p,q) \mapsto a_i(|\mathcal{G}_\psi f|)(p,q) \in \mathbb{R}$ are smooth and either $D = 0$ (pure convection) or $D^T = D > 0$ (with $D = [D_{ij}]$ $i,j = 1,\ldots,2d$), so Hörmander's condition [44] (which guarantees smooth solutions $\tilde{W}$, provided the initial condition $\tilde{W}(\cdot,\cdot,0)$ is smooth) is satisfied because of (19).

Theorem 5. *The unique solution $\tilde{W}$ of (33) is obtained from the unique solution W of (20) by means of*

$$\tilde{W}(p,q,t) = (\mathcal{S}\,W(\cdot,\cdot,\cdot,t))(p,q)\ ,\ \textit{for all } t \geq 0 \textit{ and for all } (p,q) \in \mathbb{R}^2,$$

with in particular $\tilde{W}(p,q,0) = \mathcal{G}_\psi f(p,q) = (\mathcal{S}\mathcal{W}_\psi)(p,q) = (\mathcal{S}W(\cdot,\cdot,\cdot,0))(p,q)$.

Proof This follows by the fact that the evolutions (20) leave the function space $\mathcal{H}_n$ invariant and the fact that the evolutions (33) leave the space $\mathbb{L}_2(\mathbb{R}^2)$ invariant, so that we can apply direct conjugation with the invertible operator $\mathcal{S}$ to relate the unique solutions, where we have

$$\begin{array}{ll} \tilde{W}(p,q,t) & = (e^{t\tilde{Q}(|\mathcal{G}_\psi f|, \tilde{\mathcal{A}}_1, \tilde{\mathcal{A}}_2)}\mathcal{G}_\psi f)(p,q) \\ & = (e^{t\tilde{Q}(|\mathcal{G}_\psi f|, \mathcal{S}\mathcal{A}_1\mathcal{S}^{-1}, \mathcal{S}\mathcal{A}_2\mathcal{S}^{-1})}\mathcal{S}\mathcal{W}_\psi f)(p,q) \\ & = (e^{\mathcal{S}\circ t\,Q(|\mathcal{W}_\psi f|, \mathcal{A}_1, \mathcal{A}_2)\circ \mathcal{S}^{-1}}\mathcal{S}\mathcal{W}_\psi f)(p,q) \\ & = (\mathcal{S}\ \circ\ e^{t\,Q(|\mathcal{W}_\psi f|, \mathcal{A}_1, \mathcal{A}_2)}\ \circ\ \mathcal{S}^{-1}\mathcal{S}\circ \mathcal{W}_\psi f)(p,q) \\ & = (\mathcal{S}\,W(\cdot,\cdot,\cdot,t))(p,q) \end{array} \tag{35}$$

for all $t > 0$ on densely defined domains. For every $\psi \in \mathbb{L}_2(\mathbb{R}) \cap S(\mathbb{R})$, the space of Gabor transforms is a reproducing kernel space with a bounded and smooth reproducing kernel, so that $\mathcal{W}_\psi f$ (and thereby $|\mathcal{W}_\psi f| = |\mathcal{G}_\psi f|$) is uniformly bounded and continuous and equality (35) holds for all $(p,q) \in \mathbb{R}^2$. □

5.1. The Cauchy-Riemann Equations on Gabor Transforms and the Underlying Differential Geometry

As previously observed in [19], the Gabor transforms associated to Gaussian windows obey Cauchy-Riemann equations which are particularly useful for the analysis of convection schemes, as well as for the design of more efficient algorithms. More precisely, if the window is a Gaussian

$$\psi(\xi) = \psi_a(\xi) := e^{-\pi\frac{\xi^2}{a^2}}, \tag{36}$$

and f is some arbitrary signal in $\mathbb{L}_2(\mathbb{R})$ then we have

$$(a^{-1}\mathcal{A}_2 + ia\mathcal{A}_1)\mathcal{W}_\psi(f) = 0 \Leftrightarrow (a^{-1}\mathcal{A}_2 + ia\mathcal{A}_1)\log \mathcal{W}_\psi(f) = 0 \tag{37}$$

where we included a general scaling $a > 0$. On phase space this boils down to

$$(a^{-1}\tilde{\mathcal{A}}_2 + ia\tilde{\mathcal{A}}_1)\mathcal{G}_\psi(f) = 0 \tag{38}$$

since $\mathcal{G}_\psi(f) = \mathcal{S}\mathcal{W}_\psi(f)$ and $\mathcal{A}_i = \mathcal{S}^{-1}\tilde{\mathcal{A}}_i\mathcal{S}$ for $i = 1, 2, 3$.

For the case $a = 1$, equation (38) was noted in [19]. Regarding general scale $a > 0$ we note that

$$\mathcal{G}_{\psi_a} f(p, q) = \sqrt{a}\ (\mathcal{G}_{\mathcal{D}_a\psi}(f))(p, q) = \sqrt{a}\mathcal{G}_\psi \mathcal{D}_{\frac{1}{a}} f(\frac{p}{a}, aq)$$

with $\psi = \psi_{a=1}$ with unitary dilation operator $\mathcal{D}_a : \mathbb{L}_2(\mathbb{R}) \to \mathbb{L}_2(\mathbb{R})$ given by

$$\mathcal{D}_a(\psi)(x) = a^{-\frac{1}{2}} f(x/a), \qquad a > 0. \tag{39}$$

As a direct consequence of Eq. (38), respectively (37), we have

$$\begin{array}{lll} |\tilde{U}^a|\partial_q\tilde{\Omega}^a = -a^2\partial_p|\tilde{U}^a| & \text{and} & |\tilde{U}^a|\partial_p\tilde{\Omega}^a = a^{-2}\partial_q|\tilde{U}^a| \ + \ 2\pi q, \\ \mathcal{A}_2\Omega^a = -a^2\frac{\mathcal{A}_1|U^a|}{|U^a|} & \text{and} & \mathcal{A}_1\Omega^a = a^{-2}\frac{\mathcal{A}_2|U^a|}{|U^a|}\ , \end{array} \tag{40}$$

where $\tilde{U}^a = \mathcal{G}_{\psi_a}(f)$, $U^a = \mathcal{W}_{\psi_a}(f)$, $\tilde{\Omega}^a = \arg\{\mathcal{G}_{\psi_a}(f)\}$ and $\Omega^a = \arg\{\mathcal{W}_{\psi_a}(f)\}$.

5.2. Differential Geometrical Understanding of the Cauchy-Riemann Relations of Gabor Transforms

The proper differential-geometric context for the analysis of the evolution equations (and in particular the involved Cauchy-Riemann equations) that we study in this paper is provided by sub-Riemannian geometry. As already mentioned in Subsection 3.4 we omit $\mathcal{A}_3$ from the tangent bundle $T(H_r)$ and consider the sub-Riemannian manifold $(H_r, \mathrm{Ker}(\mathrm{d}\mathcal{A}^3), \mathfrak{G}_\beta)$, recall (26), as the domain of the evolved Gabor transforms. As in our previous work on parabolic evolutions on orientation scores (defined on the sub-Riemannian manifold $(SE(2), \mathrm{Ker}(-\sin\theta \mathrm{d}x + \cos\theta \mathrm{d}y), \mathfrak{G}_\beta^{SE(2)})$) cf.[26], we use a left-invariant first fundamental form (i.e. metric tensor) on this sub-Riemannian manifold in order to analyze our parabolic evolutions from a geometric viewpoint.

Lemma 6. *The only left-invariant metric tensors $\mathfrak{G} : H_r \times T(H_r) \times T(H_r) \to \mathbb{C}$ on the sub-Riemannian manifold $(H_r, Ker(\mathrm{d}\mathcal{A}^3), \mathfrak{G})$ are given by*

$$\mathfrak{G}_g = \sum_{(i,j)\in\{1,2\}^2} g_{ij}\ \mathrm{d}\mathcal{A}^i\big|_g \otimes \mathrm{d}\mathcal{A}^j\big|_g\,.$$

Proof Let $\mathfrak{G} : H_r \times T(H_r) \times T(H_r) \to \mathbb{C}$ be a left-invariant metric tensor on the sub-Riemannian manifold $(H_r, \mathrm{Ker}(\mathrm{d}\mathcal{A}^3), \mathfrak{G})$. Then since the horizontal part of the tangent space of $(H_r, \mathrm{Ker}(\mathrm{d}\mathcal{A}^3), \mathfrak{G})$ at $g \in H_r$ is spanned by $\mathrm{Ker}(\mathrm{d}\mathcal{A}^3\big|_g) = \mathrm{span}\{\mathcal{A}_1|_g\,, \mathcal{A}_2|_g\}$ we have

$$\mathfrak{G}_g = \sum_{(i,j)\in\{1,2\}^2} g_{ij}(g)\ \mathrm{d}\mathcal{A}^i\big|_g \otimes \mathrm{d}\mathcal{A}^j\big|_g$$

for some $g_{ij}(g) \in \mathbb{C}$. Now $\mathfrak{G}$ is left-invariant, meaning $\mathfrak{G}_{gh}((L_g)_* X_h, (L_g)_* Y_h) = \mathfrak{G}_h(X_h, Y_h)$ for all vector fields X, Y on H_r, and since our basis of left-invariant vector fields satisfies $(L_g)_*\,\mathcal{A}_i|_h = \mathcal{A}_i|_{gh}$ and $\langle \mathrm{d}\mathcal{A}^i, \mathcal{A}_j\rangle = \delta^i_j$ we deduce $g_{ij}(gh) = g_{ij}(h) = g_{ij}(e)$ for all $g, h \in H_r$. □

Just as for the related quadratic forms in the generator of our parabolic evolutions, we restrict ourselves to the case where the metric tensor is diagonal

$$\mathfrak{G}_\beta = \sum_{(i,j)\in\{1,2\}^2} g_{ij}\mathrm{d}\mathcal{A}^i \otimes \mathrm{d}\mathcal{A}^j = \beta^4\mathrm{d}\mathcal{A}^1 \otimes \mathrm{d}\mathcal{A}^1 + \mathrm{d}\mathcal{A}^2 \otimes \mathrm{d}\mathcal{A}^2. \tag{41}$$

Here the fundamental positive parameter β^{-1} has physical dimension length, so that this first fundamental form is consistent with respect to physical dimensions (observe from Eq. (26) that $\mathrm{d}\mathcal{A}^1$ has physical dimension length, where as $\mathrm{d}\mathcal{A}^2$ has physical dimension one over length). Intuitively, the parameter β sets a global balance between changes in frequency space and changes in position space within the induced sub-Riemannian metric

$$d(g,h) = \inf_{\substack{\gamma \in C([0,1],H_3),\\ \gamma(0)=g,\gamma(1)=h,\\ \langle \mathrm{d}\mathcal{A}^3|_\gamma, \dot{\gamma}\rangle = 0}} \int_0^1 \sqrt{\mathfrak{G}_\beta|_{\gamma(t)}(\dot{\gamma}(t),\dot{\gamma}(t))}\,\mathrm{d}t.$$

Note that the metric tensor $\mathfrak{G}_\beta$ is bijectively related to the linear operator $G : \mathfrak{H} \to \mathfrak{H}'$, where

$$\mathfrak{H} = \mathrm{Ker}(\mathrm{d}\mathcal{A}^3) = \mathrm{span}\{\mathcal{A}_1, \mathcal{A}_2\}$$

denotes the horizontal part of the tangent space, that maps $\mathcal{A}_1$ to $\beta^4\mathrm{d}\mathcal{A}^1$ and $\mathcal{A}_2$ to $\mathrm{d}\mathcal{A}^2$. The inverse operator of G is bijectively related to

$$\mathfrak{G}_\beta^{-1} = \sum_{(i,j)\in\{1,2\}^2} g^{ij}\mathcal{A}_i \otimes \mathcal{A}_j = \beta^{-4}\mathcal{A}_1 \otimes \mathcal{A}_1 + \mathcal{A}_2 \otimes \mathcal{A}_2\ .$$

The fundamental parameter β is inevitable when dealing with flows in the Gabor domain, since position p and frequency q have different physical dimension. Later, in Section 11, we will need this metric in the design of adaptive diffusion on Gabor transforms. In this section we primarily use it for geometric understanding of the Cauchy-Riemann relations on Gabor transforms, which we will employ in our convection schemes in the subsequent section.

In potential theory and fluid dynamics the Cauchy-Riemann equations for complex-valued analytic functions, impose orthogonality between flowlines and equipotential lines. A similar geometrical interpretation can be deduced from the Cauchy-Riemann relations (40) on Gabor transforms :

Lemma 7. *Let $U := \mathcal{W}_{\psi_a} f = |U|e^{i\Omega}$ be the Gabor transform of a signal $f \in \mathbb{L}_2(\mathbb{R})$. Then*

$$\mathfrak{G}^{-1}_{\beta=\frac{1}{a}}(\mathrm{d}\log|U|, \mathbb{P}_{\mathfrak{H}^*}\mathrm{d}\Omega) = \mathfrak{G}^{-1}_{\beta=\frac{1}{a}}(\mathrm{d}|U|, \mathbb{P}_{\mathfrak{H}^*}\mathrm{d}\Omega) = 0, \tag{42}$$

where the left-invariant gradient of modulus and phase equal

$$\mathrm{d}\Omega = \sum_{i=1}^{3}\mathcal{A}_i\Omega\ \mathrm{d}\mathcal{A}^i, \quad \mathrm{d}|U| = \sum_{i=1}^{2}\mathcal{A}_i|U|\ \mathrm{d}\mathcal{A}^i,$$

whose horizontal part equals $\mathbb{P}_{\mathfrak{H}^*}\mathrm{d}\Omega = \sum_{i=1}^{2}\mathcal{A}_i\Omega\ \mathrm{d}\mathcal{A}^i$, $\mathbb{P}_{\mathfrak{H}^*}\mathrm{d}|U| \equiv \mathrm{d}|U|$.

Proof By the second line in (40) we have

$$a^{-2}\mathfrak{G}^{-1}_{\beta=a^{-1}}(\mathrm{d}\log|U|, \mathbb{P}_{\mathfrak{H}^*}\mathrm{d}\Omega) = a^2\frac{\mathcal{A}_1|U|\mathcal{A}_1\Omega}{|U|} + a^{-2}\frac{\mathcal{A}_2|U|\mathcal{A}_2\Omega}{|U|} = 0,$$

from which the result follows. □

Corollary 8. *Let $g_0 \in H_r$. Let $\mathcal{W}_{\psi_a} f = |U|e^{i\Omega}$. Then the horizontal part $\mathbb{P}_{\mathfrak{H}^*}\ \mathrm{d}\Omega|_{g_0}$ of the normal covector $\mathrm{d}\Omega|_{g_0}$ to the equi-phase surface $\{(p,q,s) \in H_r \mid \Omega(p,q,s) = \Omega(g_0)\}$ is $\mathfrak{G}_\beta$-orthogonal to the normal covector $\mathrm{d}|U||_{g_0}$ to the equi-amplitude surface $\{(p,q,s) \in H_r \mid |U|(p,q,s) = |U|(g_0)\}$.*

For a visualization of the Cauchy-Riemannian geometry see Fig.2, where we also include the exponential curves along which our diffusion and convection (Eq.(20)) take place.

Remark 9. *As in our framework of left-invariant evolutions on orientation scores [26], one expresses the left-invariant evolutions on Gabor transforms (Eq.(20)) in covariant derivatives, so that transport and diffusion takes place along the covariantly constant curves (auto-parallels) w.r.t. Cartan Connection on the*

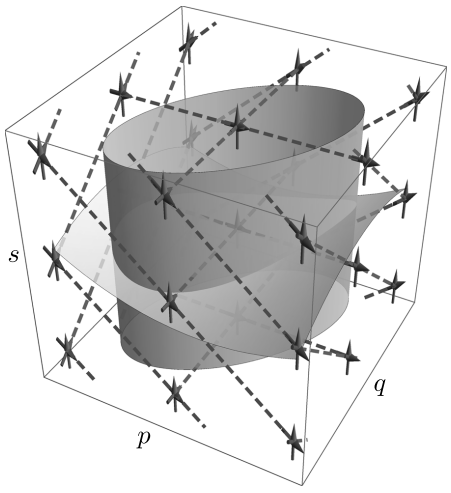

Figure 2: Equi-amplitude plane (cylindrical surface) and equi-phase plane (hyperbolic surface) in the Gabor transform of a chirp signal, that we shall compute exactly in Section 10. The left-invariant horizontal gradients of these surfaces are locally $\mathfrak{G}_\beta$-orthogonal to each other, cf. Eq. (42), with $\mathfrak{G}_\beta = \beta^4 \mathrm{d}\mathcal{A}^1 \otimes \mathrm{d}\mathcal{A}^1 + \mathrm{d}\mathcal{A}^2 \otimes \mathrm{d}\mathcal{A}^2$ with $\beta = a^{-1}$. The left-invariant vector fields $\{\mathcal{A}_1, \mathcal{A}_2, \mathcal{A}_3\} = \{\partial_p + \frac{q}{2}\partial s, \partial_q - \frac{p}{2}\partial s, \partial_s\}$ form a local frame of reference which is indicated by the arrows. Some exponential curves (the auto-parallel curves w.r.t. Cartan connection) are indicated by dashed lines.

sub-Riemannian manifold $(H_r, Ker(\mathrm{d}\mathcal{A}^3), \mathfrak{G}_\beta)$. *A brief computation (for analogous details see [26]) shows that the auto-parallels* $t \mapsto \gamma(t)$ *w.r.t. the Cartan connection* ∇ *coincide with the horizontal exponential curves. Auto-parallels are by definition curves that satisfy*

$$\nabla_{\dot\gamma}\dot\gamma = 0 \Leftrightarrow \ddot\gamma^i - \sum_{k,j} c^i_{kj}\dot\gamma^k\dot\gamma^j = \ddot\gamma^i = 0, \tag{43}$$

where in case of the Cartan-connection the Christoffel-symbols coincide with minus the anti-symmetric Lie algebra structure constants and with $\dot\gamma^i = \langle \mathrm{d}\mathcal{A}^i\big|_\gamma, \dot\gamma\rangle$. *So indeed Eq. (43) holds iff* $\dot\gamma^i = c^i \in \mathbb{R}$, $i = 1, 2$, *i.e.* $\gamma(t) = \gamma(0)\,\exp(t\sum_{i=1}^{2} c^i A_i)$ *for all* $t \in \mathbb{R}$.

6. Convection operators on Gabor Transforms that are both phase-covariant and phase-invariant

In differential reassignment, cf. [14, 18, 19] the practical goal is to sharpen Gabor distributions towards lines (minimal energy curves [29, App.D]) in H_r, while maintaining the signal as much as possible.

We would like to achieve this by left-invariant convection on Gabor transforms $U := \mathcal{W}_\psi(f)$. This means one should set $D = 0$ in Eq. (20) and (33) while considering the mapping $U \mapsto W(\cdot, t)$ for a suitably chosen fixed time $t > 0$. Let us denote this mapping by $\Phi_t : \mathcal{H}_n \to \mathcal{H}_n$ given by $\Phi_t(U) = W(\cdot, t)$. Such a mapping is called *phase invariant* if

$$\arg\left((\Phi_t(U))(p,q,s)\right) = \arg\left(U(p,q,s)\right),$$

for all $(p, q, s) \in H_r$ and all $U \in \mathcal{H}_n$, allowing us to write $\Phi_t(|U|e^{i\Omega}) = e^{i\Omega} \cdot \Phi_t^{\mathrm{net}}(|U|)$ where Φ_t^{net} is the effective operator on the modulus. Such a mapping is called *phase covariant* if the phase moves along with the flow (characteristic curves of transport), i.e. if Eq. (24) is satisfied. Somewhat contrary to intuition, the two properties are not exclusive.

Our convection operators Φ_t (obtained by setting $D = 0$ in Eq. (20) and Eq. (21)) are both phase covariant and phase invariant iff their generator is. In order to achieve both phase invariance and phase covariance one should construct the generator such that the flow is along equi-phase planes of the initial Gabor transform $\mathcal{W}_\psi f$. As we restricted ourselves to horizontal convection there is only one direction in the horizontal part of the tangent space we can use.

Lemma 10. *Let Ω_{g_0} be an open set in H_r and let $U : \Omega_{g_0} \to \mathbb{C}$ be differentiable. The only horizontal direction in the tangent bundle above Ω_{g_0} that preserves the phase of U is given by*

$$span\{-\mathcal{A}_2\Omega\mathcal{A}_1 + \mathcal{A}_1\Omega\mathcal{A}_2\},$$

with $\Omega = \arg\{U\}$.

Proof The horizontal part of the tangent space is spanned by $\{\mathcal{A}_1, \mathcal{A}_2\}$, the horizontal part of the phase gradient is given by $\mathbb{P}_{\mathfrak{H}^*}\mathrm{d}\Omega = \mathcal{A}_1\Omega\mathrm{d}\mathcal{A}^1 + \mathcal{A}_2\Omega\mathrm{d}\mathcal{A}^2$. Solving for

$$\langle \mathbb{P}_{\mathfrak{H}^*}\mathrm{d}\Omega, \alpha^1\mathcal{A}_1 + \alpha^2\mathcal{A}_2\rangle = 0$$

yields $(\alpha^1, \alpha^2) = \lambda(-\mathcal{A}_2\Omega, \mathcal{A}_1\Omega)$, $\lambda \in \mathbb{C}$. □

As a result it is natural to consider the following class of convection operators.

Lemma 11. *The horizontal, left-invariant, convection generators $\mathcal{C} : \mathcal{H}_n \to \mathcal{H}_n$ given by*

$$\mathcal{C}(U) = \mathcal{M}(|U|)(-\mathcal{A}_2\Omega\mathcal{A}_1U + \mathcal{A}_1\Omega\mathcal{A}_2U), \qquad \text{where } \Omega = \arg\{U\},$$

and where $\mathcal{M}(|U|)$ a multiplication operator naturally associated to a bounded monotonically increasing differentiable function $\mu : [0, \max(|U|)] \to [0, \mu(\max(|U|))] \subset \mathbb{R}$ with $\mu(0) = 0$, i.e. $(\mathcal{M}(|U|)V)(p, q) = \mu(|U|(p, q))\, V(p, q)$ for all $V \in \mathcal{H}_n, (p, q) \in \mathbb{R}^2$, are well-defined and both phase covariant and phase invariant.

Proof Phase covariance and phase invariance follows by Lemma 10. The operators are well-posed as the absolute value of Gabor transform is almost everywhere smooth (if ψ is a Schwarz function) bounded and moreover $\mathcal{C}$ can be considered as an unbounded operator from $\mathcal{H}_n$ into $\mathcal{H}_n$, as the bi-invariant space $\mathcal{H}_n$ is invariant under bounded multiplication operators that do not depend on the phase $z = e^{2\pi is}$. □

For Gaussian kernels $\psi_a(\xi) = e^{-a^{-2}\xi^2\pi}$ we may apply the Cauchy-Riemann relations (38) which simplify for the special case $\mathcal{M}(|U|) = |U|$ to

$$\mathcal{C}(e^{i\Omega}|U|) = (a^2(\partial_p|U|)^2 + a^{-2}(\partial_q|U|)^2)\, e^{i\Omega}. \tag{44}$$

Now consider the following phase-invariant adaptive convection equation on H_r,

$$\boxed{\begin{cases} \partial_t W(g,t) = -\mathcal{C}(W(\cdot,t))(g), \\ W(g,0) = U(g) \end{cases}} \tag{45}$$

with either

$$\boxed{\begin{array}{l} 1.\ \ \mathcal{C}(W(\cdot,t)) = \mathcal{M}(|U|)\,(-\mathcal{A}_2\Omega, \mathcal{A}_1\Omega)\cdot(\mathcal{A}_1W(\cdot,t), \mathcal{A}_2W(\cdot,t)) \text{ or} \\ 2.\ \ \mathcal{C}(W(\cdot,t)) = e^{i\Omega}\left(a^2\frac{(\partial_p|W(\cdot,t)|)^2}{|W(\cdot,t)|} + a^{-2}\frac{(\partial_q|W(\cdot,t)|)^2}{|W(\cdot,t)|}\right). \end{array}} \tag{46}$$

In the first choice we stress that $\arg(W(\cdot,t)) = \arg(W(\cdot,0)) = \Omega$, since transport only takes place along iso-phase surfaces. Initially, in case $\mathcal{M}(|U|) = 1$ the two approaches are the same since at $t = 0$ the Cauchy-Riemann relations (40) hold, but as time increases the Cauchy-Riemann equations are violated (this directly follows by the preservation of phase and non-preservation of amplitude). Consequently, generalizing the single step convection schemes in [19, 14] to a continuous time axis produces two options:

1. With respect to the first choice in (46) in (45) (which is much more cumbersome to implement) we follow the authors in [19] and consider the equivalent equation on phase space:

$$\begin{cases} \partial_t\tilde{W}(p,q,t) = -\tilde{\mathcal{C}}(\tilde{W}(\cdot,t))(p,q), \\ \tilde{W}(p,q,0) = \mathcal{G}_\psi f(p,q) =: \tilde{U}(p,q) = e^{i\tilde{\Omega}(p,q)}|\tilde{U}(p,q)| = e^{i\tilde{\Omega}(p,q)}|U|(p,q) \end{cases} \tag{47}$$

with generator

$$\tilde{C}(\tilde{W}(\cdot,t)) = \mathcal{M}(|U|)\left(-\tilde{\mathcal{A}}_2\tilde{\Omega}\tilde{\mathcal{A}}_1\tilde{W}(\cdot,t) + (\partial_q\tilde{\Omega} - 2\pi q)\tilde{\mathcal{A}}_2\tilde{W}(\cdot,t)\right),$$

where we recall $\mathcal{G}_\psi = \mathcal{S}\mathcal{W}_\psi$ and $\mathcal{A}_i = \mathcal{S}^{-1}\tilde{\mathcal{A}}_i\mathcal{S}$ for $i = 1, 2, 3$. Note that the authors in [19] consider the case $\mathcal{M} = 1$. In addition to [19] we provide in Section 9 an explicit computational finite difference scheme acting on discrete subgroups of H_r, which is non-trivial due to the phase oscillations in the Gabor domain.

2. The second choice in Eq. (46) within Eq. (45) is just a phase-invariant inverse Hamilton Jacobi equation on H_r, with a Gabor transform as initial solution. Rather than computing the viscosity solution cf. [32] of this non-linear PDE, we may as well store the phase and apply an inverse Hamilton Jacobi system on $\mathbb{R}^2$ with the amplitude $|U|$ as initial condition and multiply with the stored phase factor afterwards. More precisely, the viscosity solution of the Hamilton Jacobi system on the modulus is given by a basic inverse convolution over the $(\max, +)$ algebra, [13], (also known as erosion operator in image analysis)

$$\tilde{W}(p, q, t) = (\tilde{\Phi}_t(U))(p, q, t) = (K_t \ominus |U|)(p, q)e^{i\Omega(p,q,t)} \ , \tag{48}$$

with kernel

$$K_t(p, q) = \frac{a^{-2}p^2 + a^2q^2}{4t} \tag{49}$$

where

$$(f \ominus g)(p, q) = \inf_{(p',q')\in\mathbb{R}^2} [g(p', q') + f(p - p', q - q')] \, .$$

Here the homomorphism between erosion and inverse diffusion is given by the Cramer transform $C = \mathfrak{f} \circ \log \circ \mathcal{L}$, [13], [1], that is a concatenation of the multi-variate Laplace transform, logarithm and Fenchel transform on $\mathbb{R}^2$. The Fenchel transform $\mathfrak{f}$ maps a convex function $c : \mathbb{R}^d \to \mathbb{R}$ onto the function

$$\mathbf{x} \mapsto [\mathfrak{f}c](\mathbf{x}) = \sup\{\langle \mathbf{x}, \mathbf{y}\rangle - c(\mathbf{y}) \mid \mathbf{y} \in \mathbb{R}^d\}. \tag{50}$$

where $\mathbf{x}$ is a linear functional (co-vector) on $\mathbb{R}^d$ that is (in the case of $\mathbb{R}^d$) commonly naturally identified with elements in $\mathbb{R}^d$. Typically, the Fenchel transform (also known as Legendre-Fenchel transform) maps[6] a Lagrangian onto the corresponding Hamiltonian (and vice versa) on $\mathbb{R}^d$ [32, Ch:3.2.2]. The isomorphic property of the Cramer transform follows by

$$\mathcal{C}(f * g) = \mathfrak{f} \log \mathcal{L}(f * g) = \mathfrak{f}(\log \mathcal{L}f + \log \mathcal{L}g) = \mathcal{C}f \oplus \mathcal{C}g,$$

with convolution on the $(\max, +)$-algebra given by $f \oplus g(\mathbf{x}) = \sup_{\mathbf{y}\in\mathbb{R}^d} [f(\mathbf{x} - \mathbf{y}) + g(\mathbf{y})]$.

7. Discrete Gabor Transforms

In order to derive various suitable algorithms for differential reassignment and diffusion we consider discrete Gabor transforms. We show that Gabor transforms are defined on a (finite) group quotient in the discrete Heisenberg group. In the subsequent section we shall construct left-invariant shift operators for the generators in our left-invariant evolutions on this quotient group.

Throughout Sections 7 and 8 the Schrödinger representation index n will be set to 1 and we will use the symbol n to index discrete time.

Let the discrete signal be given by $\mathbf{f} = \{\mathbf{f}[n]\}_{n=0}^{N-1} := \{f\left(\frac{n}{N}\right)\}_{n=0}^{N-1} \in \mathbb{R}^{2N-1}$. Let the discrete kernel be given by a sampled Gaussian kernel

$$\boldsymbol{\psi} = \{\boldsymbol{\psi}[n]\}_{n=0}^{N-1} := \{e^{-\frac{(n-\frac{N-1}{2})^2\pi}{N^2a^2}}\}_{n=0}^{N-1} \in \mathbb{R}^N, \tag{51}$$

with $\frac{\pi}{a^2} = \frac{1}{2\sigma^2}$ where σ^2 is the variance of the Gaussian and note that in the following $\boldsymbol{\psi}$ will be regarded as periodic.

The discrete Gabor transform of $\mathbf{f}$ is then given by

$$(\mathcal{W}^D_{\boldsymbol{\psi}}\mathbf{f})[l, m, k] \quad := e^{-2\pi i(\frac{k}{Q} - \frac{mlL}{2M})} \frac{1}{N} \sum_{n=0}^{N-1} \overline{\boldsymbol{\psi}[n - lL \ \mathrm{Mod} \ N]}\mathbf{f}[n] \, e^{-\frac{2\pi inm}{M}} \tag{52}$$

[6] This also holds on other (sub-)Riemannian manifolds on (/within) Lie groups [54, 28].

with $L, K, N, M, Q \in \mathbb{N}$ and

$$k = 0, 1, \ldots, Q-1 \text{ and } l = 0, \ldots, K-1,\ m = 0, \ldots, M-1, \text{ with } L = \frac{N}{K}, \tag{53}$$

and integer oversampling $P = M/L \in \mathbb{Z}$. Note that we follow the notational conventions of the review paper [8]. One has

$$\frac{1}{M} = \frac{K}{P}\frac{1}{N} \text{ and } N = KL. \tag{54}$$

It is important that the discrete kernel is N periodic since $N = KL$ implies

$$\forall_{\mathbf{f}\in\ell_2(I)}\forall_{l,m,k}\mathcal{W}^D_{\boldsymbol{\psi}}\mathbf{f}[l+K,m,k] = \mathcal{W}^D_{\boldsymbol{\psi}}\mathbf{f}[l,m,k] \Leftrightarrow \forall_{n=0,\ldots N-1}\boldsymbol{\psi}[n-N] = \boldsymbol{\psi}[n],$$

where $I = \{0, \ldots, N-1\}$.

Let the continuous signal $f : \mathbb{R} \to \mathbb{R}$ be Riemann-integrable with support within $[1/4, 3/4]$ and let us for the moment assume that the continuous window $\psi : \mathbb{R} \to \mathbb{R}$ is smooth with support within $[-1/4, 1/4]$ (at this point excluding Gaussian windows). Let $\mathbf{f}$ and $\boldsymbol{\psi}$ denote the corresponding discrete signal and window. Then we obtain the pointwise limit (in the reproducing kernel space of Gabor transforms)

$$(W^D_{\boldsymbol{\psi}}\mathbf{f})[l,m,k] \to \mathcal{W}_\psi f(p = \frac{l}{K}, q = \frac{mK}{P}, s = \frac{k}{Q}) \text{ as } N \to \infty, \tag{55}$$

as we will show next. Recall that the continuous Gabor transform was given by

$$\mathcal{W}_\psi f(p,q,s) = e^{-2\pi i(s-\frac{pq}{2})}\int_{\mathbb{R}} \overline{\psi(\xi-p)}f(\xi)e^{-2\pi i\xi q}\,\mathrm{d}\xi,$$

Due to the support restrictions the Mod operator in Eq. (52) can be dispensed with, since

$$\left(\psi\left(\frac{n - l\,L + k\,N}{N}\right)\,f\left(\frac{n}{N}\right) \neq 0\ \wedge\ k \in \mathbb{Z}\ \wedge\ \mathrm{supp}(f) \subset \left[\frac{1}{4}, \frac{3}{4}\right]\ \wedge\ \mathrm{supp}(\psi) \subset \left[-\frac{1}{4}, \frac{1}{4}\right]\right) \Rightarrow k = 0.$$

Consequently, the discrete Gabor transform indeed provides the Riemann-sum approximation of the continuous Gabor transform as $N \to \infty$:

$$\begin{aligned}(W^D_{\boldsymbol{\psi}}\mathbf{f})[l,m,k] &= e^{-2\pi i(\frac{k}{Q}-\frac{mlL}{2M})}\frac{1}{N}\sum_{n=0}^{N-1}\overline{\boldsymbol{\psi}[n-lL]}\mathbf{f}[n]\,e^{-\frac{2\pi inm}{M}}\\ &= e^{-2\pi i(\frac{k}{Q}-\frac{mlL}{2M})}\frac{1}{N}\sum_{n=0}^{N-1}\overline{\psi(n/N-l/K)}f(n/N)\,e^{-2\pi i\frac{mN}{M}\frac{n}{N}}\\ &\to \mathcal{W}_\psi f(p=\tfrac{l}{K}, q=\tfrac{mK}{P}, s=\tfrac{k}{Q}) \text{ as } N\to\infty.\end{aligned}$$

where we used $N = KL$ and Eq. (54). Now let us return to Schwartz functions ψ (such as Gaussians, Eq. (51)).

Remark 12. *In case of rapidly decaying windows a truncated version $\psi_0 = \psi 1_{[-1/4,1/4]}$ can be controlled by*

$$\begin{aligned}&\|\mathcal{W}_\psi f - \mathcal{W}_{\psi_0} f\|_{\mathbb{L}_2(H_r)} = \|\mathcal{W}_{\psi-\psi_0} f\|_{\mathbb{L}_2(H_r)} = \|\psi-\psi_0\|_{\mathbb{L}_2(\mathbb{R}^d)}\|f\|_{\mathbb{L}_2(\mathbb{R}^d)},\\ &\|\mathcal{W}_\psi f - \mathcal{W}_{\psi_0} f\|_{\mathbb{L}_\infty(H_r)} \le \|\psi-\psi_0\|_{\mathbb{L}_2(\mathbb{R}^d)}\|f\|_{\mathbb{L}_2(\mathbb{R}^d)}\end{aligned}$$

the first identity follows by the orthogonality relation for Gabor transforms, whereas the second inequality is due to Cauchy-Schwarz. For these reasons we will continue using Gaussians in the discrete setting as well.

7.1. Diagonalization of the Gabor transform

In our algorithms, we follow [46] and [8] and use the diagonalization of the discrete Gabor transform by means of the discrete Zak-transform. The finite frame operator $\mathfrak{F} : \ell_2(I) \to \ell_2(I)$ equals

$$[\mathfrak{F}\mathbf{f}][n] = \sum_{l=0}^{K-1}\sum_{m=0}^{M-1}(\boldsymbol{\psi}_{lm}, \mathbf{f})\boldsymbol{\psi}_{lm}[n], \qquad n \in I = \{0, \ldots, N-1\},$$

with $\boldsymbol{\psi}_{lm} = \mathcal{U}_{[l,m,k=-\frac{Qlm}{2P}]}\boldsymbol{\psi}$. The operator $\mathfrak{F} = \mathfrak{F}^*$ is coercive and has the following orthonormal eigenvectors:

$$\mathbf{u}_{nk}[n'] = \frac{1}{\sqrt{K}} v[n'-n]\, e^{\frac{2\pi i k}{N}(n'-n)}, \text{ with } v(n) = \sum_{l=-\infty}^{\infty} \delta[n-lL]$$

for $n \in \{0,\dots,L-1\}, k \in \{0,\dots,K-1\}$, where $N = KL$, and it is diagonalized by:

$$\mathfrak{F} = (Z^D)^{-1} \circ \Lambda \circ Z^D \ ,$$

with Discrete Zak transform given by $[Z^D\mathbf{f}][n,k] = (\mathbf{u}_{nk}, \mathbf{f})_{\ell_2(I)}$, i.e. $\mathfrak{F}\mathbf{f} = \sum_{n=0}^{L-1}\sum_{k=0}^{K-1} \lambda_{nk}(\mathbf{u}_{nk}, \mathbf{f})\mathbf{u}_{nk}$, with eigenvalues $\lambda_{nk} = L\sum_{p=0}^{P-1} |Z\boldsymbol{\psi}^D[n, k - p\frac{N}{M}]|^2$ and integer oversampling factor $P = M/L$.

8. Discrete Left-invariant vector fields

Let the discrete signal be given by $\mathbf{f} = \{\mathbf{f}[n]\}_{n=0}^{N-1} := \{f\left(\frac{n}{N}\right)\}_{n=0}^{N-1} \in \mathbb{R}^N$. Then similar to the continuous case the discrete Gabor transform of $\mathbf{f}$ can be written

$$[\mathcal{W}_{\boldsymbol{\psi}}^D\mathbf{f}][l,m,k] = (\mathcal{U}_{[l,m,k]}\boldsymbol{\psi}, \mathbf{f})_{\ell_2(I)}, \tag{56}$$

where $I = \{0,\dots,N-1\}$ and $(\mathbf{a},\mathbf{b}) = \frac{1}{N}\sum_{i=0}^{N-1} \overline{a}_i b_i$ and where

$$\mathcal{U}_{[l,m,k]}\boldsymbol{\psi}[n] = e^{2\pi i(\frac{k}{Q} - \frac{ml}{2P})} e^{\frac{2\pi i n m}{M}} \boldsymbol{\psi}[n - lL], \tag{57}$$

$l = 0,\dots,K-1, m = 0,\dots,M-1, k = 0,\dots,Q-1$. Next we will show that (under minor additional conditions) Eq. (57) gives rise to a group representation of a finite dimensional Heisenberg group $\mathfrak{h}_r$, obtained by taking the quotient of the discrete Heisenberg group h_r with a normal subgroup.

Definition 13. *If $\frac{Q}{2P} \in \mathbb{N}$ then the group h_r is the set $\mathbb{Z}^3/(\{0\}\times\{0\}\times Q\mathbb{Z})$ endowed with group product*

$$[l,m,k][l',m',k'] = [l+l', m+m', k+k' + \frac{Q}{2P}(ml' - m'l)\,\mathrm{Mod}Q]. \tag{58}$$

Lemma 14. *Assume $\frac{Q}{2P} \in \mathbb{N}$ and $\frac{K}{P} \in \mathbb{N}$ and L even, N even. Then the subgroup*

$$[K\mathbb{Z}, M\mathbb{Z}, Q\mathbb{Z}] := \{[lK, mM, kQ] \mid l,m,k \in \mathbb{Z}\}$$

is a normal subgroup of h_r. Thereby, the quotient $\mathfrak{h}_r := h_r/([K\mathbb{Z}, M\mathbb{Z}, Q\mathbb{Z}])$ is a group with product

$$[l,m,k][l',m',k'] = [l+l'\ ModK, m+m'\ ModM, k+k' + \frac{Q}{2P}(ml' - m'l)\ Mod(Q)]. \tag{59}$$

Eq. (57) defines a representation of this group and thereby $\mathfrak{h}_r$ is the domain of discrete Gabor transforms[7] *endowed with the group product given by Eq. (59).*

Proof Direct computation yields

$$\begin{aligned}[l,m,k][l'K, m'M, k'Q] &= [l+l'K, m+m'M, k+k'Q + \tfrac{Q}{2P}(ml'K - m'Ml) + \mathrm{Mod}Q] = \\ [l'K, m'M, k'Q][l,m,k] &= [l+l'K, m+m'M, k+k'Q - \tfrac{Q}{2P}(ml'K - m'Ml) + \mathrm{Mod}Q]\end{aligned}$$

[7] The result in Lemma 14 relates to Gabor analysis over finite Abelian groups, cf. [34] for details.

since $M/P = L \in \mathbb{N}$ and we assumed $K/P \in \mathbb{N}$. Consequently, $H := [K\mathbb{Z}, M\mathbb{Z}, Q\mathbb{Z}]$ is a normal subgroup and thereby (since $g_1 H g_2 H] = g_1 g_2 H$) the quotient $\mathfrak{h}_r := h_r/([K\mathbb{Z}, M\mathbb{Z}, Q\mathbb{Z}])$ is a group with well-defined group product (59). The remainder now follows by direct verification of

$$\mathcal{U}_{[l,m,k]}\mathcal{U}_{[l',m',k']} = \mathcal{U}_{[l,m,k][l',m',k']}$$

and $\mathcal{U}_{[l,m,k]} = \mathcal{U}_{[l+K,m+M,k+Q]}$. □

In view of Eq. (55) we define a monomorphism between h_r and H_r as follows.

Lemma 15. *The mapping $\phi : h_r \to H_r$ defined by*

$$\phi[l,m,k] = \left(\frac{l}{K}, \frac{mK}{P}, \frac{k}{Q}\right)$$

sets a monomorphism between $h_r$and the continuous Heisenberg group H_r.

Proof Straightforward computation yields

$$\begin{aligned}\phi[l,m,k]\phi[l',m',k'] &= \left(\tfrac{l}{K}, \tfrac{mK}{P}, \tfrac{k}{Q}\right)\left(\tfrac{l}{K}, \tfrac{mK}{P}, \tfrac{k}{Q}\right)\\ &= \left(\tfrac{l+l'}{K}, \tfrac{(m+m')K}{P}, \tfrac{k+k'+\frac{Q}{2P}(ml'-lm')}{Q}\right) = \phi[[l,m,k][l',m',k']].\end{aligned}$$

from which the result follows. □

The mapping ϕ maps the discrete variables on a uniform grid in the continuous domain:

$$s \in [0,1) \leftrightarrow k \in [0,Q) \cap \mathbb{Z}, \quad p \in [0,1) \leftrightarrow l \in [0,K) \cap \mathbb{Z}, \quad q \in [0,N) \leftrightarrow m \in [0,M) \cap \mathbb{Z}.$$

On the quotient-group $\mathfrak{h}_r$ we define the forward left-invariant vector fields on discrete Gabor-transforms as follows (where we again use the identities (54)):

$$\begin{aligned}(\mathcal{A}_1^{D^+} W_{\boldsymbol{\psi}}^D \mathbf{f})[l,m,k] &= K\,(\mathrm{d}\mathcal{R}^{D^+}[1,0,0] W_{\boldsymbol{\psi}}^D \mathbf{f})[l,m,k] &&= \tfrac{W_{\boldsymbol{\psi}}^D \mathbf{f}([l,m,k][1,0,0]) - W_{\boldsymbol{\psi}}^D \mathbf{f}[l,m,k]}{K^{-1}}\\ &= \tfrac{e^{-\frac{\pi i m}{P}} W_{\boldsymbol{\psi}}^D \mathbf{f}[l+1,m,k] - W_{\boldsymbol{\psi}}^D \mathbf{f}[l,m,k]}{K^{-1}} &&= K\left(e^{-\frac{\pi i m L}{M}} W_{\boldsymbol{\psi}}^D \mathbf{f}[l+1,m,k] - W_{\boldsymbol{\psi}}^D \mathbf{f}[l,m,k]\right)\\ (\mathcal{A}_2^{D^+} W_{\boldsymbol{\psi}}^D \mathbf{f})[l,m,k] &= \tfrac{M}{N}\,(\mathrm{d}\mathcal{R}^{D^+}[0,1,0] W_{\boldsymbol{\psi}}^D \mathbf{f})[l,m,k] &&= \tfrac{M}{N}\left(e^{+\frac{\pi i l L}{M}} W_{\boldsymbol{\psi}}^D \mathbf{f}[l,m+1,k] - W_{\boldsymbol{\psi}}^D \mathbf{f}[l,m,k]\right),\\ (\mathcal{A}_3^{D^+} W_{\boldsymbol{\psi}}^D \mathbf{f})[l,m,k] &= Q(\mathrm{d}\mathcal{R}^{D^+}[0,0,1] W_{\boldsymbol{\psi}}^D \mathbf{f})[l,m,k] &&= Q\,(e^{\frac{-2\pi i}{Q}} - 1) W_{\boldsymbol{\psi}}^D \mathbf{f}[l,m,k]),\end{aligned} \tag{60}$$

and the backward discrete left-invariant vector fields

$$\begin{aligned}(\mathcal{A}_1^{D^-} W_{\boldsymbol{\psi}}^D \mathbf{f})[l,m,k] &= K\left(W_{\boldsymbol{\psi}}^D \mathbf{f}[l,m,k] - e^{+\frac{\pi i m L}{M}} W_{\boldsymbol{\psi}}^D \mathbf{f}[l-1,m,k]\right),\\ (\mathcal{A}_2^{D^-} W_{\boldsymbol{\psi}}^D \mathbf{f})[l,m,k] &= \tfrac{M}{N}\left(W_{\boldsymbol{\psi}}^D \mathbf{f}[l,m,k] - e^{-\frac{\pi i l L}{M}} W_{\boldsymbol{\psi}}^D \mathbf{f}[l,m-1,k]\right),\\ (\mathcal{A}_3^{D^-} W_{\boldsymbol{\psi}}^D \mathbf{f})[l,m,k] &= Q\,(1 - e^{\frac{2\pi i}{Q}}) W_{\boldsymbol{\psi}}^D \mathbf{f}[l,m,k]\ .\end{aligned} \tag{61}$$

Remark 16. *With respect to the step-sizes in (60) and (61) we have set $p = \frac{l}{K}$, $q = \frac{m}{M}N$, $\xi = \frac{n}{N}$, $s = \frac{k}{Q}$, so that the actual discrete steps are $\Delta p = K^{-1}$, $\Delta q = N\,M^{-1}$ and $\Delta s = Q^{-1}$. This discretization is chosen such that both the continuous Gabor transform and the continuous left-invariant vector fields follow from their discrete counterparts by $N \to \infty$, e.g. recall Eq. (55).*

As in the continuous case, we map Gabor transforms $W_{\boldsymbol{\psi}}^D$ onto phase space representations $G_{\boldsymbol{\psi}}^D$, using the following discrete version S^D of the operator $\mathcal{S}$ from Section 4:

$$G_{\boldsymbol{\psi}}^D \mathbf{f}[l,m] := (S^D W_{\boldsymbol{\psi}}^D)\mathbf{f}[l,m] = W_{\boldsymbol{\psi}}^D \mathbf{f}[l,m,-\frac{Qlm}{2P}],$$

with oversampling factor $P = M/L$. The inverse is given by

$$W_{\boldsymbol{\psi}}^D \mathbf{f}[l,m,k] = ((S^D)^{-1} G_{\boldsymbol{\psi}}^D \mathbf{f})[l,m,k] = e^{-2\pi i\left(\frac{k}{Q} + \frac{lmL}{2M}\right)} G_{\boldsymbol{\psi}}^D \mathbf{f}[l,m].$$

Again we can use the conjugation with S^D to map the left-invariant discrete vector fields $\{\mathcal{A}_i^{D^\pm}\}_{i=1}^3$ to the corresponding discrete vector fields on the discrete phase space: $\tilde{\mathcal{A}}_i^{D^\pm} = (S^D) \circ \mathcal{A}_i^{D^\pm} \circ (S^D)^{-1}$. A brief computation yields the following forward left-invariant differences

$$\begin{aligned}
(\tilde{\mathcal{A}}_1^{D^+} G_{\boldsymbol{\psi}}^D \mathbf{f})[l,m] &= K \left(e^{\frac{-2\pi i L m}{M}} (G_{\boldsymbol{\psi}}^D \mathbf{f})[l+1,m] - G_{\boldsymbol{\psi}}^D \mathbf{f}[l,m] \right), \\
(\tilde{\mathcal{A}}_2^{D^+} G_{\boldsymbol{\psi}}^D \mathbf{f})[l,m] &= M\, N^{-1} \left(G_{\boldsymbol{\psi}}^D \mathbf{f}[l,m+1] - G_{\boldsymbol{\psi}}^D \mathbf{f}[l,m] \right), \\
(\tilde{\mathcal{A}}_3^{D^+} G_{\boldsymbol{\psi}}^D \mathbf{f})[l,m] &= Q(e^{\frac{-2\pi i}{Q}} - 1)\, G_{\boldsymbol{\psi}}^D \mathbf{f}[l,m]
\end{aligned} \tag{62}$$

and the following backward left-invariant differences:

$$\begin{aligned}
(\tilde{\mathcal{A}}_1^{D^-} G_{\boldsymbol{\psi}}^D \mathbf{f})[l,m] &= K \left(G_{\boldsymbol{\psi}}^D \mathbf{f}[l,m] - e^{\frac{2\pi i L m}{M}} G_{\boldsymbol{\psi}}^D \mathbf{f}[l-1,m] \right), \\
(\tilde{\mathcal{A}}_2^{D^-} G_{\boldsymbol{\psi}}^D \mathbf{f})[l,m] &= M\, N^{-1} \left(G_{\boldsymbol{\psi}}^D \mathbf{f}[l,m] - G_{\boldsymbol{\psi}}^D \mathbf{f}[l,m-1] \right), \\
(\tilde{\mathcal{A}}_3^{D^-} G_{\boldsymbol{\psi}}^D \mathbf{f})[l,m] &= Q(1 - e^{\frac{2\pi i}{Q}})\, G_{\boldsymbol{\psi}}^D \mathbf{f}[l,m]\ .
\end{aligned} \tag{63}$$

The discrete operators are defined on the discrete quotient group $\mathfrak{h}_r$ and do not involve approximations in the setting of discrete Gabor transforms. They are first order approximation of the corresponding continuous operators on H_r as we motivate next. For f compactly supported on $[0,1]$ and both f and ψ Riemann-integrable on $\mathbb{R}$:

$$\begin{aligned}
\tilde{\mathcal{A}}_1 \mathcal{G}_\psi f(p = \tfrac{l}{K}, q = \tfrac{mK}{P}) &= (\partial_p - 2\pi q)(e^{2\pi i p q} \int_{\mathbb{R}} \overline{\psi(\xi - p)} f(\xi) e^{-2\pi i \xi q}\, \mathrm{d}\xi)(\tfrac{l}{K}, \tfrac{mK}{P}) \\
&= -e^{\frac{2\pi i l}{P}} \int_{\mathbb{R}} \overline{\psi}'(\xi - \tfrac{l}{K}) f(\xi) e^{-\frac{2\pi i n m K}{NP}}\, \mathrm{d}\xi \\
&= O(\tfrac{1}{N}) - \tfrac{1}{N} e^{\frac{2\pi i l m}{P}} \sum_{n=0}^{N-1} \overline{\psi}' \left(\tfrac{n}{N} - \tfrac{l}{K} \right) f\left(\tfrac{n}{N} \right) e^{-\frac{2\pi i n m}{M}}.
\end{aligned} \tag{64}$$

Moreover, we have

$$[G_{\boldsymbol{\psi}}^D \mathbf{f}](l,m) = \frac{1}{N} e^{\frac{2\pi i m l}{P}} \sum_{n=0}^{N-1} e^{-\frac{2\pi i n m}{M}} \overline{\psi} \left(\frac{n}{N} - \frac{l}{K} \right) f\left(\frac{n}{N} \right)$$

so that straightforward computation yields

$$\begin{aligned}
\tilde{\mathcal{A}}_1^{D^+} G_{\boldsymbol{\psi}}^D \mathbf{f}[l,m] &= \tfrac{1}{N} e^{2\pi i \frac{lm}{P}} \sum_{n=0}^{N-1} \frac{\overline{\psi}\left(\frac{n}{N} - \frac{l+1}{K} \right) - \overline{\psi}\left(\frac{n}{N} - \frac{l}{K} \right)}{K^{-1}} f\left(\tfrac{n}{N} \right) e^{-\frac{2\pi i n m}{N}} \\
&= O\left(\tfrac{1}{K} \right) O\left(\tfrac{1}{N} \right) - \tfrac{1}{N} e^{\frac{2\pi i l m}{P}} \sum_{n=0}^{N-1} \overline{\psi}' \left(\tfrac{n}{N} - \tfrac{l}{K} \right) f\left(\tfrac{n}{N} \right) e^{-\frac{2\pi i n m}{M}}
\end{aligned} \tag{65}$$

So from (64) and (65) we deduce that

$$\tilde{\mathcal{A}}_1^{D^+} G_{\boldsymbol{\psi}}^D \mathbf{f}[l,m] = O\left(\frac{1}{N} \right) + \tilde{\mathcal{A}}_1 \mathcal{G}_\psi f(p = \frac{l}{K}, q = \frac{mK}{P}).$$

So clearly the discrete left-invariant vector fields acting on the discrete Gabor-transforms converge to the continuous vector fields acting on the continuous Gabor transforms pointwise as $N \to \infty$.

In our algorithms it is essential that one works on the finite group with corresponding left-invariant vector fields. This is simply due to the fact that one computes finite Gabor-transforms (defined on the group $\mathfrak{h}_r$) to avoid sampling errors on the grid. Standard finite difference approximations of the continuous left-invariant vector fields do not appropriately deal with phase oscillations in the (discrete) Gabor transform.

Remark 17. *In the PDE-schemes which we will present in the next sections, such as for example the diffusion scheme in Section 11, the solutions will leave the space of Gabor-transforms. In such cases one has to apply a left-invariant finite difference to a smooth function $U \in \mathbb{L}_2(H_r)$ defined on the Heisenberg-group H_r or, equivalently, one has to apply a finite difference to a smooth function $\tilde{U} \in \mathbb{L}_2(\mathbb{R}^2)$ defined on phase*

space. If U is not the Gabor transform of an image it is usually inappropriate to use the final results in (61) and (60) on the group H_r. Instead one should just use

$$\begin{array}{l}(\mathcal{A}_1^{D^+}U)[l,m,k] = K\,(\,U[[l,m,k][1,0,0]] - U[l,m,k]\,)\,,\\ (\mathcal{A}_1^{D^-}U)[l,m,k] = K\,(\,U[l,m,k] - U[[l,m,k][-1,0,0]]\,)\,,\\ (\mathcal{A}_2^{D^+}U)[l,m,k] = \frac{M}{N}\,(\,U[[l,m,k][0,1,0]] - U[l,m,k]\,)\,,\\ (\mathcal{A}_2^{D^-}U)[l,m,k] = \frac{M}{N}\,(\,U[l,m,k] - U[[l,m,k][0,-1,0]]\,)\,,\end{array} \tag{66}$$

which does not require any interpolation between the discrete data iff $\frac{Q}{2P} \in \mathbb{N}$. The left-invariant operators on phase space (62) and (63) are naturally extendable to $\mathbb{L}_2(\mathbb{R}^2)$. For example, $(\mathcal{A}_1^{D^+}U)[l,m] = [\mathcal{S}^D \circ \mathcal{A}_1^{D^+} \circ (\mathcal{S}^D)^{-1}\tilde{U}][l,m] = K(e^{-\frac{2\pi i m}{P}}\tilde{U}[l+1,m] - \tilde{U}[l,m])$ for all $\tilde{U} \in \ell_2(\{0,\dots,K-1\}\times\{0,\dots,M-1\})$.

9. Algorithm for the PDE-approach to Differential Reassignment

Here we provide an explicit algorithm on the discrete Gabor transform $G_{\boldsymbol{\psi}}^D\mathbf{f}$ of the discrete signal $\mathbf{f}$, that consistently corresponds to the theoretical PDE's on the continuous case as proposed in [19], i.e. convection equation (45) where we apply the first choice (46). Although the PDE studied in [19] is not as simple as the second approach in (46) (which corresponds to a standard erosion step on the absolute value $|\mathcal{G}_\psi f|$ followed by a restoration of the phase afterwards) we do provide an explicit numerical scheme of this PDE, where we stay entirely in the *discrete phase space*.

It should be stressed that taking straightforward central differences of the continuous differential operators of section 6 does not work, due to the fast oscillations (of the phase) of Gabor transforms. We need the left-invariant differences on discrete Heisenberg groups discussed in the previous subsection.

Explicit upwind scheme with left-invariant finite differences in pseudo-code for $\mathcal{M} = 1$

For $l = 1,\dots,K-1$, $m = 1,\dots M-1$ set $\tilde{W}[l,m,0] := G_{\boldsymbol{\psi}}^D\mathbf{f}[l,m]$.
For $t = 1,\dots,T$
For $l = 0,\dots,K-1$, for $m = 1,\dots,M-1$ set
$\tilde{v}^1[l,m] := -\frac{aK}{2}(\log|\tilde{W}|[l+1,m,t=0] - \log|\tilde{W}|[l-1,m,t=0])$
$\tilde{v}^2[l,m] := -\frac{aM}{2}(\log|\tilde{W}|[l,m+1,t=0]| - \log|\tilde{W}|[l,m-1,t=0])$
$\tilde{W}[l,m,t] := \tilde{W}[l,m,t-1] + K\,\Delta t\left(z^+(\tilde{v}^1)[l,m]\;[\tilde{\mathcal{A}}_1^{D^-}\tilde{W}][l,m,t] + z^-(\tilde{v}^1)[l,m]\;[\tilde{\mathcal{A}}_1^{D^+}\tilde{W}][l,m,t]\right) +$
$M\Delta t\left(z^+(\tilde{v}^2)[l,m]\;[\tilde{\mathcal{A}}_2^{D^-}\tilde{W}][l,m,t] + z^-(\tilde{v}^2)[l,m]\;[\tilde{\mathcal{A}}_2^{D^+}\tilde{W}][l,m,t]\right)$.

Explanation of all involved variables:

l	discrete position variable $l = 0,\dots,K-1$.
m	discrete frequency variable $m = 1,\dots,M-1$.
t	discrete time $t = 1,\dots T$, where T is the stopping time.
$\boldsymbol{\psi}$	discrete window $\boldsymbol{\psi} = \boldsymbol{\psi}_a^C = \{\psi_a(nN^{-1})\}_{n=-(N-1)}^{N-1}$ or $\boldsymbol{\psi} = \{\boldsymbol{\psi}_a^D[n]\}_{n=-(N-1)}^{N-1}$see below.
$G_{\boldsymbol{\psi}}^D\mathbf{f}[l,m]$	discrete Gabor transform computed by diagonalization via Zak transform [46].
$\tilde{W}[l,m,t]$	discrete evolving Gabor transform evaluated at position l, frequency m and time t.
$\tilde{\mathcal{A}}_i^{D^\pm}$	forward (+), backward (-) left-invariant position ($i=1$) and frequency ($i=2$) shifts.
$z^\pm$	$z^+(\phi)[l,m,t] = \max\{\phi(l,m,t),0\}$, $z^-(\phi)[l,m,t] = \min\{\phi(l,m,t),0\}$ for upwind.

The discrete Cauchy-Riemann window $\boldsymbol{\psi}_a^D$ is derived in Appendix C.4 and satisfies the system

$$\forall_{l=0,\dots,K-1}\forall_{m=0,\dots,M-1}\forall_{\mathbf{f}\in\ell_2(I)}\;:\;\left(\tfrac{1}{a}(\tilde{\mathcal{A}}_2^{D^+}+\tilde{\mathcal{A}}_2^{D^-}) + i\,a(\tilde{\mathcal{A}}_1^{D^+}+\tilde{\mathcal{A}}_1^{D^-})\right)(G_{\boldsymbol{\psi}_a^D}^D\mathbf{f})[l,m] = 0\;, \tag{67}$$

which has a unique solution in case of extreme oversampling $K = M = N$, $L = 1$.

9.1. Evaluation of Reassignment

We distinguished between two approaches to apply left-invariant adaptive convection on discrete Gabor-transforms (that we diagonalize by discrete Zak transform [46], recall subsection 7.1). Either we apply the numerical upwind PDE-scheme described in subsection 9 using the discrete left-invariant vector fields (62), or we apply erosion (48) on the modulus and restore the phase afterwards. Within each of the two approaches, we can use the discrete Cauchy-Riemann window $\boldsymbol{\psi}_a^D$ or the sampled continuous Cauchy-Riemann window $\boldsymbol{\psi}_a^C$.

To evaluate these 4 methods we apply the reassignment scheme to the reassignment of a linear chirp that is multiplied by a modulated Gaussian and is sampled using $N = 128$ samples. A visualization of this complex valued signal can be found Fig. 4 (top). The other signals in this figure are the reconstructions from the reassigned Gabor transforms that are given in Fig. 6. Here the topmost image shows the Gabor transform of the original signal. One can also find the reconstructions and reassigned Gabor transforms respectively using the four methods of reassignment. The parameters involved in generating these figures are $N = 128$, $K = 128$, $M = 128$, $L = 1$. Furthermore $a = 1/6$ and the time step for the PDE based method is set to $\Delta t = 10^{-3}$. All images show a snapshot of the reassignment method stopped at $t = 0.1$. The signals are scaled such that their energy equals the energy of the input signal. This is needed to correct for the numerical diffusion the discretization scheme suffers from. Clearly the reassigned signals resemble the input signal quite well. The PDE scheme that uses the sampled continuous window shows some defects. In contrast, the PDE scheme that uses $\boldsymbol{\psi}_a^D$ resembles the modulus of the original signal the most. Table 9.1 shows the relative ℓ_2-errors for all 4 experiments. Advantages of the erosion scheme (48) over the PDE-scheme of Section 9 are:

1. The erosion scheme does not produce numerical approximation-errors in the phase, which is evident since the phase is not used in the computations.
2. The erosion scheme does not involve numerical diffusion as it does not suffer from finite step-sizes.
3. The separable erosion scheme is much faster.

The convection time in the erosion scheme is different from the convection time in the upwind-scheme, due to violation of the Cauchy-Riemann equations. Using a discrete window (that satisfies the discrete Cauchy-Riemann relations, see Appendix C.4) in the PDE-scheme is more accurate. Thereby one can obtain more visual sharpening in the Gabor domain while obtaining similar relative errors in the signal domain. For example $t = 0.16$ for the PDE-scheme roughly corresponds to erosion schemes with $t = 0.1$ in the sense that the ℓ_2-errors nearly coincide, see Table 1. The method that uses a sampled version of the continuous window shows large errors and indeed in Fig. 6 the defects are visible. This shows the importance of the window selection, i.e. in the PDE-schemes it is better to use window $\boldsymbol{\psi}_a^D$ rather than window $\boldsymbol{\psi}_a^C$. However, Fig. 5 and Table 1 clearly indicate that in the erosion schemes it is better to choose window $\boldsymbol{\psi}_a^C$ than $\boldsymbol{\psi}_a^D$.

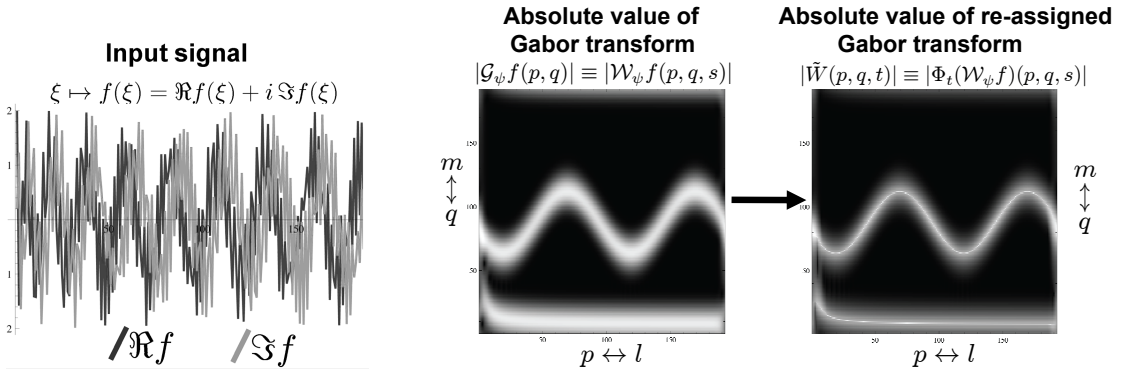

Figure 3: Illustration of reassignment by adaptive phase-invariant convection explained in Section 6, using the upwind scheme of subsection 9 applied on a Gabor transform.

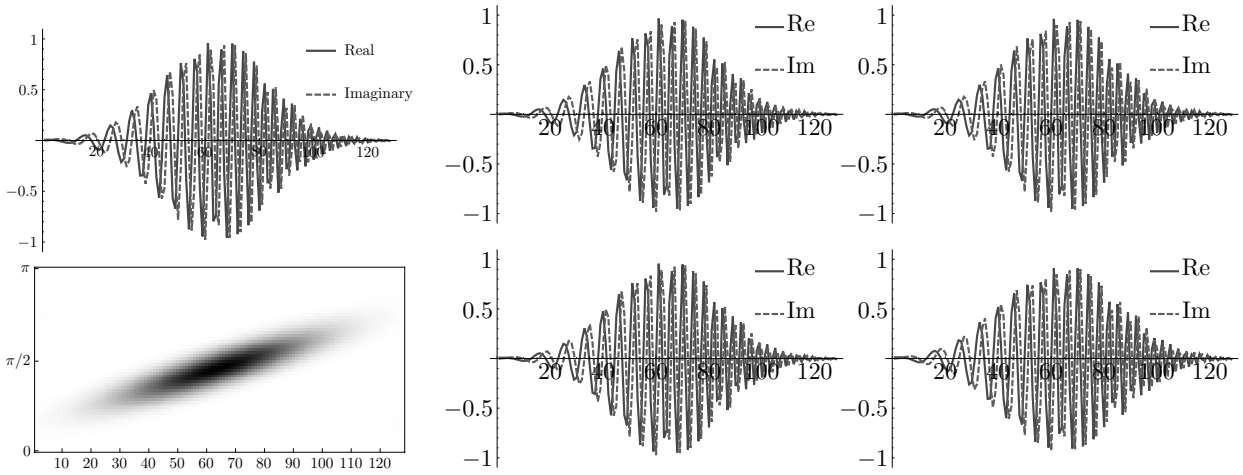

Figure 4: Reconstructions of the reassigned Gabor transforms of the original signal that is depicted on the top left whose absolute value of the Gabor transform is depicted on bottom left. In the right: First row corresponds to reassignment by the upwind scheme ($\mathcal{M} = 1$) of subsection 9, where on the left we used $\boldsymbol{\psi}_a^C$ and on the right we used $\boldsymbol{\psi}_a^D$. The parameters involved are grid constants $K = M = N = 128$, window scale $a = 1/6$, time step $\Delta t = 10^{-3}$ and time $t = 0.1$. The first row corresponds to reassignment by finite differences, whereas the second row corresponds to reassignment by morphological erosion where again in the left we used kernel $\boldsymbol{\psi}_a^C$ and in the right we used $\boldsymbol{\psi}_a^D$. The goal of reassignment is achieved; all reconstructed signals are close to the original signal, whereas their corresponding Gabor transforms depicted in Fig. 6 are much sharper than the absolute value of the Gabor transform of the original depicted on the bottom left of this figure.

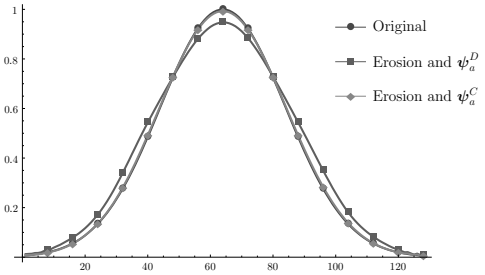

Figure 5: The modulus of the signals in the bottom row of Fig. 4. For erosion $\boldsymbol{\psi}_a^C$ performs better than erosion applied on a Gabor transform constructed by $\boldsymbol{\psi}_a^D$.

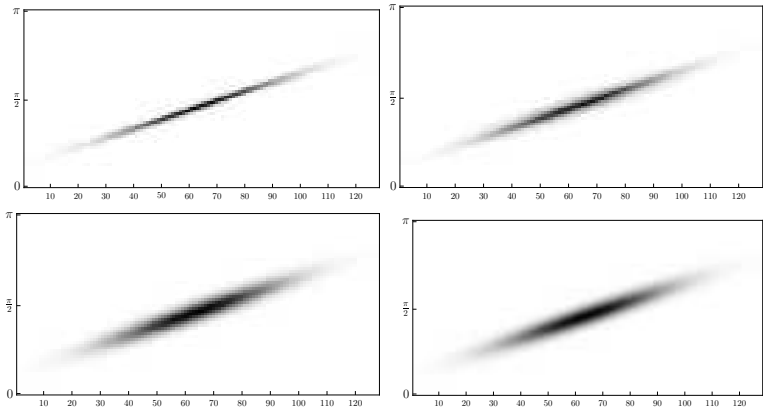

Figure 6: Absolute value of reassigned Gabor transforms of the signals depicted in the right of Fig. 4.

	ϵ_1	ϵ_2	t
Erosion continuous window	$2.41 \cdot 10^{-2}$	$8.38 \cdot 10^{-3}$	0.1
Erosion discrete window	$8.25 \cdot 10^{-2}$	$7.89 \cdot 10^{-2}$	0.1
PDE continuous window	$2.16 \cdot 10^{-2}$	$2.21 \cdot 10^{-3}$	0.1
PDE discrete window	$1.47 \cdot 10^{-2}$	$3.32 \cdot 10^{-4}$	0.1
	$2.43 \cdot 10^{-2}$	$6.43 \cdot 10^{-3}$	0.16

Table 1: The first column shows $\epsilon_1 = (\| \mathbf{f} - \tilde{\mathbf{f}} \|_{\ell_2(I)}) \|\mathbf{f}\|_{\ell_2}^{-1}$, the relative error of the complex valued reconstructed signal compared to the input signal. In the second column $\epsilon_2 = (\| \, |\mathbf{f}| - |\tilde{\mathbf{f}}| \, \|_{\ell_2(I)}) \|\mathbf{f}\|_{\ell_2}^{-1}$ can be found which represents the relative error of the modulus of the signals. Parameters involved are $K = M = N = 128$, window scale $a = \frac{1}{8}$ and convection time $t = 0.1$, with times step $\Delta t = 10^{-3}$ if applicable. PDE stands for the upwind scheme presented in subsection 9 and erosion means the morphological erosion method given by eq. (48).

10. The Exact Analytic Solutions of Reassigned Gabor Transforms of 1D-chirp Signals

In the previous section we have introduced several numerical algorithms for differential reassignment. We compared them experimentally on the special case where the initial 1D-signal (i.e. $d = 1$) is a chirp. In this section we aim for an analytic description of the behaviour of reassignment. The first major result of this section is Theorem 21, which spells out that the Gabor transform of a chirp signal with respect to a Gaussian window is a twodimensional chirp. In particular, the isocontours of the Gabor transform modulus are ellipses. We then describe the effect of reassignment on the isocontours of the solution, showing that as time progresses, the isocontours collapse towards a line pointing in the direction of the longer principal axis of the initial ellipse, but with increasing anisotropy that can be interpreted as a measure of sharpening in the time-frequency image, see Theorem 26.

These geometrical properties that can also be observed in Figure 7 and Figure 8. Some of the more technical results and proofs have been relegated to the appendix.

Lemma 18. *Let $t > 0$, $\eta \in [\frac{1}{2}, \infty)$. Let $\Phi_t^\eta : \mathcal{H}_n \to C(H_r)$ be the operator that maps a Gabor transform $\mathcal{W}_{\psi_a} f$ to its reassigned Gabor transform*

$$Q_{t,a,\eta}(|\mathcal{W}_{\psi_a} f|) \, e^{i arg\{\mathcal{W}_{\psi_a} f\}}$$

where $Q_{t,a,\eta}$ maps the absolute value $|\mathcal{W}_{\psi_a} f|$ of the Gabor transform to the unique viscosity solution $Q_{t,\eta}(|\mathcal{W}_{\psi_a} f|) := \tilde{W}(\cdot, t)$ of the Hamilton-Jacobi equation

$$\begin{cases} \frac{d\tilde{W}}{dt}(p,q,t) = -\frac{1}{2\eta} \left(a^{-2} \frac{d^2 \tilde{W}}{dp^2}(p,q,t) + a^2 \frac{d^2 \tilde{W}}{dq^2}(p,q,t) \right)^{2\eta}, & (p,q) \in \mathbb{R}^2, t > 0, \\ \tilde{W}(p,q,0) = |\mathcal{W}_{\psi_a} f(p,q,s)| = |\mathcal{G}_{\psi_a} f(p,q)|, & (p,q) \in \mathbb{R}^2, \end{cases} \tag{68}$$

at fixed time $t > 0$. Set

$$\Xi_t^{a,\eta} := \Phi_t^\eta \circ \mathcal{W}_{\psi_a}. \tag{69}$$

Let $\mathcal{D}_a$ be the unitary scaling operator given by (39). Then

$$(\Xi_t^{a,\eta} f)(p,q,s) = \sqrt{a} \, (\Xi_t^{1,\eta} \mathcal{D}_{a^{-1}} f)(a^{-1}p, aq, s) \tag{70}$$

Proof First of all one has by substitution in integration that

$$(\mathcal{W}_{\psi_a} f)(p,q,s) = \sqrt{a} (\mathcal{W}_{\psi_{a=1}} \mathcal{D}_{a^{-1}} f)(\frac{p}{a}, aq, s) \ . \tag{71}$$

for all $f \in \mathbb{L}_2(\mathbb{R}^d)$, $(p,q,s) \in H_r$. So if we introduce the scaling operator $\mathbf{D}_a : \mathbb{L}_2(H_r) \to \mathbb{L}_2(H_r)$ by

$$(\mathbf{D}_a U)(p,q,s) = U(a^{-1}p, qa, s) \ , a > 0,$$

then (71) can be written as $\mathcal{W}_{\psi_a} = \sqrt{a} \mathbf{D}_a \mathcal{W}_{\psi_1}$ and by the chain-law for differentiation one has $Q_{t,a,\eta} = \mathbf{D}_a Q_{t,1,\eta} \mathbf{D}_{a^{-1}}$ (where we note that the viscosity condition, cf. [32] is scaling covariant). Consequently, we obtain

$$\begin{aligned} (\Xi_t^{a,\eta} f)(p,q,s) &= \sqrt{a} \, e^{i \arg\{\mathcal{W}_{\psi_a} f(p,q,s)\}} \, (\mathbf{D}_a Q_{t,1,\eta} \mathbf{D}_{a^{-1}} \mathbf{D}_a \mathcal{W}_{\psi_1} \mathcal{D}_{a^{-1}} f)(p,q,s) \\ &= \sqrt{a} \, e^{i \arg\{\mathcal{W}_{\psi_1} f(a^{-1}p, aq, s)\}} \, (Q_{t,1,\eta} (\mathcal{D}_{a^{-1}} f))(a^{-1}p, aq, s) \\ &= \sqrt{a} \, (\Xi_t^{1,\eta} f)(a^{-1}p, aq, s) \end{aligned}$$

□

Corollary 19. *By means of the scaling relation Eq. (70) we may as well restrict ourselves to the case $a = 1$ for analytic solutions.*

Lemma 20. *Let $g(\xi) = e^{w\xi^2+u\xi+t}$, with $Re(w) < 0$ and $Im(w) > 0$. Then*

$$\int_{\mathbb{R}} g(\xi)\,\mathrm{d}\xi = \sqrt{\frac{\pi}{-w}} e^{\frac{4tw-u^2}{4w}}$$

where the complex square root is taken using the usual branch-cut along the positive real axis.

Proof By contour integration where the contour encloses the two-sided section in the complex plane given by the intersection of the ball with radius R with $0 < \arg(z) < -\frac{1}{2}\arg(-w)$ (positively) and $-\pi < \arg(z) < -\pi + -\frac{1}{2}\arg(-w)$ (negatively) then one has by Cauchy's formula of integration and letting $R \to \infty$ that

$$\int_{\mathbb{R}} g(\xi)\,\mathrm{d}\xi = \int_{\arg(z)=-\frac{1}{2}\arg(-w)} e^{|w|e^{i\arg(w)}z^2-\frac{u^2}{4w}}\,\mathrm{d}z = \sqrt{\frac{|w|}{-w}}\sqrt{\frac{\pi}{|w|}} e^{-\frac{u^2}{4w}}$$

from which the result follows. □

Theorem 21. *Let $r, b > 0$. Let f be (a chirp signal) given by*

$$f(\xi) = e^{-\frac{\xi^2}{2b^2}} e^{i\pi r\xi^2}\ , \tag{72}$$

(a) The Gabor transform of f (with $\psi(\xi) = e^{-\pi\xi^2}$) equals

$$\mathcal{W}_\psi f(p,q,s) = \sqrt{\frac{1}{2\pi b^2 - ir + 1}}\, e^{-2\pi i(s+\frac{pq}{2})} e^{(p,q)B_{r,b}(p,q)^T} \tag{73}$$

with $B_{rb} = Re(B_{r,b}) + i\,Im(B_{r,b})$, $Re(B_{r,b}) < 0$, $(Im(B_{r,b}))^T = Im(B_{r,b})$, $(Re(B_{r,b}))^T = Re(B_{r,b})$ given by

$$\begin{aligned} B_{rb} \quad &= \tfrac{1}{r^2b^4+(\frac{1}{2\pi}+b^2)^2}\left(\begin{pmatrix} -\frac{1}{2}(b^2+\frac{1}{2\pi}) - \pi r^2 b^4 & \pi r b^4 \\ \pi r b^4 & -\pi b^2(b^2+\frac{1}{2\pi}) \end{pmatrix}\right. \\ &\left. + i\begin{pmatrix} \pi r b^4 & \frac{1}{4\pi}+\frac{b^2}{2}+\pi r^2 b^4 \\ \frac{1}{4\pi}+\frac{b^2}{2}+\pi r^2 b^4 & -\pi r b^4 \end{pmatrix}\right)\ . \end{aligned}$$

(b) For $\eta \in (\frac{1}{2}, 1]$, the reassigned Gabor transform is given by

$$\begin{aligned} &(\Xi_t^{a,\eta} f)(p,q,s) = \sqrt{a}\,(\Xi_t^{1,\eta}\mathcal{D}_{a^{-1}} f)(a^{-1}p, aq, s)\ , a > 0,\ \textit{with} \\ &(\Xi_t^{1,\eta} f)(p,q,s) = e^{2\pi i(s-\frac{pq}{2})} e^{i\,Im(B_{rb})}(k_t^\eta \ominus e^{(\cdot,\cdot)Re(B_{rb})(\cdot,\cdot)^T})(p,q)\ , \end{aligned} \tag{74}$$

with (positive) erosion kernel at time $t > 0$ given by

$$k_t^\eta(p,q) = \frac{2\eta-1}{2\eta} t^{-\frac{1}{2\eta-1}} (p^2+q^2)^{\frac{\eta}{2\eta-1}} \tag{75}$$

for $\eta \in (\frac{1}{2}, 1]$ and

$$k_t^{\eta=\frac{1}{2}}(p,q) = \begin{cases} \infty & \text{if } p^2+q^2 \geq t^2 \\ 0 & \text{if } p^2+q^2 < t^2 \end{cases} \tag{76}$$

Proof Consider Eq. (5) where we set $n = 1$, $d = 1$, Eq. (72) and $\psi(\xi) = e^{-\pi\xi^2}$. We apply Lemma 20 with $w = i\pi r - \frac{1}{2b^2} - \pi$, $u = -2\pi p - 2\pi i q$, $t = 2\pi i pq - \pi p^2$ and Eq. (73) follows. Then we note that when transporting along equiphase planes, phase-covariance is the same as phase invariance and indeed by Lemma 18 the main result (74) follows. Finally, we note that the viscosity solutions of the erosion PDE is given by morphological convolution with the erosion kernel which by the Hopf-Lax formula equals $k_t^\eta(p,q) = t\mathcal{L}_\eta(t^{-1}(p,q)^T)$ where the Lagrangian $\mathcal{L}_\eta(p,q) = (\mathfrak{f}H_\eta)(p,q)$ is obtained, cf. [32, ch:3.2.2], by the Fenchel-transform of the hamiltonian $H_\eta(a^{-1}u, av) = \frac{1}{2\eta}(a^{-2}(u)^2 + a^2(v)^2)^{2\eta}$ that appears in the righthand side of the Hamilton-Jacobi equation Eq. (68), cf. [59, ch:2,p.24], Eq. (48), from which the result follows. □

Remark 22. *In Theorem 21 we considered a chirp signal centered in position, frequency and phase. The general case follows by:* $(\mathcal{W}_\psi \mathcal{U}_{(p_0,q_0,s_0)} f)(p,q,s) = (\mathcal{W}_\psi f)((p_0,q_0,s_0)^{-1}(p,q,s))$.

Remark 23. *Note that trace*$\{Re(B_{rb})\} < 0$ *and Det*$\{Re(B_{rb})\} > 0$*, so both eigenvalues of the symmetric matrix* $Re(B_{rb})$ *are negative. Consequently, the equi-contours of the spectrogram* $(p,q) \mapsto |G_\psi f|(p,q)$ *are ellipses. In a chirp signal (without window, i.e.* $b \to \infty$*) frequency increases linearly with* ξ *via rate* r *and thereby one expects the least amount of decay in the spectrogram along* $q = r\,p$*, i.e. one expects* $(1,r)^T$ *to be the eigenvector with smallest absolute eigenvalue of* $Re(B_{r,b})$*. This is indeed only the case if* $b \to \infty$ *as*

$$Re(B_{r,b}) \begin{pmatrix} 1 \\ r \end{pmatrix} = \frac{(b^2/2)}{r^2 b^4 + ((2\pi)^{-1} + b^2)^2} \left(\begin{pmatrix} 1 \\ r \end{pmatrix} + \begin{pmatrix} \frac{1}{2\pi b^2} \\ 0 \end{pmatrix} \right).$$

Remark 24. *Note that Det*$\{Re(B_{rb})\} < 0$*, so the eigenvalues of the symmetric matrix* $Re(B_{rb})$ *have different sign and consequently the equiphase lines in phase space (where we have set* $s = -pq/2$*) are hyperbolic as can be observed the left column in Figure 7 and Figure 8.*

In case $\eta \to \infty$ the Lagrangian is homogeneous, the Hamilton-Jacobi equation (that describes the evolution of geodesically equidistant surfaces $\{(p,q) \in \mathbb{R}^2 \mid \tilde{W}(p,q,t) = c\}$) becomes time-independent, cf. [59, ch:4,p.170]

$$1 = a^{-2} \frac{d^2}{dp^2} \tilde{W}(p,q,t) + a^2 \frac{d^2}{dp^2} \tilde{W}(p,q,t).$$

In case $\eta = \frac{1}{2}$ the Hamiltonian is homogeneous and the erosion kernels are flat accordingly. The non-flatness of the erosion kernels can be controlled via the parameter $\eta \in (\frac{1}{2}, \infty)$. Furthermore, the Hamilton-Jacobi equation in (68) is invariant under monotonic transformations iff $\eta = \frac{1}{2}$ and this allows us to compute $(\Xi_t^{1,\frac{1}{2}} f)(p,q,s)$.

The next theorem provides the exact solution $\Xi_t^{1,\frac{1}{2}} f : H_r \to \mathbb{C}$ of an eroded Gabor transform of a chirp signal at time $t > 0$. In the subsequent theorem we will show that the isocontours of the spectogram are non-ellipsoidal Jordan curves that shrink towards the principal eigenvector of $\mathrm{Re}(B_{r,b})$ where they collaps as t increases. This collapsing behavior can also be observed in the bottom rows of Figure 7 and 8.

For details on the derivations of $\Xi_t^{1,\frac{1}{2}} f$ and the collapsing of its iso-contours see Appendix C.

Theorem 25. *Let* $\eta = \frac{1}{2}$ *and let* $t > 0$*. Let* f *be a chirp signal given by (72) then the reassigned Gabor transform of* f *(with window scale* $a = 1$*) is given by*

$$\begin{aligned}
&(\Xi_t^{1,\frac{1}{2}} f)(p,q,s) = \sqrt{\tfrac{1}{2\pi b^2 - ir + 1}}\, e^{-2\pi i (s + \frac{pq}{2})} e^{i\,(p,q)\,Im(B_{rb})(p,q)^T} (k_t^{\eta=\frac{1}{2}} \ominus e^{(\cdot,\cdot) Re(B_{rb})(\cdot,\cdot)^T})(p,q) \\
&= \sqrt{\tfrac{1}{2\pi b^2 - ir + 1}}\, e^{-2\pi i (s + \frac{pg}{2})} \cdot \\
&\begin{cases}
e^{(\lambda_t(p,q))^2 \left(\frac{|\alpha_1(p,q)|^2 \lambda_1}{(\lambda_1 - \lambda_t(p,q))^2} + \frac{|\alpha_2(p,q)|^2 \lambda_2}{(\lambda_2 - \lambda_t(p,q))^2} \right)} & \text{if } \alpha_1(p,q)\alpha_2(p,q) \neq 0, \\
e^{|(\alpha_2(p,q)| + t)^2 \lambda_2} & \text{if } \alpha_1(p,q) = 0, \\
e^{(|\alpha_1(p,q)| + t)^2 \lambda_1} & \text{if } \alpha_2(p,q) = 0 \text{ and } t \leq t_{max}(p, \tau p).
\end{cases}
\end{aligned} \tag{77}$$

Here λ_1, λ_2 *denote the negative eigenvalues (with* $|\lambda_1| < |\lambda_2|$*) of* $Re(B_{r,b})$*, explicitly derived in Lemma 32, and* $(p,q) = \alpha_1(p,q)\boldsymbol{k}_1 + \alpha_2(p,q)\boldsymbol{k}_2$ *with* $\{\boldsymbol{k}_1, \boldsymbol{k}_2\}$ *the normalized eigenvectors of* $Re(B_{r,b})$*. Te Euler-Lagrange multiplier* $\lambda_t := \lambda_t(p,q)$ *corresponds to the unique zero* $P_t(\lambda_t) = 0$ *of the 4-th order polynomial*

$$P_t(\lambda) := t^2 \prod_{i=1}^{2} (\lambda - \lambda_i)^2 - \sum_{i=1}^{2} (\lambda_i \alpha_i(p,q))^2 (\lambda - \lambda_{-i+3})^2, \tag{78}$$

such that, for $\alpha_1(p,q)\alpha_2(p,q) \neq 0$*, the corresponding unique solution* (p', q') *of*

$$(Re(B_{r,b}) - \lambda_t(p,q)) \begin{pmatrix} p' \\ q' \end{pmatrix} = -\lambda_t(p,q) \begin{pmatrix} p \\ q \end{pmatrix} \tag{79}$$

has maximum $\sum_{k=1}^{2} \lambda_k |\alpha_k(p',q')|^2$. *The polynomial has at least 2 real-valued zeros. For each* $(p,q) \in \mathbb{R}^2$ *there exists a* $t = t_{max}(p,q) \geq 0$ *such that* P_t *has 3 real-valued zeros and* P_s *has 4 real-valued zeros for all* $s > t$. *Finally, the Lagrange multiplier satisfies the following scaling property*

$$\lambda_t(p,q) = \lambda_{\zeta t}(\zeta p, \zeta q) \text{ for all } \zeta > 0. \tag{80}$$

Proof See Appendix C.1. □

Theorem 26. *Let* $c > 0$. *Let* $\lambda_1, \lambda_2 < 0$ *be the eigenvalues of* $Re(B_{r,b})$ *with* $|\lambda_1| < |\lambda_2|$ *and with corresponding eigenvectors* $\boldsymbol{k}_1$, $\boldsymbol{k}_2$. *The isocontours*

$$\{(p,q) \in \mathbb{R}^2 \mid |\Xi_t^{1,\frac{1}{2}} f|(p,q,s) = c\}$$

of $|\Xi_t^{1,\frac{1}{2}} f|$ *with* $t > 0$ *are non-ellipsoidal Jordan curves that retain the reflectional symmetry in the principal axes of* $Re(B_{r,b})$. *The interior*

$$\Omega_{t,c} = \{(p,q) \in \mathbb{R}^2 \mid |\Xi_t^{1,\frac{1}{2}} f|(p,q) > c\}$$

of these Jordan curves is convex. If $\mathfrak{B}_{t,c}$ *denote the smallest rectangular box containing this interior with sides parallel to* $\boldsymbol{k}_1$ *and* $\boldsymbol{k}_2$, *then the aspect ratio of* $\mathfrak{B}_{t,c}$ *equals*

$$\left(\sqrt{\frac{c}{\lambda_1}} - t\right)\left(\sqrt{\frac{c}{\lambda_2}} - t\right)^{-1} \tag{81}$$

for $0 \leq t \leq t_{fin} := \sqrt{\frac{c}{\lambda_2}}$. *The isocontour* $\{(p,q) \mid |\Xi_t^{1,\frac{1}{2}} f(p,q,s)| = c\}$ *collapses to the span of* $\boldsymbol{k}_1$ *as* $t \uparrow t_{fin}$.

Proof See Appendix C.3. □

10.1. Plots of the Exact Re-assigned Gabor Transforms of Chirp Signals

For a plot of the exact $\Xi_t^{1,\frac{1}{2}} f$ in Theorem 25 using Gardano's formula for the zeros of the fourth order polynomial given by Eq. (78) we refer to Figure 7 (for the case $(b,r) = (\frac{1}{2},1)$) and Figure 8 (for the case $(b,r) = (1,1)$). Within these Figures one can clearly see that during the erosion process isocontours collapse towards the eigenspace $\langle \mathbf{k}_1 \rangle$ with smallest eigenvalue. This in accordance with Theorem 26.

Moreover for $(b,r) = (1,1)$ one has $\mathbf{k}_1 \approx \frac{1}{\sqrt{1+r^2}}(1,r)^T$ and finally, we note that the discrete Gabor transforms closely approximate the exact Gabor transforms as can be seen in the top row of Figure 8. Despite the fact that, for $\eta = \frac{1}{2}$, the eroded ellipses are no longer ellipses the principal axis $\langle \mathbf{k}_1 \rangle$ is preserved as a symmetry-axis for the isolines in phase space (where $s = -\frac{pq}{2}$). This in accordance with Theorem 26, Theorem 21 and the convergence results from discrete to continuous setting shown in Section 7.

11. Left Invariant Diffusion on Gabor transforms

A common technique in imaging to enhance images $f : \mathbb{R}^2 \to \mathbb{R}$ via non-linear adaptive diffusions are so-called coherence enhancing diffusion (CED) schemes, cf. [64, 16, 55]. Within these CED schemes one considers a diffusion equation, where the diffusivity/conductivity matrix in between the divergence and gradient is data-adaptive. Typically the diffusivity is adapted to the Gaussian gradient (structure tensor) or Hessian tensor computed from the data. Here the aim is to diffuse strongly along edges/lines and little orthogonal to them. In case of edge-adaptation the anisotropic diffusivity matrix is diagonalized along the eigenvectors of auxiliary matrix

$$\mathbf{A}(u_f(\cdot,s))(x,y) = (G_\epsilon * (\nabla u_f(\cdot,s)(\nabla u_f(\cdot,s))^T))(x,y) \tag{82}$$

where ∇u_f denotes either the Gaussian gradient of image f or the gradient of the non-linearly evolved image $u_f(\cdot,s)$ and where the final convolution, with Gaussian kernel $G_\epsilon(x,y) = (4\pi\epsilon)^{-1} e^{-\frac{\|\mathbf{x}\|^2}{4\epsilon}}$ with $\epsilon > 0$ small, is

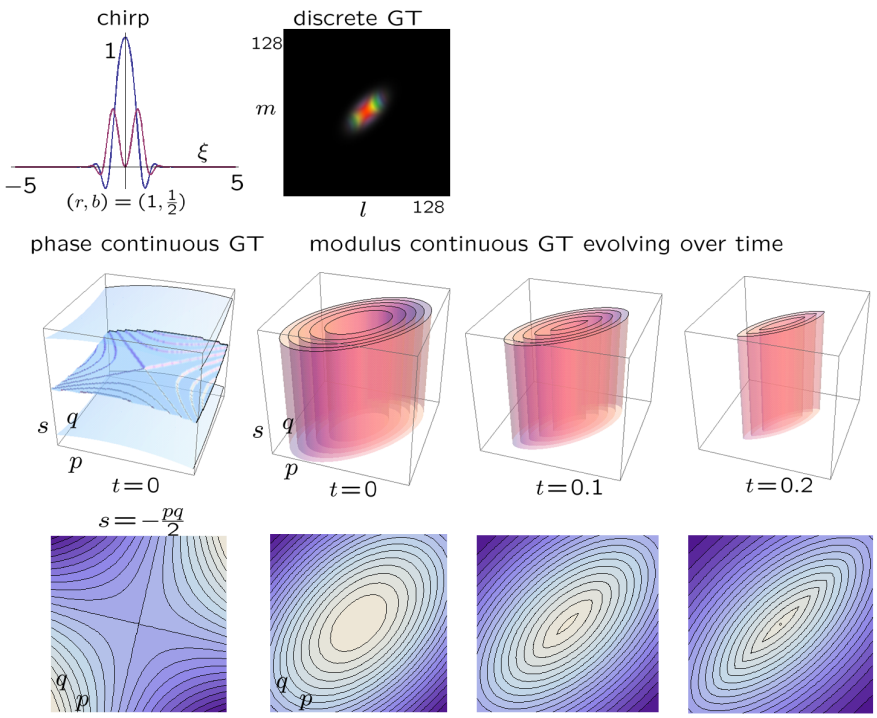

Figure 7: Visualization of $(p,q,s) \mapsto (\Xi_t^{1,\frac{1}{2}} f)(p,q,s)$ where f is the chirp signal (72) with $(b,r) = (\frac{1}{2},1)$. Top row: left; the input chirp signal, right: We have sampled the chirp signal on 128-grid and depicted the corresponding discrete Gabor transform $(K = M = N, L = a = 1)$ where color represents phase and where intensity represents the modulus. Middle row; equisurfaces of the phase and modulus of our exact solutions for $\Xi_t^{1,\frac{1}{2}} f$ in Theorem 25, phase is constant over time whereas the modulus is considered for $t = 0$, $t = 0.1$ and $t = 0.2$. Iso-intensities have been fixed $(-0.05, -0.09, -0.14, -0.18, -0.23)$ over time to show their collapsing behavior towards $\mathbf{k}_1$ in accordance with Corollary 35. Bottom row; Restrictions to the surface $s = -\frac{pq}{2}$ yields the solutions in phase space.

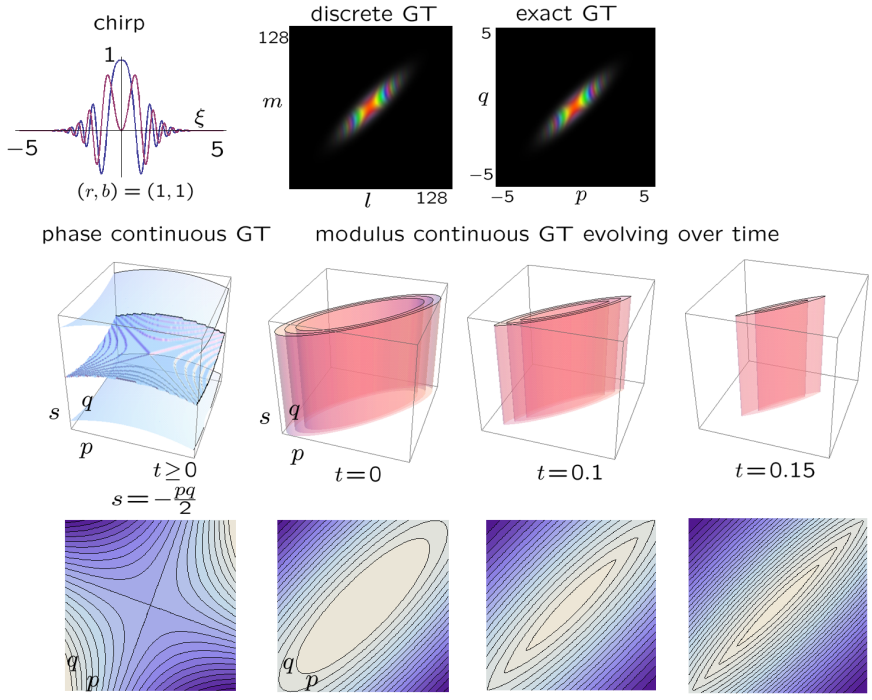

Figure 8: Same settings as in Figure 7 except for $(b,r) = (1,1)$ and iso-intensities $(-0.06, -0.08, -0.1)$.

applied componentwise. In case of line-adaptation the auxiliary matrix is, for each position $\mathbf{x} = (x, y) \in \mathbb{R}^2$, obtained by the Hessian at that position:

$$(\mathbf{A}(u_f(\cdot,s)))(\mathbf{x}) = (G_\epsilon * Hu_f(\cdot,s))(\mathbf{x}) = [(G_\epsilon * \partial_{x_i}\partial_{x_j} u_f(\cdot,s))(\mathbf{x})]_{i,j=1,2} = [(\partial_{x_i}\partial_{x_j} G_\epsilon * u_f(\cdot,s))(\mathbf{x})]_{i,j=1,2}\ . \tag{83}$$

Given the eigen system of the auxiliary matrix, standard coherence enhancing diffusion equations on images cf. [64] can be formulated as

$$\begin{cases} \partial_s u_f(\mathbf{x},s) & = \left(\nabla_{\mathbf{x}} \cdot\ \mathbf{S} \cdot \begin{pmatrix} \varepsilon & 0 \\ 0 & (1-\varepsilon)e^{-\frac{c}{\lambda_1-\lambda_2}} + \varepsilon \end{pmatrix} \cdot\ \mathbf{S}^{-1} \cdot\ (\nabla_{\mathbf{x}} u_f(\cdot,s))^T\right)(\mathbf{x}) \\ & = \begin{pmatrix} \partial_u & \partial_v \end{pmatrix} \begin{pmatrix} \varepsilon & 0 \\ 0 & (1-\varepsilon)e^{-\frac{c}{(\lambda_1-\lambda_2)^2}} + \varepsilon \end{pmatrix} \begin{pmatrix} \partial_u \\ \partial_v \end{pmatrix} u_f(\mathbf{x},s), \quad \mathbf{x} \in \mathbb{R}^2, s > 0, \\ u_f(\mathbf{x},0) & = f(\mathbf{x}), \qquad \mathbf{x} \in \mathbb{R}^2. \end{cases} \tag{84}$$

Here we expressed the diffusion equations in both the global standard basis $\{\mathbf{e}_x, \mathbf{e}_y\} := \{(1,0),(0,1)\} \leftrightarrow \{\partial_x, \partial_y\}$ and in the locally adapted basis of eigenvectors of auxiliary matrix $\mathbf{A}(u_f(\cdot,s))(\mathbf{x})$, recall Eq. (82) and Eq. (83):

$$\{\mathbf{e}_1, \mathbf{e}_2\} := \{\mathbf{e}_1\left(\mathbf{A}(u_f(\cdot,s))(\mathbf{x})\right), \mathbf{e}_2\left(\mathbf{A}(u_f(\cdot,s))(\mathbf{x})\right)\} \leftrightarrow \{\partial_u, \partial_v\},$$

with respective eigenvalues $\lambda_k := \lambda_k(\mathbf{A}(u_f(\cdot,s))(\mathbf{x}))$, $k = 1, 2$. The corresponding orthogonal basis transform which maps the standard basis vectors to the eigenvectors $\{\mathbf{e}_1, \mathbf{e}_2\}$ is denoted by $\mathbf{S} = (\mathbf{e}_1 \mid \mathbf{e}_2)$ and we have $(\partial_u\ \ \partial_v) = (\partial_x\ \ \partial_y) \cdot \mathbf{S}$. Note that

$$\mathbf{A} = \mathbf{S} \cdot \mathrm{diag}\{\lambda_1, \lambda_2\} \cdot \mathbf{S}^{-1}.$$

In isotropic areas $\lambda_1 \to \lambda_2$. Here the conductivity matrix becomes a multiple of the identity, yielding isotropic diffusion, which is desirable for noise-removal in these areas.

A typical drawback of this type of coherence enhancing diffusion directly applied to images is that the direction of the image gradient (or Hessian eigenvectors) is ill-posed in the vicinity of crossings and junctions. Therefore, in their recent works on orientation scores, cf. [39, 26, 38] Franken and Duits developed coherence enhancing diffusion via invertible orientation scores (CEDOS) where crossings are generically disentangled allowing crossing preserving diffusion, see Figure 9. The key idea here is to replace the image domain $\mathbb{R}^2$ by a larger Lie group $SE(2) = \mathbb{R}^2 \rtimes SO(2)$, where the left-invariant vector fields provide per spatial position a whole family of oriented reference frames cf. [23, 22]. This allows the inclusion of coherent alignment ("context") of disentangled local line fragments visible in the orientation score.

In this section we would like to extend this general idea to Gabor transforms defined on the Heisenberg group, where the left-invariant vector fields provide per spatial position a whole family of reference frames with respect to frequency and phase. Again we would like to achieve coherent alignment of all Gabor atoms in the Gabor domain via left-invariant diffusion.

In order to generalize the CED (coherence enhancing diffusion) schemes to Gabor transforms we must replace the left-invariant vector fields $\{\partial_x, \partial_y\}$ on the additive group $(\mathbb{R}^2, +)$, by the left-invariant vector fields on H_r. Furthermore, we replace the 2D-image by the Gabor transform of a $1D$-signal, the group $\mathbb{R}^2$ by H_r, the standard inner product on $\mathbb{R}^2$ by the first fundamental form (41) parameterized by β. Finally, we replace the basis of normalized left-invariant vector fields $\{\mathbf{e}_x, \mathbf{e}_y\} := \{(1,0),(0,1)\} \leftrightarrow \{\partial_x, \partial_y\}$ on $\mathbb{R}^2$ by the normalized left-invariant vector fields $\{\mathbf{e}_x, \mathbf{e}_y\} := \{(1,0),(0,1)\} \leftrightarrow \{\beta^{-2}\mathcal{A}_1, \mathcal{A}_2\}$ on H_r.

These steps produce the following system for adaptive left-invariant diffusion on Gabor transforms:

$$\begin{cases} \partial_t W(p,q,s,t) & = \left(\begin{pmatrix} \beta^{-2}\mathcal{A}_1 & \mathcal{A}_2 \end{pmatrix} \cdot \mathbf{S} \cdot \begin{pmatrix} \varepsilon & 0 \\ 0 & (1-\varepsilon)e^{-\frac{c}{\lambda_1-\lambda_2}} + \varepsilon \end{pmatrix} \cdot \mathbf{S}^{-1} \begin{pmatrix} \beta^{-2}\mathcal{A}_1 W \\ \mathcal{A}_2 W \end{pmatrix}\right)(p,q,s,t) \\ & = \begin{pmatrix} \partial_u & \partial_v \end{pmatrix} \begin{pmatrix} \varepsilon & 0 \\ 0 & (1-\varepsilon)e^{-\frac{c}{(\lambda_1-\lambda_2)^2}} + \varepsilon \end{pmatrix} \begin{pmatrix} \partial_u \\ \partial_v \end{pmatrix} W(p,q,s,t), \\ & \text{for all } (p,q,s) \in H_r, t > 0 \text{ and fixed } c > 0, \varepsilon > 0, \\ W(p,q,s,0) & = \mathcal{W}_\psi f(p,q,s), \text{ for all } (p,q,s) \in H_r. \end{cases} \tag{85}$$

with $\mathbf{S} := (\mathbf{e}_1 \mid \mathbf{e}_2)$ and $(\partial_u W\ \ \partial_v W) = (\beta^{-2}\mathcal{A}_1 W\ \ \mathcal{A}_2 W)\mathbf{S}$ and where

$$\begin{aligned} &\lambda_k := \lambda_k(\mathbf{A}(|\mathcal{W}_\psi f|)(p,q,s)), k = 1,2, |\lambda_1| \le |\lambda_2| \\ &\mathbf{e}_k := \mathbf{e}_k(\mathbf{A}(|\mathcal{W}_\psi f|)(p,q,s)), k = 1,2, \end{aligned} \tag{86}$$

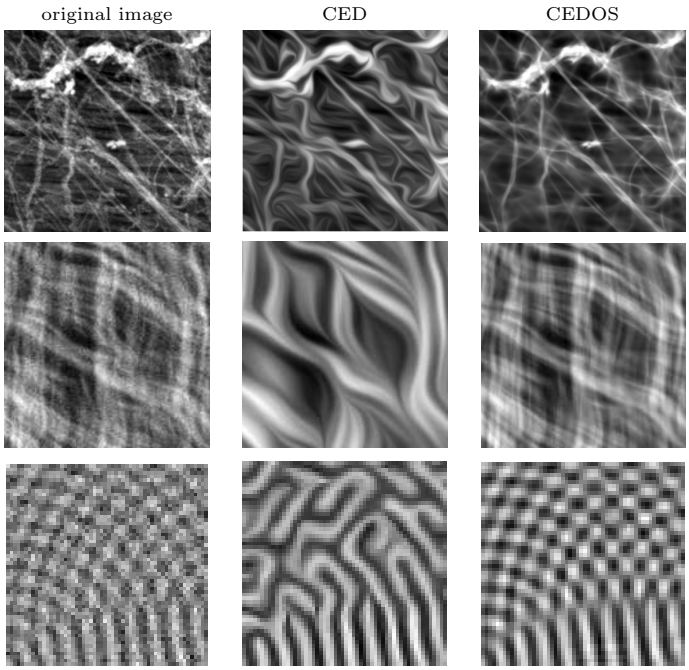

Figure 9: Left-invariant processing via invertible orientation scores is the right approach to generically deal with crossings and bifurcations. Left column: original images. Middle column: result of coherence enhancing diffusion on images (CED), cf. [64]. Right column: coherence enhancing diffusion via orientation score, cf. [26, 39]. Top row: 2-photon microscopy image of bone tissue. 2nd row : collagen fibers of the heart. 3rd row: artificial pattern. coherence enhancing diffusion on orientation scores (CEDOS) is capable of handling crossings and bifurcations, whereas (CED) produces spurious artifacts.

denote the eigenvalues and $\{\mathbf{e}_1, \mathbf{e}_2\} \leftrightarrow \{\partial_u, \partial_v\}$ the corresponding normalized eigenvectors of a local auxiliary matrix $\mathbf{A}(|\mathcal{W}_\psi f|)(p,q,s)$:

$$\mathbf{A}(|\mathcal{W}_\psi f|)(p,q,s)\ \mathbf{e}_k = \lambda_k\, \mathbf{e}_k.$$

The eigenvectors are normalized w.r.t. first fundamental form (41) parameterized by β, i.e.

$$\begin{array}{l} \mathfrak{G}_\beta(\partial_u,\partial_u) = \mathfrak{G}_\beta(\partial_v,\partial_v) = \mathfrak{G}_\beta(\beta^{-2}\mathcal{A}_1, \beta^{-2}\mathcal{A}_1) = \mathfrak{G}_\beta(\mathcal{A}_2,\mathcal{A}_2) = 1 \quad \leftrightarrow \\ \mathbf{e}_1^T\mathbf{e}_1 = \mathbf{e}_2^T\mathbf{e}_2 = \mathbf{e}_x^T\mathbf{e}_x = \mathbf{e}_y^T\mathbf{e}_y = 1 \Rightarrow \mathbf{S}^T = \mathbf{S}^{-1}. \end{array}$$

This auxiliary matrix $\mathbf{A}(|\mathcal{W}_\psi f|)(p,q,s)$ at each position $(p,q,s) \in H_r$ is chosen such that it depends only on the absolute value $|\mathcal{W}_\psi f|$ (so it is independent of phase parameter s) of the *initial condition*. The same holds for the corresponding conductivity matrix-valued function appearing in Eq. (85):

$$\mathbf{C} = \mathbf{S} \cdot \begin{pmatrix} \varepsilon & 0 \\ 0 & (1-\varepsilon)e^{-\frac{c}{\lambda_1 - \lambda_2}} + \varepsilon \end{pmatrix} \cdot \mathbf{S}^{-1},$$

where we note that $\mathbf{A} = \mathbf{S} \cdot \mathrm{diag}\{\lambda_1, \lambda_2\} \cdot \mathbf{S}$.

We propose the following specific choices of auxiliary matrices

$$\begin{array}{l} \mathbf{A}(|\mathcal{W}_\psi f|)(p,q,s) = [(\partial_{p_i}\partial_{p_j} G_\sigma * |\mathcal{W}_\psi f|)(p,q)]_{i,j=1,2}\ , \\ \mathbf{A}(|\mathcal{W}_\psi f|)(p,q,s) = [(\partial_{p_i} G_\sigma * |\mathcal{W}_\psi f|)(p,q)\ (\partial_{p_j} G_\sigma * |\mathcal{W}_\psi f|)(p,q)]_{i,j=1,2} \end{array}$$

with $p_1 = \beta^2 p$ and $p_2 = q$ and separable Gaussian kernel $G_\sigma(p,q) = \frac{\beta^2}{2\pi\sigma^2} e^{-\frac{\beta^4 p^2 + q^2}{2\sigma^2}}$. Note that $\mathcal{A}_1|\mathcal{W}_\psi f| = \partial_p|\mathcal{W}_\psi f|$ and $\mathcal{A}_2|\mathcal{W}_\psi f| = \partial_q|\mathcal{W}_\psi f|$. Now since $|\mathcal{W}_\psi f| = |\mathcal{G}_\psi f|$ and $\tilde{\mathcal{A}}_i = \mathcal{S} \circ \mathcal{A}_i \circ \mathcal{S}^{-1}$ (recall (32)) and

$\mathcal{S} \circ \mathcal{W}_\psi f = \mathcal{G}_\psi f$ we get the following equivalent non-linear left-invariant diffusion equations on phase space:

$$\begin{cases} \partial_t \tilde{W}(p,q,t) & = \left(\begin{pmatrix} \beta^{-2}\tilde{\mathcal{A}}_1 & \tilde{\mathcal{A}}_2 \end{pmatrix} \cdot \mathbf{S} \cdot \begin{pmatrix} \varepsilon & 0 \\ 0 & (1-\varepsilon)e^{-\frac{c}{\lambda_1-\lambda_2}} + \varepsilon \end{pmatrix} \cdot \mathbf{S}^{-1} \begin{pmatrix} \beta^{-2}\tilde{\mathcal{A}}_1 \tilde{W} \\ \tilde{\mathcal{A}}_2 \tilde{W} \end{pmatrix} \right)(p,q,t) \\ & = \begin{pmatrix} \partial_{\tilde{u}} & \partial_{\tilde{v}} \end{pmatrix} \begin{pmatrix} \varepsilon & 0 \\ 0 & (1-\varepsilon)e^{-\frac{c}{(\lambda_1-\lambda_2)^2}} + \varepsilon \end{pmatrix} \begin{pmatrix} \partial_{\tilde{u}} \\ \partial_{\tilde{v}} \end{pmatrix} \tilde{W}(p,q,t), \\ & \text{for all } (p,q) \in \mathbb{R}^2, t > 0 \text{ and fixed } c > 0, \varepsilon > 0, \\ \tilde{W}(p,q,0) & = \mathcal{G}_\psi f(p,q), \text{ for all } (p,q) \in \mathbb{R}^2. \end{cases} \tag{87}$$

with again $\mathbf{S} = (\mathbf{e}_1 \mid \mathbf{e}_2)$ and $(\partial_u W \quad \partial_v W) = (\beta^{-2}\mathcal{A}_1 W \quad \mathcal{A}_2 W)\,\mathbf{S}$ and where we recall from (86) that λ_k, $\mathbf{e}_k$ denote the eigenvalues and normalized eigenvectors of the local auxiliary-matrix $\mathbf{A}(|\mathcal{W}_\psi f|)(\mathbf{x}, s) = \mathbf{A}(|\mathcal{G}_\psi f|)(\mathbf{x}, s)$. In phase space, these eigenvectors (in $\mathbb{R}^2$) correspond to

$$\{\mathbf{e}_1, \mathbf{e}_2\} \leftrightarrow \{\partial_{\tilde{u}}, \partial_{\tilde{v}}\} = \{\mathcal{S} \circ \partial_u \circ \mathcal{S}^{-1}, \mathcal{S} \circ \partial_v \circ \mathcal{S}^{-1}\}\ ,$$

Consequently we indeed get the right correspondence between (87) and (85).

Theorem 27. *Let W be the solution of PDE-system (85). Let $\tilde{W}$ be the solution of PDE-system (87). Then*

$$\tilde{W}(\cdot,\cdot,t) = \mathcal{S} \circ W(\cdot,\cdot,\cdot,t) \text{ for all } t \geq 0.$$

Proof Via direct computations and conjugations we find

$$\begin{aligned} &\forall_{(p,q,s)\in H_r, t>0} : \quad \partial_t W(p,q,s,t) = \begin{pmatrix} \partial_u & \partial_v \end{pmatrix} \begin{pmatrix} \varepsilon & 0 \\ 0 & (1-\varepsilon)e^{-\frac{c}{(\lambda_1-\lambda_2)^2}} + \varepsilon \end{pmatrix} \begin{pmatrix} \partial_u \\ \partial_v \end{pmatrix} W(p,q,s,t) \Leftrightarrow \\ &\forall_{(p,q,s)\in H_r, t>0} : \quad \partial_t(\mathcal{S}^{-1}\tilde{W})(p,q,s,t) = \begin{pmatrix} \partial_u & \partial_v \end{pmatrix} \begin{pmatrix} \varepsilon & 0 \\ 0 & (1-\varepsilon)e^{-\frac{c}{(\lambda_1-\lambda_2)^2}} + \varepsilon \end{pmatrix} \begin{pmatrix} \partial_u \\ \partial_v \end{pmatrix} (\mathcal{S}^{-1}\tilde{W})(p,q,s,t) \quad \Leftrightarrow \\ &\forall_{(p,q,s)\in H_r, t>0} : \quad \partial_t(\mathcal{S}^{-1}\tilde{W})(p,q,s,t) = \begin{pmatrix} \partial_u & \partial_v \end{pmatrix} \mathcal{S}^{-1} \begin{pmatrix} \varepsilon & 0 \\ 0 & (1-\varepsilon)e^{-\frac{c}{(\lambda_1-\lambda_2)^2}} + \varepsilon \end{pmatrix} \mathcal{S} \begin{pmatrix} \partial_u \\ \partial_v \end{pmatrix} (\mathcal{S}^{-1}\tilde{W})(p,q,s,t) \Leftrightarrow \\ &\forall_{(p,q)\in\mathbb{R}^2, t>0} : \quad \partial_t \tilde{W}(p,q,t) = \begin{pmatrix} \partial_{\tilde{u}} & \partial_{\tilde{v}} \end{pmatrix} \begin{pmatrix} \varepsilon & 0 \\ 0 & (1-\varepsilon)e^{-\frac{c}{(\lambda_1-\lambda_2)^2}} + \varepsilon \end{pmatrix} \begin{pmatrix} \partial_{\tilde{u}} \\ \partial_{\tilde{v}} \end{pmatrix} \tilde{W}(p,q,t) \end{aligned}$$

so that the uniqueness of the solutions $\tilde{W}$ of (87) and W of (85) implies that

$$\tilde{W}(\cdot,\cdot,0) = \mathcal{G}_\psi f = \mathcal{S} \circ \mathcal{W}_\psi f = \mathcal{S} \circ W(\cdot,\cdot,\cdot,0) \Rightarrow \forall_{t\geq 0} : \tilde{W}(\cdot,\cdot,t) = \mathcal{S} \circ W(\cdot,\cdot,\cdot,t)\ ,$$

which shows the result. □

Clearly, Problem (87) is preferable over problem (85) if it comes to numerical schemes as it is a 2D-evolution.

See Figure 10 for an explicit example, where we applied adaptive nonlinear diffusion on the Gabor transform of a noisy chirp signal. Due to left-invariance of our diffusions the phase is treated appropriately and thereby the effective corresponding denoising operator on the signal is sensible. Moreover, the tails of the enhanced chirp are smoothly dampened.

12. Reassignment, Texture Enhancement and Frequency Estimation in 2D-images ($d = 2$)

In Section 6 we applied differential reassignment to 1D-signals. This technique can also be applied to Gabor transform of 2D-images. Here we choose for the second option in (46) as the corresponding algorithm is faster. In this case the reassigned Gabor transforms concentrate towards the lines $\{(p^1, p^2, q_1, q_2, s) \in H_5 \mid \partial_{p^i}|\mathcal{G}_\psi f|(p,q,s) = \partial_{q_i}|\mathcal{G}_\psi f|(p,q,s) = 0, i = 1,2, p = (p^1,p^2), q = (q_1,q_2) \in \mathbb{R}^2\}$, which coincides with the stationary solutions of the corresponding Hamilton Jacobi equation on the modulus. See Figure 11, where the amount of large Gabor coefficients is strongly reduced while maintaining the original image.

12.1. Left-invariant Diffusion on Phase Space as a Pre-processing Step for Differential Reassignment

Gabor transforms of noisy medical images often require smoothing as pre-processing before differential reassignment can be applied. Here we aim for pre-processing before reassignment rather than signal enhancement. The Dunford-Pettis Theorem [12] shows minor conditions for a linear operator on $\mathbb{L}_2(X)$, with X a measurable space, to be a kernel operator. Furthermore, all linear left-invariant kernel operators on $\mathbb{L}_2(H_r)$ are convolution operators. Next we classify all left-invariant kernel operators on phase space (i.e. all operators that commute with $\tilde{\mathcal{L}}_{(p,q,s)} := \mathcal{S}\mathcal{L}_{(p,q,s)}\mathcal{S}^{-1}$).

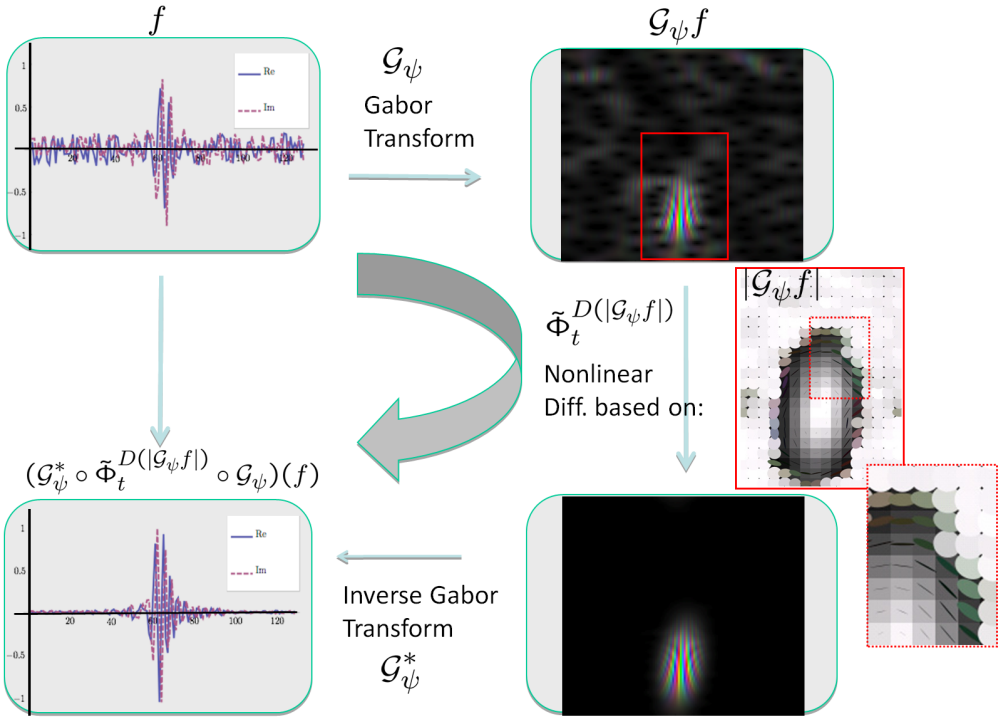

Figure 10: Illustration of the left-invariant diffusions on Gabor transforms that are adapted to the Hessian of the absolute value. The corresponding operator $f \mapsto \mathcal{G}_\psi^* \tilde{\Phi}_t^D \mathcal{G}_\psi$ in the signal domain smoothly enhances the signal without tresholding of Gabor coefficients. In the most right plot we depicted ellipses representing the local eigenvectors of the Hessian of $|\mathcal{G}_\psi|$ along which the diffusion locally takes place. The directions of the ellipses coincide with the eigenvectors of the Hessian, whereas the anisotropy of the ellipses is determined by the fraction $|\lambda_1/\lambda_2|$ of the eigenvalues $\{\lambda_1, \lambda_2\}$ with $|\lambda_1| > |\lambda_2|$, the colors indicate the directions of the largest eigenvector and the intensity reflects the relative damping factor $(p,q) \mapsto 1+\epsilon^{-1}(1-\epsilon)e^{-c(\lambda_1(p,q)-\lambda_2(p,q))^{-2}}\lambda_1(p,q)$ of the second eigenvector.

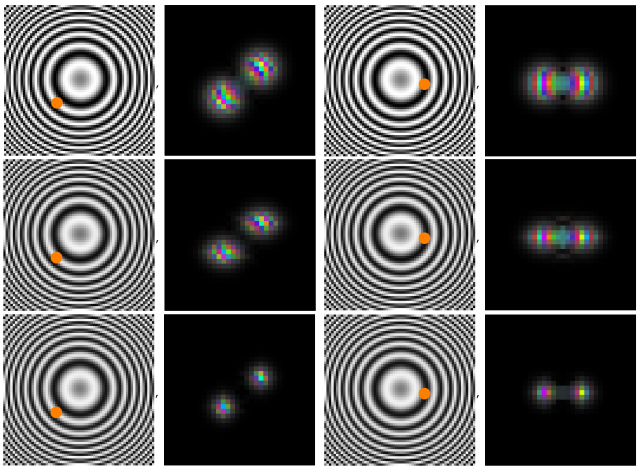

Figure 11: Application of re-assignment of Gabor transforms of 2D-images. The dot indicates the position $(p^1, p^2) \in \mathbb{R}^2$ in the image (left) where we depicted the local frequency distribution $(q^1, q^2) \mapsto \mathcal{G}_\psi f(p^1, p^2, q^1, q^2)$ (right) where we color-coded the phase. Top row input at two locations. Middle row output for $t = 0.1$. Bottom row output for $t = 4$. Further parameter settings: $a = 1$, $N = 64$, $K = M = 32$, $L = 2$, $D^{11} = D^{22} = 1$.

Lemma 28. *A kernel operator $\mathcal{K}_k : \mathbb{L}_2(\mathbb{R}^{2d}) \to \mathbb{L}_\infty(\mathbb{R}^{2d}) \cap \mathbb{L}_2(\mathbb{R}^{2d})$ given by*

$$(\mathcal{K}_k\tilde{U})(p,q) = \int_{\mathbb{R}^{2d}} \tilde{k}(p,q,p',q')\tilde{U}(p',q')\mathrm{d}p'\mathrm{d}q',$$

with $k \in \mathbb{L}_1(\mathbb{R}^{2d} \times \mathbb{R}^{2d})$ is left-invariant if

$$\tilde{k}(p,q,p',q') = e^{2\pi i\overline{q}(p'-p)}\tilde{k}(p+\overline{p},q+\overline{q},p'+\overline{p},q'+\overline{q}) \tag{88}$$

for almost every $(p,q),(p',q'),(\overline{p},\overline{q}) \in \mathbb{R}^{2d}$.

Proof We have $\tilde{\mathcal{L}}_g\tilde{U}(p',q') = (\mathcal{S}\tilde{\mathcal{L}}_g\mathcal{S}^{-1}\tilde{U})(p',q') = e^{2\pi is+\pi i(2qp'-pq)}\tilde{U}(p'-p,q'-q)$ so that

$$\begin{array}{l}(\mathcal{K}_k\mathcal{L}_g\tilde{U})(\tilde{p},\tilde{q}) = \int_{\mathbb{R}^{2d}} \tilde{k}(\tilde{p},\tilde{q},p',q')e^{2\pi is+\pi i(2qp'-pq)}\tilde{U}(p'-p,q'-q)\mathrm{d}p'\mathrm{d}q' \\ = e^{2\pi is}\int_{\mathbb{R}^{2d}} e^{\pi i(2q\tilde{p}-pq)}\tilde{k}(\tilde{p}-p,\tilde{q}-q,p'',q'')\tilde{U}(p'',q'')\mathrm{d}p''\mathrm{d}q'' = (\mathcal{L}_g\mathcal{K}_k\tilde{U})(\tilde{p},\tilde{q})\end{array}$$

from which the result follows by substitution $p'' = p'-p$, $q'' = q'-q$. □

Theorem 29. *Let $d \in \mathbb{N}$. Let Φ_t be a left-invariant semi-group operator on H_r given by*

$$(\Phi_t(U))(g) = (U * K_t)(g) := \int_{H_r} K_t(h^{-1}g)U(h)\,\mathrm{d}\mu(h)$$

with μ the left-invariant measure on H_r, $t > 0$. Then the corresponding operator on phase space $\tilde{\Phi}_t = \mathcal{S} \circ \Phi_t \circ \mathcal{S}^{-1}$ is given by

$$\begin{array}{l}(\tilde{\Phi}_t(\mathcal{G}_\psi f))(p,q) = \int\limits_{\mathbb{R}^d}\int\limits_{\mathbb{R}^d} \tilde{k}_t(p,q,p',q')\mathcal{G}_\psi f(p',q')\,\mathrm{d}p'\mathrm{d}q', \\ \text{with } \tilde{k}_t(p,q,p',q') = \int\limits_0^1 e^{-\pi ip'\cdot q'}K_t(p-p',q-q',\frac{-p\cdot q}{2}-s'-\frac{1}{2}(p\cdot q'-q\cdot p'))e^{-2\pi is'}\,\mathrm{d}s'.\end{array} \tag{89}$$

In particular, this applies to the hypo-elliptic diffusion kernel $K_t : H_r \to \mathbb{R}^+$ where the diffusion is generated by $D^{11}\sum\limits_{i=1}^{d}(\mathcal{A}_i)^2 + D^{22}\sum\limits_{i=d+1}^{2d}(\mathcal{A}_i)^2$.

Proof Eq. (89) follows by direct computation where we note $h^{-1} = (p',q',s')^{-1} = (-p',-q',-s')$ and taking the phase inside, which is possible since $(\mathcal{S}\mathcal{W}_\psi f)(p',q') = (\mathcal{G}_\psi f)(p',q')$ is independent of s'. The heat kernel on H_r is obtained by the heat kernel on H_{2d+1} via $K_t^{H_r}(p,q,s) = \sum\limits_{k\in\mathbb{Z}} K_t^{H_{2d+1}}(p,q,s+k)$. □

As the analytic closed form solution of this kernel is complicated, cf. [41, 23], we consider the well-known local analytic approximation

$$K_t(p,q,s) = \frac{c}{8t\sqrt{D^{11}D^{22}}}\frac{1}{(4\pi tc^{-1}D^{11})^{\frac{d}{2}}(4\pi tc^{-1}D^{22})^{\frac{d}{2}}}e^{-\left(\frac{|s|}{\sqrt{D^{11}D^{22}}}+\frac{\|p\|^2}{D^{11}}+\frac{\|q\|^2}{D^{22}}\right)\frac{c}{4t}}. \tag{90}$$

This approximation is due to the ball-box theorem [7] or theory of weighted sub-coercive operators on Lie groups [61], where we assign weights $w_i = 1$, $i = 1\ldots,2d$ and $w_{2d+1} = 2$ to the left-invariant vector fields $\{\mathcal{A}_1,\ldots,\mathcal{A}_{2d+1}\}$.

Lemma 30. *Let $K_t : H(2d+1) \to \mathbb{R}^+$ be given by Eq. (90). Then the corresponding kernel on phase space is given by*

$$\tilde{k}_t(p,q,p',q') = e^{-\left(\frac{\|p-p'\|^2}{D^{11}}+\frac{\|q-q'\|^2}{D^{11}}\right)\frac{c}{4t}}e^{-\pi i(p'-p)\cdot(q'+q)}\frac{\left(\frac{c}{4\pi t\sqrt{D^{11}D^{22}}}\right)^d}{1+64D^{11}D^{22}t^2c^{-2}}. \tag{91}$$

and satisfies Eq. (88).

Proof By Eq. (90) and Eq. (89) we find by substitution $v = s'-s-k+\frac{1}{2}(p\cdot q'-q\cdot p')$ that

$$\begin{array}{l}\tilde{k}_t(p,q,p',q') = e^{\pi i(p\cdot q'-q\cdot p')}e^{-2\pi s}e^{-ip'\cdot q'}\frac{c}{8t\sqrt{D^{11}D^{22}}}\frac{1}{(4\pi tc^{-1}D^{11})^{\frac{d}{2}}(4\pi tc^{-1}D^{22})^{\frac{d}{2}}}\cdot \\ \sum\limits_{k\in\mathbb{Z}}\int\limits_{s'-k+\frac{1}{2}(p\cdot q'-q\cdot p')}^{1+s'-k+\frac{1}{2}(p\cdot q'-q\cdot p')} e^{-|v|\frac{c}{4t\sqrt{D^{11}D^{22}}}}e^{-2\pi vi}\,\mathrm{d}v.\end{array}$$

The integral can be computed by means $\int_{\mathbb{R}} e^{-|v|\gamma}e^{-2\pi iv}\,\mathrm{d}v = \frac{2\gamma}{\gamma^2+4\pi^2}$ for $\gamma > 0$. The kernel in Eq.(91) satisfies the left-invariance constraint (88) since $-(\tilde{p}-\overline{p})(\tilde{q}+\overline{q}) = 2q(\tilde{p}-\overline{p}) - (\tilde{p}-\overline{p})(\tilde{q}+\overline{q}+2q)$ □

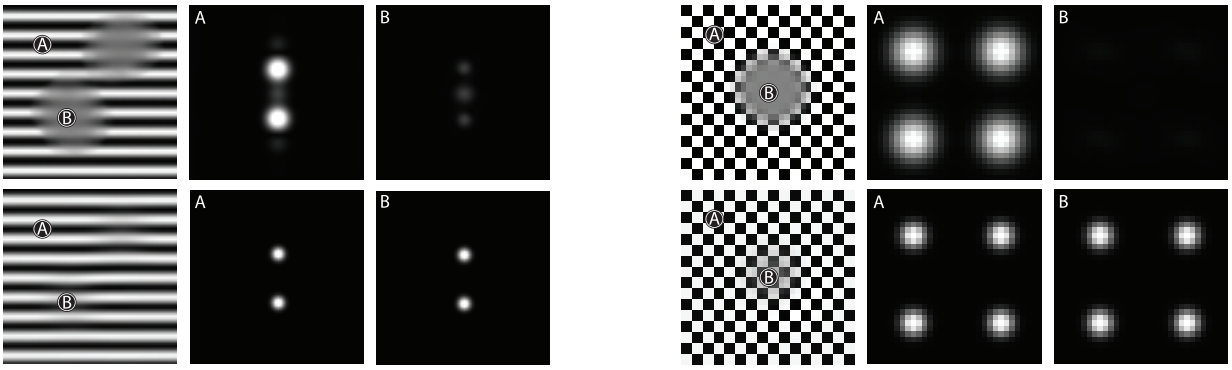

Figure 12: Top row: Input image f_i and two slices $|\mathcal{G}_\psi f_i(\mathbf{p}_k, \cdot, \cdot)|$, $k = 1, 2$, in the Gabor domain centered around the indicated positions. Bottom row: output in spatial and Gabor domain of linear diffusion combined with a squaring of the modulus. (Left: input image f_1, i.e. $i = 1$, right: input image f_2, i.e. $i = 2$). Similar to left-invariant diffusions on orientation scores where we can generically diffuse along crossing lines (Recall Figure 9) we can apply left-invariant diffusion on Gabor transforms and thereby diffuse along crossing frequencies.

12.1.1. Possible Extension to Texture Enhancement in 2D images via Left-invariant Evolutions

The techniques signal enhancement by non-linear left-invariant diffusion on Gabor transforms in Section 11 can be extended to enhancement of local 2D-frequency patterns and/or textures. This can have similar applications as the enhancement of lines via non-linear diffusion on invertible orientation scores, cf. [39, 26] and Figure 9. However, such an extension would yield a technical and slow algorithm. Instead, similar to our earlier works on contour enhancement via invertible orientation scores, cf. [24, 25], we can use the (more basic) concatenation of linear left-invariant diffusion and monotonic transformations in the co-domain. Figure 12 shows a basic experiment of such an approach.

12.2. Gabor Analysis Application: Cardiac Tagged MRI Images

In the limiting case (where the evolution time tends to infinity) differential reassignment concentrates around local maxima of the absolute value of a Gabor transform. These local maxima produce per position $(p^1, p^2) \in \mathbb{R}^2$ a local frequency $(q_1, q_2) \in \mathbb{R}^2$ estimation. In this section we briefly explain a 2D medical imaging application where local frequency estimation is important for measuring heart wall deformations during a systole. For more details, see [10].

Quantification of cardiac wall motion may help in (early) diagnosis of cardiac abnormalities such as ischemia and myocardial infarction. To characterize the dynamic behavior of the cardiac muscle, non-invasive acquisition techniques such as MRI tagging can be applied. This allows to locally imprint brightness patterns in the muscle, which deform accordingly and allow detailed assessment of myocardial motion. Several optical flow techniques have been considered in this application. However, as the constant brightness assumption [45, 9, 35] in this application is invalid, this approach requires the a concatenation of several rather technical procedures, [30, 4, 5, 36] yielding a complicated overall model and algorithm. For example, instead of tracking constant brightness one can track local extrema in scale space [48] (taking into account covariant derivatives and Helmholtz decomposition of the flow field [30]) or one can compute optical flow fields [36, 63] that follow equiphase lines, where the phase is computed by Gabor filtering techniques known as the harmonic phase method (HARP), cf. [56]. Gabor filtering techniques were also used in a recent applied approach [2] where one obtains cardiac wall deformations directly from local scalar-valued frequency estimations in tagging directions. Here we aim for a similar short-cut, but in contrast to the approach in [2] we extract the maxima from all Gabor transform coefficients producing per tagging direction and per time an accurate frequency covector field $\mathbf{q}^{t,i} = q_1^{t,i}\mathrm{d}x^1 + q_2^{t,i}\mathrm{d}x^2$ (not necessarily aligned with the tagging direction). From these covector fields one can deduce the required deformation gradients of the cardiac wall by duality as we explain next.

12.2.1. Frequency Fields from Tagged MRI Images

Let $f_t^{\theta_i} : \mathbb{R}^2 \to \mathbb{R}$ be the images corresponding to tag-direction $\theta_i \in [0, 2\pi)$, $i = 1, \ldots, N$, with $N \geq 2$ the total number of tags at time $t > 0$ corresponding to (independent) tag-direction $(\cos(\theta_i), \sin(\theta_i))$ with

$\theta_i \in [0, 2\pi)$. We compute the Gabor transforms $\mathcal{G}_\psi(f_t^{\theta_i}) : \mathbb{R}^4 \to \mathbb{C}$ and apply a linear left-invariant evolution and extract per position $\mathbf{p}$ the remaining maxima w.r.t. the frequency variable $\mathbf{q}$. For each position $\mathbf{p} = (p^1, p^2) \in \mathbb{R}^2$ the Gabor transform $\mathcal{G}_\psi(f_t^{\theta_i})(\mathbf{p}, \cdot)$ typically shows only two dominant, noisy blobs (for t small), cf. Figure 13. The 2 blobs relate to each other by reflection $\mathbf{q} \mapsto -\mathbf{q}$.

The best frequency estimates are obtained by extracting maxima after applying a large time evolution. By the results in [52] this maximum converges to the center of mass, which gives a sub-pixel accurate estimate. This yields per position $(p^1, p^2) \in \mathbb{R}^2$ and per tagging direction θ_i the local frequency estimate $\mathbf{q}^{t,i}(p^1, p^2) := \pm(q_1^{t,i}(p^1, p^2), q_2^{t,i}(p^1, p^2))$ that we store in a covector field

$$\mathbf{q}^{t,i} = q_1^{t,i} \mathrm{d}x^1 + q_2^{t,i} \mathrm{d}x^2,$$

where $\mathrm{d}x^1 = \mathrm{d}x$, $\mathrm{d}x^2 = \mathrm{d}y$.

12.2.2. Deformation Fields from Tagged MRI Images

Next we will derive a novel principle to compute deformation gradients from the frequency fields obtained from (dynamic) tagged MRI images obtained at discrete times $t \in \mathbb{N}$ (e.g. 30 time frames).

Regarding deformation gradients we first introduce some notation. Let $\chi_t : V_{t-1} \to V_t$ be the diffeomorphic warping of the cardiac wall (located at $V_t \subset \mathbb{R}^2$ at time t) in between two subsequent time frames. Suppose $\mathbf{x}_t \in \mathbb{R}^2$ denotes the position of a material point in the heart wall at time $t > 0$. Then in particular we have $\mathbf{x}_t = \chi_t(\mathbf{x}_{t-1})$. Now the objective is to estimate the deformation gradient field $D(\chi_t)$ from the frequency fields $\{\mathbf{q}^{t,i}(p^1, p^2), \mathbf{q}^{t-1,i}(p^1, p^2)\}_{i=1,\ldots,N}$.

To this end we impose the following duality principle

$$\langle (\chi_t)^* \mathbf{q}^{t,i}(\mathbf{x}_t), \mathbf{v} \rangle := \langle \mathbf{q}^{t,i}(\mathbf{x}_t), (\chi_t)_*(\mathbf{v}) \rangle = \langle \mathbf{q}^{t-1,i}(\mathbf{x}_{t-1}), \mathbf{v} \rangle \tag{92}$$

for all tangent vectors $\mathbf{v} \in T_{\mathbf{x}_{t-1}}(V_{t-1})$ (denoting the tangent space at $\mathbf{x}_{t-1} \in V_{t-1} \subset \mathbb{R}^2$). Here the push-forward[8] $(\chi_t)_*(\mathbf{v}) \in T_{\mathbf{x}_t}(V_t)$ of $\mathbf{v}$ is a tangent vector at $\mathbf{x}_t$, whereas the pull-back $(\chi_t)^* \mathbf{q}^{t,i}(\mathbf{x}_t)$ of $\mathbf{q}^{t,i}(\mathbf{x}_t)$ is a co-vector at $\mathbf{x}_{t-1}$. By means of the chain-law for differentiation (and the natural association of the push-forward $(\chi_t)_*$ to the deformation gradient $D(\chi_t)$) we have

$$\begin{gathered}
\sum_{k,j=1}^{2} q_j^{t,i}(\mathbf{x}_t)\, D_k^j(\mathbf{x}_{t-1})\, v^k = \sum_{j=1}^{2} q_j^{t,i}(\mathbf{x}_t)\, ((\chi_t)_*(\mathbf{v}))^j \\
= \langle \mathbf{q}^{t,i}(\mathbf{x}_t), (\chi_t)_*(\mathbf{v}) \rangle = \langle \mathbf{q}^{t-1,i}(\mathbf{x}_{t-1}), \mathbf{v} \rangle = \sum_{j=1}^{2} q_j^{t-1,i}(\mathbf{x}_{t-1})\, v^j \\
\Leftrightarrow \\
\mathbf{Q}_t(\mathbf{x}_t)\, \mathbf{D}_t(\mathbf{x}_{t-1})\, \mathbf{v} = \mathbf{Q}_{t-1}(\mathbf{x}_{t-1})\, \mathbf{v}
\end{gathered}$$

with $\mathbf{D}_t = [D_k^j] = \left[\frac{\partial x_t^j}{\partial x_{t-1}^k}\right] \in \mathbb{R}^{2\times 2}$ represents the deformation gradient matrix representing $D(\chi_t)$ expressed in the standard basis, $\mathbf{Q}_t = \left[q_j^{t,i}\right] \in \mathbb{R}^{N\times 2}$. Furthermore, $\mathbf{v} = (v^1, v^2)^T \in \mathbb{R}^2$ is a column vector representing the *arbitrary* vector $\mathbf{v} \in T_{\mathbf{x}_{t-1}}(V_{t-1})$. Consequently, we have

$$\mathbf{Q}_t(\mathbf{x}_t)\mathbf{D}_t(\mathbf{x}_{t-1}) = \mathbf{Q}_{t-1}(\mathbf{x}_{t-1}).$$

Provided that the frequency estimates are smooth and slowly varying with respect to the position variable one can apply first order Taylor expansion on the left-hand side and evaluate $\mathbf{Q}_t(\mathbf{x}_{t-1})$ instead of $\mathbf{Q}_t(\mathbf{x}_t)$. This corresponds to linear deformation theory, where $\mathbf{D}_t(\mathbf{x}_t) \approx \mathbf{D}_t(\mathbf{x}_{t-1})$ provided that displacements $\|\mathbf{x}_t - \mathbf{x}_{t-1}\|$ are small. Consequently, we use for each spatial position $\mathbf{x} \in \mathbb{R}^2$, the least squares solution of $\mathbf{Q}_t(\mathbf{x})\mathbf{D}_t(\mathbf{x}) = \mathbf{Q}_{t-1}(\mathbf{x})$ given by

$$\mathbf{D}_t(\mathbf{x}) = ((\mathbf{Q}_t(\mathbf{x}))^T \mathbf{Q}_t(\mathbf{x}))^{-1} (\mathbf{Q}_t(\mathbf{x}))^T \mathbf{Q}_{t-1}(\mathbf{x}) \tag{93}$$

as our deformation gradient estimate.

[8] Considering $\mathbf{v} \in T_{\mathbf{x}_{t-1}}(V_{t-1})$ as differential operator on locally defined smooth realvalued functions ϕ, the push-forward is defined by $((\chi_t)_*(\mathbf{v}))|_{\mathbf{x}_t = \chi_t(\mathbf{x}_{t-1})}(\phi) := \mathbf{v}(\phi \circ \chi_t)$, with $\phi \circ \chi_t$ locally defined around $\mathbf{x}_{t-1}$ and ϕ locally defined around $\mathbf{x}_t$. The corresponding pull-back acting on co-vector fields is defined by duality such as in the first equality in Eq. (92).

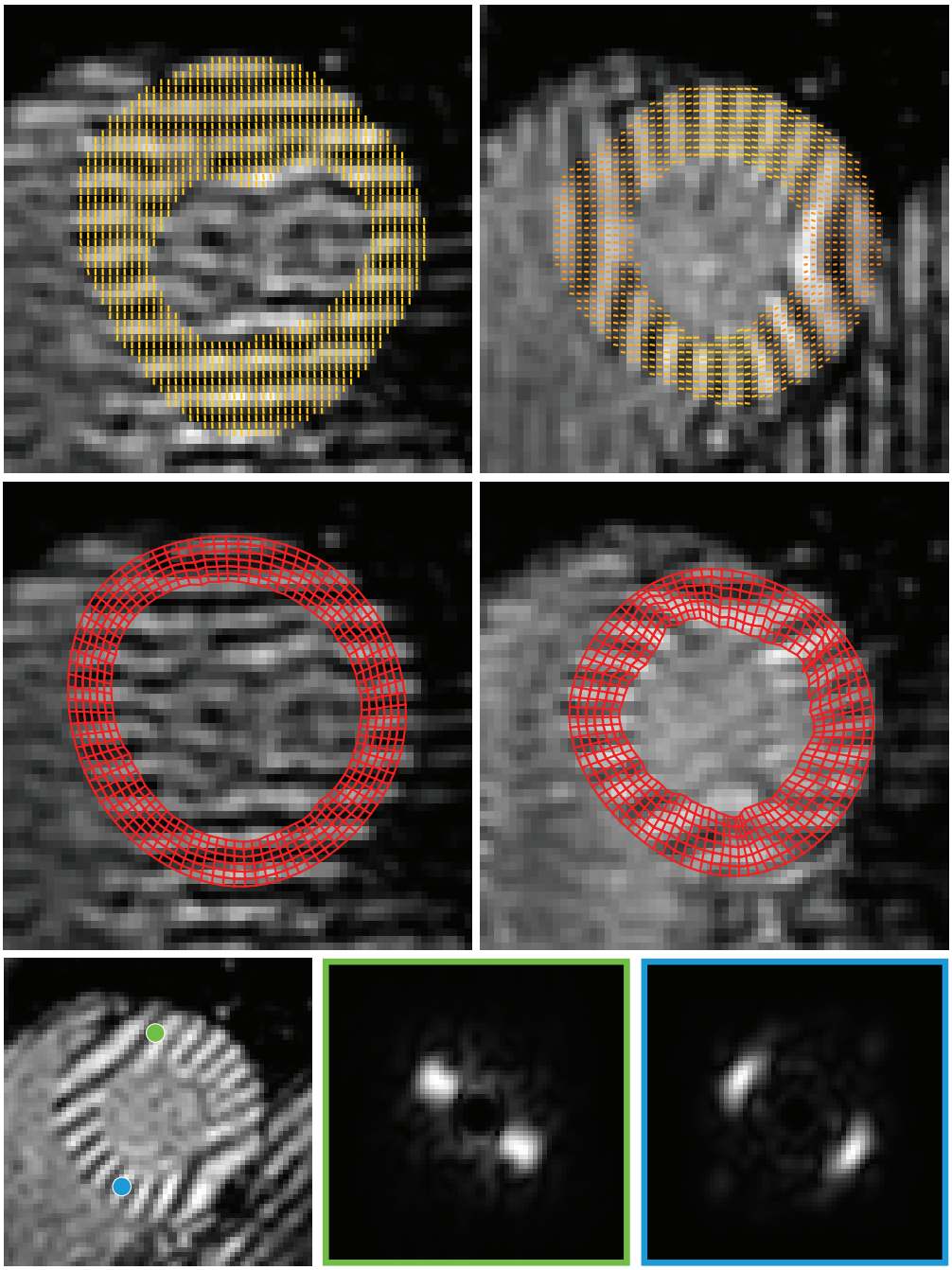

Figure 13: Top row: MRI-tagging images (on a 64×64-grid) at time frame $t = 2$ and time frame $t = 8$ (the cardiac cycle is sampled in 30 time frames), scanned in 4 tag-directions, i.e. $N = 4$. Left: horizontal tag $\theta_1 = 0$ at $t = 2$ with estimated frequency field $\mathbf{q}^{2,1}$, right: vertical tag $\theta_3 = \pi/2$ with estimated frequency field $\mathbf{q}^{8,3}$ plotted on top. In the frequency estimates we used maximum over-sampling $L = 1$, $K = 64$ in the discrete Gabor transform Eq. (52) with Gaussian window-size with a standard deviation of $\sigma = 6$ (pixel lengths). Middle row: Corresponding deformation nets computed from the frequency fields and outer boundary via Eq. (93) and Eq. (94) Bottom row: Plots of the absolute value of the Gabor transform $(q_1, q_2) \mapsto |\mathcal{G}_\psi f(p^1, p^2, q_1, q_2)|$ of MRI-tagging image f with orientation $\theta_2 = \pi/4$ restricted to the green and blue point (p^1, p^2) of interest. We have masked the low frequencies to show the 2 frequency blobs of the tagging lines.

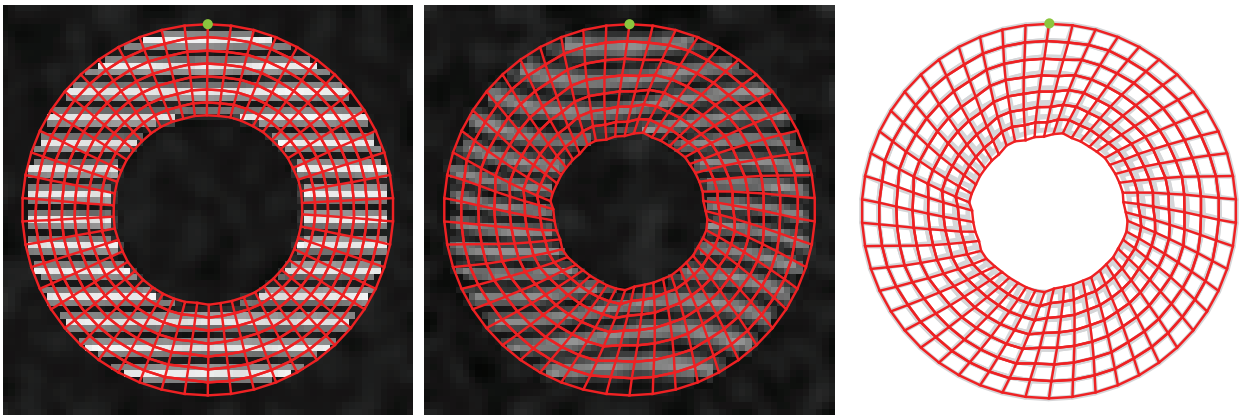

Figure 14: Ground truth phantom where the middle image at time $t > 0$ is obtained from the left image $t = 0$ via both non-uniform scaling and non-uniform rotation. The phantom includes a strong fading of the tag-line intensities in this phantom. The deformation net depicted on top in red is computed according to Eq. (94), with $N = 4$, $R = 8$ and $J = 50$. The deformation net is entirely computed from a single indicated material point at the boundary. The right image shows a comparison between the computed deformation net (red) with the ground-truth deformation net (grey).

12.3. Experiments: Deformation Nets on Tagged MRI Images

A deformation net is a means of approximating and visualizing deformations that are sufficiently close to the identity map. It is computed by fixing a polar grid and estimating the images of the gridpoints under the deformation. Displaying the estimated image of the grid yields an intuitive global visualization of the deformation, see Figure 14, and provides an easily evaluated approximation of the deformation by interpolation.

For experiments on a phantom with both considerable non-uniform scaling, fading, and non-uniform rotation see Figure 14. The iteratively computed deformation net is close to the ground truth deformation net.

The deformation nets are computed as follows. We fix a single material point at the boundary (the green point in Figure 14) and first compute the grid points on the outer contour in circumferential direction. From these points we compute the inner grid-points iteratively in inward radial direction. Let $\mathbf{x}_t^{r,j}$ denote the j-th grid-point in the deformation net at time $t > 0$ on the r-th closed contour. Let J denote the number of points on one closed circumferential contour and let R denote the number of points on a radial contour, let T be the total time (number of frames), then

$$\begin{array}{l}\text{Single material point } \mathbf{x}_t^{1,1} \text{ given for all } t \in \{0, \dots T-1\},\\ \text{Initial polar grid } \mathbf{x}_0^{r,j} \text{ given for all } r \in \{1, \dots R\}, j \in \{1, \dots J\},\\ \text{Deformation field } D_t \text{ computed for all } t \geq 0 \text{ from the local frequency fields } \{\mathbf{q}^{t,i}\}_{i=1}^N \text{ via Eq. (93)},\\ \text{Then for } t = 1 \text{ to T-1 do}\\ \text{for } j = 1 \text{ to J compute } \mathbf{x}_t^{1,j+1} := \mathbf{x}_t^{1,j} + \mathbf{D}_t|_{\mathbf{x}_t^{1,j}} (\mathbf{x}_{t-1}^{1,j+1} - \mathbf{x}_{t-1}^{1,j}),\\ \text{for } r = 1 \text{ to R compute } \mathbf{x}_t^{r+1,j} := \mathbf{x}_t^{r,j} + \mathbf{D}_t|_{\mathbf{x}_t^{r,j}} (\mathbf{x}_{t-1}^{r+1,j} - \mathbf{x}_{t-1}^{r,j}).\end{array} \tag{94}$$

In contrast to well-established optical flow methods, [45, 53, 9, 36, 35, 63] this method is robust with respect to inevitable fading of the tag-lines, and can be applied directly on the original MRI-tagging images without harmonic phase or sine phase pre-processing [56, 36]. Some of the optic flow methods, such as [49, 6, 21], do allow direct computation on the original MRI-tagging images as well, but they are relatively expensive, complicated and technical, e.g. [30].

First experiments show that our method can handle relatively large nonlinear deformations in both radial and circumferential direction. The frequency and deformation fields look very promising from the qualitative viewpoint, e.g. Figure 14 and Figure 13. Quantitative comparisons to other methods such as [2, 62, 37] and investigation of the reliability of the frequency estimates (and their connection to left-invariant evolutions on Gabor transforms) are interesting topics for future work.

13. Conclusion

We have presented a novel systematic approach to the design, implementation and analysis of left-invariant evolution schemes acting on Gabor transform, primarily for applications in signal and image analysis. In order to obtain a translation and modulation invariant operator on the space of signals, the corresponding operator on the reproducing kernel space of Gabor transforms must be left invariant, i.e. it should commute with the left regular action of the reduced Heisenberg group H_r. By using the left-invariant vector fields on H_r in the generators of our left-invariant evolution equations on Gabor transforms, we naturally employ the essential group structure on the domain of a Gabor transform. In our design for left-invariant evolutions on Gabor transforms we distinguished between two different tasks:

1. Non-linear adaptive left-invariant convection (reassignment) to sharpen Gabor transforms, while maintaining the original signal.
2. Signal/image enhancement via left-invariant diffusion on the corresponding Gabor transform.

We have provided differential geometrical underpinning, numerical experiments, analytical evidence and explicit comparisons of our methods.

The numerical implementation of such methods requires adaptation to the discrete (respectively finite) setting where we used quadratic forms on left-invariant shifts on discrete (respectively finite) Heisenberg groups. The continuous PDE-setting then follows by a limit of the discrete setting.

Regarding the first task we have included a differential geometrical understanding of the Cauchy-Riemann relations that hold for Gabor transforms with Gaussian windows. These relations are exploited in our numerical algorithms. Furthermore, we have provided a complete analytic description of differential reassignment of Gabor transforms of chirp signals, where we analyzed the collapsing of iso-contours in the absolute value of the Gabor transform towards the expected straight line in the Gabor domain.

Regarding the second task we have only included basic numerical experiments that indicate potential benefits for texture and frequency enhancement via left-invariant nonlinear diffusions on Gabor transforms. The benefit is similar to our previous work on enhancement of crossing elongated structures in 2D images (via left-invariant diffusion on orientation scores) as the left-invariant diffusions on Gabor transforms allow us to enhance crossing frequencies in the image domain. The idea seems promising and needs further investigation (e.g. efficiency of the involved algorithm, extend the techniques in section 11, Figure 10, to $d = 2$).

Finally, we have presented a novel and effective Gabor technique for deriving cardiac wall deformations in cardiac MRI. This technique is based on a basic duality principle (Eq. (92)) that relates frequency fields in MRI tagging (with multiple tagging directions) to deformations.

Despite the fact that Gabor transforms are widely used in 1D-signal processing, they are less common in 2D-imaging. However, the results in this article indicates applications of both Gabor transforms and the left-invariant evolutions acting on them in 2D-image processing.

Acknowledgements The authors gratefully acknowledge Jos Westenberg (Leiden University Medical Center) for providing us the MRI-tagging data sets that were acquired in 4 different tagging directions. Thanks are also due to the referees for their constructive criticism and detailed comments.

Appendix A. Proof of Theorem 1

For notational convenience we shall restrict ourselves to $d = 1$ as the general case follows similarly. First we shall show that $g\,\gamma^e_{\mathcal{U}_{g^{-1}f}}(t) = \gamma^g_f(t)$ for all $g \in H_r$ and all $t > 0$ and all $f \in \mathbb{L}_2(\mathbb{R})$. To this end we note that both solutions are horizontal curves, i.e.

$$\langle \mathrm{d}\mathcal{A}^3\big|_{\gamma^g_f(t)}, \dot{\gamma}^g_f(t)\rangle = \langle \mathrm{d}\mathcal{A}^3\big|_{g\,\gamma^e_{\mathcal{U}_{g^{-1}f}}(t)}, g\,\dot{\gamma}^e_{\mathcal{U}_{g^{-1}f}}(t)\rangle = 0,$$

where $\mathrm{d}\mathcal{A}^3 = \mathrm{d}s + 2(p\mathrm{d}q - q\mathrm{d}p)$. So it is sufficient to check whether the first two components of the curves coincide. Let $g = (p, q, s) \in H_r$ and define $p_e : \mathbb{R}^+ \to \mathbb{R}$, $q_e : \mathbb{R}^+ \to \mathbb{R}$ and $p_g : \mathbb{R}^+ \to \mathbb{R}$, $q_g : \mathbb{R}^+ \to \mathbb{R}$ by

$$\begin{aligned} p_e(t) &:= \langle \mathrm{d}p, g\,\dot{\gamma}^e_{\mathcal{U}_{g^{-1}f}}(t)\rangle\ , \quad p_g(t) := \langle \mathrm{d}p, \dot{\gamma}^g_f(t)\rangle\ , \\ q_e(t) &:= \langle \mathrm{d}q, g\,\dot{\gamma}^e_{\mathcal{U}_{g^{-1}f}}(t)\rangle\ , \quad q_g(t) := \langle \mathrm{d}q, \dot{\gamma}^g_f(t)\rangle\ , \end{aligned}$$

then it remains to be shown that $p_e + p = p_g$ and $p_e + q = q_g$. To this end we compute

$$\tfrac{dp_e}{dt}(t) = a^1(|\mathcal{W}_\psi \mathcal{U}_{g^{-1}} f|)(p_e(t), q_e(t)) = a^1(|\mathcal{L}_{g^{-1}} \mathcal{W}_\psi f|)(p_e(t), q_e(t)) = a^1(|\mathcal{W}_\psi f|)(p_e(t) + p, q_e(t) + q),$$

so that we see that $(p_e + p, q_e + q)$ satisfies the following ODE system:

$$\begin{cases} \frac{d}{dt}(p + p_e)(t) & = a^1(|\mathcal{W}_\psi f|)\,(p_e(t) + p, q_e(t) + q), \qquad t > 0, \\ \frac{d}{dt}(q + q_e)(t) & = a^2(|\mathcal{W}_\psi f|)\,(q_e(t) + q, q_e(t) + q), \qquad t > 0, \\ p + p_e = p, & \\ q + q_e = q. & \end{cases}$$

This initial value problem has a unique smooth solution, so indeed $p_g = p + p_e$ and $q_g = q + q_e$. Finally, we have by means of the chain-rule for differentiation:

$$\begin{aligned} \tfrac{d}{dt}(\mathcal{W}_\psi f)(\gamma_f^g(t)) &= \sum_{i=1}^{2} \langle \mathrm{d}\mathcal{A}^i\big|_{\gamma_f^g(t)}, \dot{\gamma}_f^g(t) \rangle \;\; (\mathcal{A}_i|_{\gamma_f^g(t)}\, \mathcal{W}_\psi f\Big)\,(\gamma_f^g(t)) \\ &= \dot{p}_g(t) \;\; \mathcal{A}_1|_{\gamma_f^g(t)}\, \mathcal{W}_\psi f(\gamma_f^g(t)) + \dot{q}_g(t) \;\; \mathcal{A}_2|_{\gamma_f^g(t)}\, \mathcal{W}_\psi f(\gamma_f^g(t)) \\ &= -a^1(|\mathcal{W}_\psi f|)(p_g(t), q_g(t))\; \mathcal{A}_1|_{\gamma_f^g(t)}\, \mathcal{W}_\psi(\gamma_f^g(t)) \\ &\qquad -a^2(|\mathcal{W}_\psi f|)(p_g(t), q_g(t))\; \mathcal{A}_2|_{\gamma_f^g(t)}\, \mathcal{W}_\psi(\gamma_f^g(t))\;. \end{aligned}$$

from which the result follows □

Appendix B. Existence and Uniqueness of the Evolution Solutions

The convection diffusion systems (20) have unique solutions, since the coefficients a_i and D_{ij} depend smoothly on the modulus of the initial condition $|\mathcal{W}_\psi f| = |\mathcal{G}_\psi f|$. So for a given initial condition $\mathcal{W}_\psi f$ the left-invariant convection diffusion generator $Q(|\mathcal{W}_\psi f|, \mathcal{A}_1, \ldots, \mathcal{A}_{2d})$ is of the type

$$Q(|\mathcal{W}_\psi f|, \mathcal{A}_1, \ldots, \mathcal{A}_{2d}) = \sum_{i=1}^{d} \alpha_i \mathcal{A}_i + \sum_{i,j=1}^{d} \mathcal{A}_i \beta_{ij} \mathcal{A}_j.$$

Such hypo-elliptic operators with almost everywhere smooth coefficients given by $\alpha_i(p,q) = a_i(|\mathcal{G}_\psi f|)(p,q)$ and $\beta_{ij}(p,q) = D_{ij}(|\mathcal{G}_\psi f|)(p,q)$ generate strongly continuous, semigroups on $\mathbb{L}_2(\mathbb{R}^2)$, as long as we keep the functions α_i and β_{ij} fixed, [60, 44], yielding unique solutions where at least formally we may write

$$W(p,q,s,t) = \Phi_t(\mathcal{W}_\psi f)(p,q,s) = e^{t\left(\sum_{i=1}^{d} \alpha_i \mathcal{A}_i + \sum_{i,j=1}^{d} \mathcal{A}_i\, \beta_{ij}\, \mathcal{A}_j\right)} \mathcal{W}_\psi f(p,q,s)$$

with $\lim_{t \downarrow 0} W(\cdot, t) = \mathcal{W}_\psi f$ in $\mathbb{L}_2$-sense. Note that if ψ is a Gaussian kernel and $f \neq 0$ the Gabor transform $\mathcal{G}_\psi f \neq 0$ is real analytic on $\mathbb{R}^{2d}$, so it can not vanish on a set with positive measure, so that $\alpha_i : \mathbb{R}^2 \to \mathbb{R}$ are almost everywhere smooth. This applies in particular to the first reassignment approach in (46) (mapping everything consistently into phase space using Theorem 5), where we have set $D = 0$, $a_1(|\mathcal{G}_\psi f|) = \mathcal{M}(|\mathcal{G}_\psi f|)|\mathcal{G}_\psi f|^{-1}\partial_p|\mathcal{G}_\psi f|$ and $a_2(|\mathcal{G}_\psi f|) = \mathcal{M}(|\mathcal{G}_\psi f|)|\mathcal{G}_\psi f|^{-1}\partial_q|\mathcal{G}_\psi f|$. In the second approach in (46) the operator $\tilde{U} \mapsto \tilde{\mathcal{C}}(\tilde{U})$ is non-linear, left-invariant and maps the space $\mathbb{L}_2^+(\mathbb{R}^2) = \{f \in \mathbb{L}_2(\mathbb{R}^2) \mid f \geq 0\}$ into itself again. In these cases the erosion solutions (48) are the unique viscosity solutions, of (45), see [17].

Remark 31. *For the diffusion case, [29, ch:7], [47, ch:6], we have $D = [D_{ij}]_{i,j=1,\ldots,2d} > 0$, in which case the (horizontal) diffusion generator $Q(|\mathcal{W}_\psi f|, \mathcal{A}_1, \ldots, \mathcal{A}_{2d})$ on the group is hypo-elliptic, whereas the corresponding generator $\tilde{Q}(|\mathcal{G}_\psi f|, \tilde{\mathcal{A}}_1, \ldots, \tilde{\mathcal{A}}_{2d})$ on phase space is elliptic. By the results [32, ch:7.1.1] and [51] there exists a unique weak solution $\tilde{W} = \mathcal{S}W \in \mathbb{L}_2(\mathbb{R}^+, \mathbb{H}_1(\mathbb{R}^2)) \cap \mathbb{H}_1(\mathbb{R}^+, \mathbb{L}_2(\mathbb{R}^2))$. By means of the combination of Theorem 3 and Theorem 5 we can transfer the existence and uniqueness result for the elliptic diffusions on phase space to the existence and uniqueness result for the hypo-elliptic diffusions on the group H_r (that is via conjugation with $\mathcal{S}$).*

Appendix C. Derivation of the Exact Eroded Gabor Transform of a Chirp Signal and the Proofs of Theorems 25 and 26

First we provide some preparations for the computation of $\Xi_t^{1,\frac{1}{2}} f$, that is in Lemma 32 we compute the eigen values of $\mathrm{Re}(B_{r,b})$ that appears in the modulus of the Gabor transform of a chirp. Subsequently, in Lemma 33 we address a technical issue related to a branching problem in the Euler-Lagrange problem in the erosion operator included in $\Xi_t^{1,\frac{1}{2}} f$. This branching problem is relevant in the proof of Theorem 25 and it is illustrated in Figure C.16. After these two preparations we provide the actual proof of Theorem 25, in Appendix C.1 where the full derivation of $(p,q,s) \mapsto \Xi_t^{1,\frac{1}{2}} f(p,q,s)$ is given. Finally, in Appendix C.3 we provide the proof of Theorem 26.

Lemma 32. *Let λ_1, λ_2 denote the eigenvalues (with $|\lambda_1| < |\lambda_2|$) of $Re(B_{r,b})$ with respective normalized eigenvectors $\boldsymbol{k}_1$ and $\boldsymbol{k}_2$. Then each vector in $\mathbb{R}^2$ can be written as $(p,q) = \alpha_1(p,q)\boldsymbol{k}_1 + \alpha_2(p,q)\boldsymbol{k}_2$. One has*

$$\begin{aligned}
\lambda_1 &= \tfrac{1}{d_{br}} \left(-1 - 4b^2\pi(1+\pi(b^2+r^2)) + \sqrt{(\pi r b^4)^2 + \tfrac{1}{4}\left(\tfrac{1}{4\pi} + b^2\pi(r^2-b^2)\right)^2} \right) , \\
\lambda_2 &= \tfrac{1}{d_{br}} \left(-1 - 4b^2\pi(1+\pi(b^2+r^2)) - \sqrt{(\pi r b^4)^2 + \tfrac{1}{4}\left(\tfrac{1}{4\pi} + b^2\pi(r^2-b^2)\right)^2} \right) , \\
\alpha_1(p,q) &= N_{br}^1 \, d_{br} \left(\tfrac{4b^4\pi^2 r}{c_{br}} p + \left(\tfrac{1}{2} - \left(\tfrac{-1+4b^2\pi(b^2-r^2)}{c_{br}} \right) \right) q \right) , \\
\alpha_2(p,q) &= N_{br}^2 \, d_{br} \left(-\tfrac{4b^4\pi^2 r}{c_{br}} p + \left(\tfrac{1}{2} + \left(\tfrac{-1+4b^2\pi(b^2-r^2)}{c_{br}} \right) \right) q \right) ,
\end{aligned}$$

with $d_{br} = r^2 b^4 + (b^2 + \frac{1}{2\pi})^2$ and

$$\begin{aligned}
c_{br} &= \sqrt{1 + 8b^2\pi^2(r^2 + b^2(-1 + 2\pi^2(b^4 + 2b^2(2b^2-1)r^2 + r^4)))} , \\
N_{br}^k &= \sqrt{1 + \tfrac{|1 - 4b^4\pi^2 + 4b^2\pi^2 r^2 (-1)^k c_{br}|^2}{64\pi^4 b^8 r^2}} \text{ for } k = 1,2.
\end{aligned} \tag{C.1}$$

We omit the proof as the result follows by direct computation.

Lemma 33. *Consider the ellipsoidal isolines given by*

$$\{(p',q') \in \mathbb{R}^2 \mid (p',q') B_{r,b}(p',q')^T = \lambda_1 |\alpha_1(p',q')|^2 + \lambda_2 |\alpha_2(p',q')|^2 = c\},$$

with $c > 0$ arbitrary. Consider the line spanned by the principal direction with smallest absolute eigenvalue. Applying the settings of Lemma 32 this line is given by $\alpha_2(p',q') = 0$. Consider another point (p,q) on this line, i.e. $\alpha_2(p,q) = 0 \Leftrightarrow p = \tau q$, with $p > 0$. Then there exists a unique $p^* = p^*(p,p\tau) = \frac{p}{1 - \frac{\sigma}{1+\tau^2}}$ such that the circle $(p-p^*)^2 + (\tau p - \tau p^*)^2 = t^2$ is tangent to one of the ellipses $(p',q')B_{r,b}(p',q')^T = \lambda_1|\alpha_1(p',q')|^2 + \lambda_1|\alpha_2(p',q')|^2 = c$ in $(p^*, \tau p^*)$. The corresponding time equals

$$t_{max}(p,p\tau) = \sqrt{1+\tau^2}\,\sqrt{(p-p^*(p,q))^2} = \frac{\sqrt{\sigma}|p|}{\left|1 - \sqrt{\frac{\sigma}{1+\tau^2}}\right|}.$$

where the constants σ and τ are given by

$$\begin{aligned}
\sigma &= b^4 \left(4\tfrac{N_{br}^2}{N_{br}^1}\right)^2 \pi^2 r \, \tfrac{c_{br} d_{br} (-1+c_{br}+4b^2\pi^2(b-r)(b+r))(1+c_{br}+4b^2\pi(1+\pi(b^2+r^2)))}{((1+c_{br}-4b^4\pi^2)^2 + 8b^2\pi^2(1+c_{br}+4b^4(-1+2b^2)\pi^2)r^2 + 16b^4\pi^4 r^4)^{\frac{3}{2}} (1-c_{br}+4b^2\pi(1+\pi(b^2+r^2)))}, \\
\tau &= \tfrac{4b^4\pi^2 r}{c_{br}/2 - 1 + 4b^2\pi(b^2-r^2)},
\end{aligned}$$

with the values obtained in Lemma 32, Eq. (C.1)

Proof In order to have the circle touching the ellipse in $(p^*, \tau p^*)$, we have to solve the following system

$$\begin{aligned}
&\alpha_2(p',q') = 0, \\
&(p-p')^2 + (q-q')^2 = t^2, \\
&\kappa^2(p',q') = \tfrac{1}{t^2}.
\end{aligned}$$

The curvature along isocontours of $u(p,q) = (p',q')B_{r,b}(p',q')^T$ is expressed as

$$\begin{array}{l}\kappa(p',q') = -\frac{1}{\left(\left(\frac{\partial u(p',q')}{\partial p'}\right)^2+\left(\frac{\partial u(p',q')}{\partial q'}\right)^2\right)^{\frac{3}{2}}}\cdot \\ \left(\frac{\partial u(p',q')}{\partial q'}\frac{\partial^2 u(p',q')}{\partial p'^2} - 2\frac{\partial u(p',q')}{\partial q'}\frac{\partial u(p',q')}{\partial p'}\frac{\partial^2 u(p',q')}{\partial p'\partial q'} + \left(\frac{\partial u(p',q')}{\partial p'}\right)^2\frac{\partial^2 u(p',q')}{\partial q'^2}\right) = \sigma^{-1/2}(p')^{-1}\end{array} \tag{C.2}$$

then along $\mathbf{k}_1$ we have $\alpha_2(p',q') = 0$ i.e. $q' = \tau p'$ and substitution in (C.2) yields

$$\kappa^{-2}(p',\tau p') = (p')^2\,\sigma = t^2 = (p-p')^2 + (q-q')^2 = (p-p')^2(1+\tau^2)$$

this yields $p'(p,\tau p) = \frac{p}{1\pm\sqrt{\frac{\sigma}{1+\tau^2}}}$, so since $p^* \geq p$ we find $p^*(p,p\tau) = \frac{p}{1-\sqrt{\frac{\sigma}{1+\tau^2}}}$. □

Appendix C.1. ***Proof of Theorem 25***

In case $\eta = \frac{1}{2}$ we have (up to scalar multiplication)

$$(k_t^{\frac{1}{2}} \ominus |\mathcal{W}_\psi f(\cdot,\cdot,s)| \quad \equiv \min_{(p-p')^2+(q-q')^2<t^2} e^{(p',q')\mathrm{Re}(B_{r,b})(p',q')^T} = e^{\left(\min\limits_{(p-p')^2+(q-q')^2<t^2}(p',q')\mathrm{Re}(B_{r,b})(p',q')^T\right)}, \tag{C.3}$$

where we recall that the absolute value $|\mathcal{W}_\psi f(\cdot,\cdot,s)|$ is independent of $s > 0$. Now $\mathrm{Re}(B_{r,b}) < 0$, hence the minimum of the associated continuous function can be found on the boundary of the convex domain. Application of Euler-Lagrange yields the system

$$\begin{array}{l}\mathrm{Re}(B_{r,b})\begin{pmatrix} p' \\ q' \end{pmatrix} = \lambda_t(p,q)\begin{pmatrix} p'-p \\ q'-q \end{pmatrix}, \\ (p-p')^2 + (q-q')^2 = t^2.\end{array} \tag{C.4}$$

First we must find the Euler-Lagrange multipliers $\lambda_t(p,q)$. If $\lambda_t := \lambda_t(p,q)$ is not an eigenvalue of $\mathrm{Re}(B_{r,b})$ the resolvent $(\mathrm{Re}(B_{r,b}) - \lambda_t I)^{-1}$ exists and one finds

$$t^2 = \|\mathrm{Re}(B_{r,b})(\mathrm{Re}(B_{r,b}) - \lambda_t I)^{-1}(p,q)^T\|^2,$$

which yields the 4th-order polynomial equation (78), where we note that $(p,q) = \sum_{k=1}^2 \alpha_k(p,q)\mathbf{k}_k$ with $(\mathbf{k}_i,\mathbf{k}_j) = \delta_{ij}$ so that

$$t^2 = \|\mathrm{Re}(B_{r,b})(\mathrm{Re}(B_{r,b}) - \lambda_t I)^{-1}(p,q)^T\|^2 = \sum_{k=1}^2 \left|\frac{\lambda_k\alpha_k(p,q)}{\lambda_k - \lambda_t(p,q)}\right|^2. \tag{C.5}$$

Now that the (four, three or two) Lagrange multipliers are known, we select the one associated to the global minimum and the general solution is given by

$$e^{(\lambda_t(p,q))^2(p,q)(\mathrm{Re}(B_{r,b})-\lambda_t I)^{-1}\mathrm{Re}(B_{r,b})(\mathrm{Re}(B_{r,b})-\lambda_t I)^{-1}}, \tag{C.6}$$

and substitution of $(p,q) = \sum_{i=1}^2 \alpha_i(p,q)\mathbf{k}_i$ straightforwardly yields the first case in (77). The scaling relation (70) now directly follows by (C.6) and $\alpha_i(\zeta p,\zeta q) = \zeta\alpha_i(p,q)$, for all $i = 1,2$, $(p,q) \in \mathbb{R}^2$ and $\zeta > 0$.

In case $\lambda_t(p,q)$ is equal to an eigenvalue of $\mathrm{Re}(B_{r,b})$, say λ_l then (C.4) yields $\lambda_k\alpha_k(p',q') = \lambda_t(p,q)(\alpha_k(p',q') - \alpha_k(p,q))$, $k = 1,2$, from which we deduce that Eq. (78) is still valid if the resolvent does not exist, since then $\lambda_t(p,q) = \lambda_l \Rightarrow \alpha_l(p,q) = 0$. If $\alpha_l(p,q) = 0$ then (p,q) is aligned with the $(3-l)$-th principal axis of the ellipses $\{(p,q) \in \mathbb{R}^2 \mid (p,q)\mathrm{Re}(B_{r,b})(p,q)^T = c\}$, $c > 0$ and the minimum $e^{(t+|\alpha_{3-l}|)^2\lambda_{3-l}}$ is obtained at $(p',q') = (p,q) + t\mathrm{sgn}(\alpha_{3-l}(p,q))\mathbf{k}_{3-l} = (\alpha_{3-l}(p,q) + t\mathrm{sgn}(\alpha_{3-l}))\,\mathbf{k}_{3-l}$, where only for $l = 2$ we get the extra condition $t \leq t_{\max}(p,p\tau)$. See the second row of Figure C.16, where in the third column t is chosen slightly larger than $t_{\max}(p,p\tau)$. One can see that the minimum moves along the straight main principal direction until $(p^*(p,\tau p),\tau p^*(p,\tau p))$ is reached at time $t_{\max}(p,p\tau)$, where the single minimum is cut into two minima that evolve to the side.

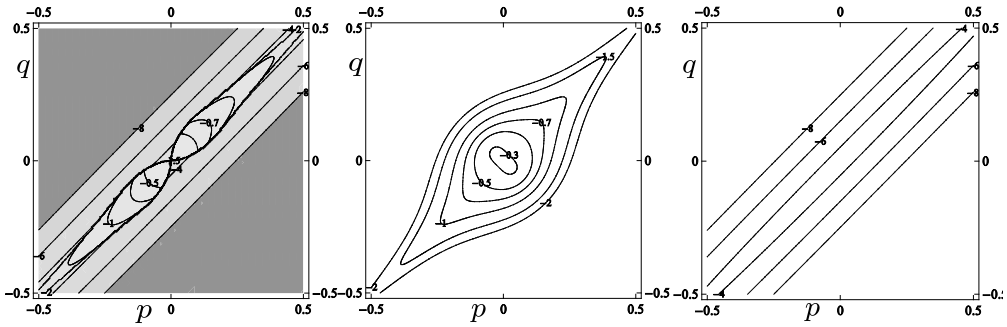

Figure C.15: The Lagrange multiplier $\lambda_t(p,q)$ for $(b,r,t) = (1,1,0.1)$ used in exact $\Xi_t^{1,1} f$, cf. Figure 8 and the corresponding approximations, in Eq. (C.8) for respectively $t > t_{\max(p,q)}$ and $t \leq t_{\max(p,q)}$ (where we have set $c = \frac{1}{2}$).

For the $l = 2$-case $\alpha_2(p,q) = 0$ (and $t \leq t_{\max}(p, p\tau)$) and the $l = 1$-case $\alpha_1(p,q) = 0$, see respectively first and second row of Figure C.16. In these cases we find (by Eq. (C.5)) the Lagrange multiplier

$$\alpha_l = 0 \Rightarrow \lambda_t = (1 + \frac{|\alpha_{3-l}|}{t})\lambda_{3-l} \tag{C.7}$$

which shows us that we indeed have a continuous transition of the solution across the principle directions in Eq. (77). Finally, we note that along the ray $\mathbb{R}^+ \ni \mu \mapsto (1+\mu)(p^*(p,p\tau), \tau p^*(p,p\tau))$ there do not exist global minimizers of the optimization problem given by (C.3). □

Appendix C.2. An Approximation of $\Xi_t^{1,\frac{1}{2}}$ and a Corollary of Theorem 25

Remark 34. *We did not succeed in finding more tangible exact closed form expressions than the general tedious Gardano formula for the Lagrange-multipliers $\lambda_t(p,q)$ which are zeros of the fourth order polynomial given by Eq. (78). For a plot of the graph of $(p,q) \mapsto \lambda_t(p,q)$, for $(b,r) = (\frac{1}{2}, 1)$, see Figure C.15. These plots do suggest a close approximation of the type*

$$\lambda_t(p,q) \approx \begin{cases} \lambda_1 \left(1 + t^{-1}\sqrt{|\alpha_1(p,q)|^2 + |\alpha_2(p,q)|^2 \left(\frac{|\alpha_2(p,q)|^2 + |\alpha_1(p,q)|^2}{t^2}\right)^{\frac{3}{2}}}\right) & \text{for } t_{max}(p,q) < t \\ \lambda_2 \left(1 + t^{-1}\sqrt{|\alpha_2(p,q)|^2 + c^2 \frac{|\lambda_1|^2}{|\lambda_2|^2}|\alpha_1(p,q)|^2}\right) & \text{for } t_{max}(p,q) \geq t\ , \end{cases} \tag{C.8}$$

with $c \in (0,1]$, where we recall that $t_{max}(p,q)$ is defined in Theorem 25. This approximation obeys the scaling property (80) and is exact along the principal axes (i.e. exact if $\alpha_1 = 0$ or $\alpha_2 = 0$).

Corollary 35. *Let $c > 0$. Let $\lambda_1, \lambda_2 < 0$ be the eigenvalues of $Re(B_{r,b})$ with $|\lambda_1| < |\lambda_2|$ and with corresponding eigenvectors $\boldsymbol{k}_1$, $\boldsymbol{k}_2$. The function $\Xi_t^{1,\frac{1}{2}} f : H_r \to \mathbb{C}$ converges pointwise towards 0 as $t \to \infty$. The isocontours*

$$\{(p,q) \in \mathbb{R}^2 \mid |\Xi_t^{1,\frac{1}{2}} f|(p,q,s) = c\}$$

of $|\Xi_t^{1,\frac{1}{2}} f|$ with $t > 0$ are non-ellipsoidal Jordan curves that retain the reflectional symmetry in the principal axes of $Re(B_{r,b})$. The aspect ratio of the intersection with the principal axes) of the isocontour at time $t > 0$ with iso-intensity $c > 0$ equals

$$\left(\sqrt{\frac{c}{\lambda_1}} - t\right)\left(\sqrt{\frac{c}{\lambda_2}} - t\right)^{-1} \tag{C.9}$$

which tends to ∞ as $t \uparrow t_{fin} := \sqrt{\frac{c}{\lambda_2}}$.

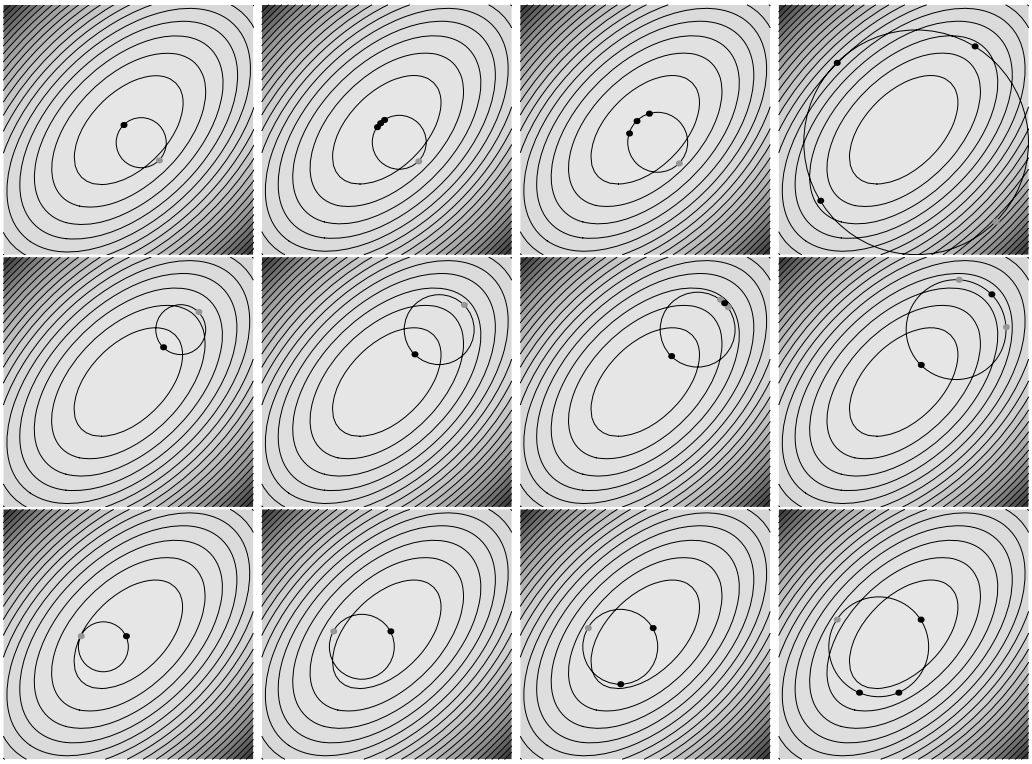

Figure C.16: Various plots of the solutions of optimization problem (C.3) arising in $\Xi_t^{1,\frac{1}{2}}$. The horizontal axis, is the p' axis, whereas the vertical axis is the q'-axis. Top row $(p,q) = (0.02, 0.02) = 0.02\mathbf{k}_1$, middle row $(p,q) = (0.05, -0.05) = -0.05\mathbf{k}_2$, bottom row $(p,q) = (-0.1, -0.05)$ for increasing time-frames $t > 0$ from left to right. The minimizer(s) on the circle is(are) indicated with a grey dot, whereas the other spurious solution(s) of Eq. (79) and Eq. (78) is(are) indicated with black dots.

Proof Set $\eta = \frac{1}{2}$. By the semi-group property of the erosion with kernel Eq. (76) and Eq. (48) (i.e. $k_t^\eta \ominus k_\delta^\eta = k_{t+\delta}^\eta$), and that the function $|\Xi_0^{1,\frac{1}{2}} f| = |\mathcal{G}_\psi f|$ vanishes at infinity and has a single critical point; a maximum at $(p,q) = (0,0)$ it follows that

$|\Xi_{t+\delta}^{1,\eta} f| = k_\delta^\eta \ominus |\Xi_t^{1,\eta} f| < |\Xi_t^{1,\eta} f|$, $|\Xi_t^{1,\eta} f|$ attains a single extremum; that is a maximum at $(p,q) = (0,0)$, $|\Xi_t^{1,\eta} f|$ is continuous , $|\Xi_t^{1,\eta} f|(p,q) \to 0$ as $\|(p,q)\| \to \infty$,

for all $t, \delta > 0$. Consequently, the isocontour of $|\Xi_{t+\delta}^{1,\eta} f|$ with value $c > 0$ is a Jordan curve that is strictly contained in the interior of the isocontour of $|\Xi_t^{1,\eta} f|$ with the same value. By Theorem 21 the isocontours are ellipsoidal for $t = 0$. For $t > 0$ these are no longer ellipsoidal since $(p,q) \mapsto \lambda_t(p,q)$ is not constant in Eq. (77). For $t \to \infty$ the kernel k_t^η, cf. Eq. (76), vanishes and the erosion, cf. Eq. (48), with the kernel k_t^η converges for each point $(p,q) \in \mathbb{R}^2$ to the global minimum of $|\mathcal{G}_\psi f|$ which is zero.

Eq. (78) is invariant under $\alpha_i \mapsto -\alpha_i$ and thereby λ_t is invariant under reflections in the principal axes of $\mathrm{Re}(B_{r,b})$. As a result, by Eq. (77), all isocontours of $|\Xi_t^{1,\eta} f|$ are invariant under these reflections. Such an isocontour is given by

$$(\lambda_t(p,q))^2 \left(\frac{|\alpha_1(p,q)|^2 \lambda_1}{(\lambda_1 - \lambda_t(p,q))^2} + \frac{|\alpha_2(p,q)|^2 \lambda_2}{(\lambda_2 - \lambda_t(p,q))^2} \right) = C, \tag{C.10}$$

for some $C \leq 0$. Now set $\alpha_1 = 0$ in Eq.(C.10) and solve for α_2, then set $\alpha_2 = 0$ in Eq.(C.10) and solve for α_1. Here one should use the exact formula, Eq. (C.7) for λ_t that holds along the principal axes. Finally, division of the 2 obtained results yields Eq. (C.9) from which the result follows. □

See Figure C.16 for solutions of the optimization problem (C.3) for various settings of $(p,q,t) \in \mathbb{R}^2 \times \mathbb{R}^+$.

Appendix C.3. ***Proof of Theorem 26***

For the proof of Theorem 26 we need a Lemma that shows that $\Omega_{t,c}$ is convex.

Lemma 36. *Let $c > 0$, $t > 0$ then the interior of the iso-contour of the absolute value of the reassigned Gabor transform of chirp signal f with value $c > 0$, i.e.*

$$\Omega_{t,c} := \{(p,q) \in \mathbb{R}^2 \mid |\Xi_t^{1,\frac{1}{2}} f|(p,q) > c\},$$

with $0 < c < |\Xi_t^{1,\frac{1}{2}} f|(0,0)$, is bounded and convex and again symmetric along the principle axes $\boldsymbol{k}_1$ and $\boldsymbol{k}_2$ of the ellipsoidal iso-contours of the absolute value of the Gabor transform $|\Xi_0^{1,\frac{1}{2}} f|$ at time $t = 0$.

Proof By the formal definition of $\Xi_t^{1,\frac{1}{2}}$ (erosions with $\eta = \frac{1}{2}$) we have

$$|\Xi_t^{1,\frac{1}{2}} f|(p,q) = \inf\{|\mathcal{G}_\psi f|(y) \mid y \in \mathbb{R}^2 \text{ with } \|y - (p,q)^T\| < t\}.$$

By continuity of $(p,q) \mapsto |\Xi_t^{1,\frac{1}{2}} f|(p,q)$ it follows that $\Omega_{t,c}$ is indeed the interior of the iso-contour $|\Xi_t^{1,\frac{1}{2}} f|$ with iso-intensity c, from which we directly deduce $\Omega_{t,c} \subset \Omega_{0,c}$ with $\Omega_{0,c}$ bounded. Reflection symmetry follows from the fact that reflection of balls of radius $t > 0$ are again balls of the same radius.

Next we show $\Omega_{t,c}$ is convex. To this end we first note that the set $\Omega_{0,c}$ is convex since the quadratic form $(\cdot,\cdot)\mathbf{B}_{r,b}(\cdot,\cdot)$ (whose iso-contours coincide with iso-contours of $|\mathcal{G}_\psi f|$) is a convex function.

Now let $t > 0$. Let x_1, x_2 be two arbitrary points within $\Omega_{t,c}$. Let $y = sx_1 + (1-s)x_2$ with $s \in [0,1]$ be some convex combination. We want to prove $|\mathcal{G}_\psi f|(z) > c$ for all $\|z - y\| < t$ since this will entail $y \in \Omega_{t,c}$. For this purpose fix a $z \in \mathbb{R}^2$ with $\|z - y\| < t$ and set $z_i = x_i + z - y$ for $i = 1, 2$. Note that $\|z_i - x_i\| < t$ and since $x_i \in \Omega_{t,c}$ we have

$$|\mathcal{G}_\psi f|(z_i) > c \quad \text{for } i = 1, 2. \tag{C.11}$$

Via direct computation we find $z = sz_1 + (1-s)z_2$. Now the required result $|\mathcal{G}_\psi f|(z) > c$ follows by Eq. (C.11) and the convexity of the set $\Omega_{0,c} = \{y \in \mathbb{R}^2 \mid |\mathcal{G}_\psi f|(y) > c\}$. □

Now that we know the set $\Omega_{t,c}$ is convex we proceed with the actual proof.

Let (p_j, q_j) denote the intersection of the iso-contour with value c with axis $\mathbf{k}_j$. Consequently, we have $|\Xi_t^{1,\frac{1}{2}} f|(p_j, q_j) = c$. Suppose there exists a point $(p_0, q_0) \in \Omega_{t,c} \setminus \mathfrak{B}_{t,c}$.

Then there exists a $j \in \{1, 2\}$ such that $(p_0, q_0) \cdot \mathbf{k}_j > (p_j, q_j) \cdot \mathbf{k}_j$. Now due to the reflection symmetry and the convexity of $\Omega_{t,c}$ the projection of (p_0, q_0) on the span of $\mathbf{k}_j$ given by $((p_0, q_0) \cdot \mathbf{k}_j)\mathbf{k}_j$ is also within $\Omega_{t,c}$ but this contradicts the fact that the restrictions of the function $|\Xi_t^{1,\frac{1}{2}} f|$ to the principal axes is monotonically decreasing as can be deduce from Eq. (77). Due to Corollary 35 in Appendix C the aspect ratio of the box $\mathfrak{B}_{t,c}$ equals Eq. (81). The rest follows by taking the limit $t \uparrow t_{\text{fin}} := \sqrt{\frac{c}{\lambda_2}}$. □

Appendix C.4. The Cauchy-Riemann relations in the discrete case

We aim for a discrete kernel $\boldsymbol{\psi}_a^D := \{\psi[n]\}_{n=-(N-1)}^{N-1}$ such that the following discrete Cauchy-Riemann equation in discrete phase space (using central left-invariant differences) holds

$$\forall_{l=0,\ldots,K-1} \forall_{m=0,\ldots,M-1} \forall_{\mathbf{f} \in \ell_2(I)} \; : \; (\tfrac{1}{a}(\tilde{\mathcal{A}}_2^{D^+} + \tilde{\mathcal{A}}_2^{D^-}) + i\, a(\tilde{\mathcal{A}}_1^{D^+} + \tilde{\mathcal{A}}_1^{D^-}))(G^D_{\boldsymbol{\psi}_a^D}\mathbf{f})[l,m] = 0 \;, \tag{C.12}$$

which is (by left-invariance of the discrete left-invariant vector fields) equivalent to

$$\begin{aligned} &\forall_{l=0,\ldots,K-1} \forall_{m=0,\ldots,M-1} \; \forall_{n'=0,\ldots,L-1} : (\tfrac{1}{a}(\tilde{\mathcal{A}}_2^{D^+} + \tilde{\mathcal{A}}_2^{D^-}) + i\, a(\tilde{\mathcal{A}}_1^{D^+} + \tilde{\mathcal{A}}_1^{D^-}))(G^D_{\boldsymbol{\psi}_a^D}\delta_{n'})[l,m] = 0, \\ &\text{with } \delta_{n'}[n] = \delta_{nn'} \;, \end{aligned}$$

Now $G_{\boldsymbol{\psi}}\delta_{n'}[l,m] = \frac{1}{N}\psi[n' - lL]e^{2\pi i(lm\frac{L}{M} - n')}$ and by straightforward application of the discrete left-invariant vector fields we find

$$K\frac{ia}{2}\frac{e^{\frac{2\pi i l m L}{M}}}{N}(\psi[n' - (l+1)L] - \psi[n' - (l-1)L]) + \frac{e^{\frac{2\pi i l m L}{M}}}{a}\frac{M}{2N^2}(\psi[n' - l\,L])(e^{2\pi i \frac{lL}{M}} - e^{-2\pi i \frac{lL}{M}}) = 0.$$

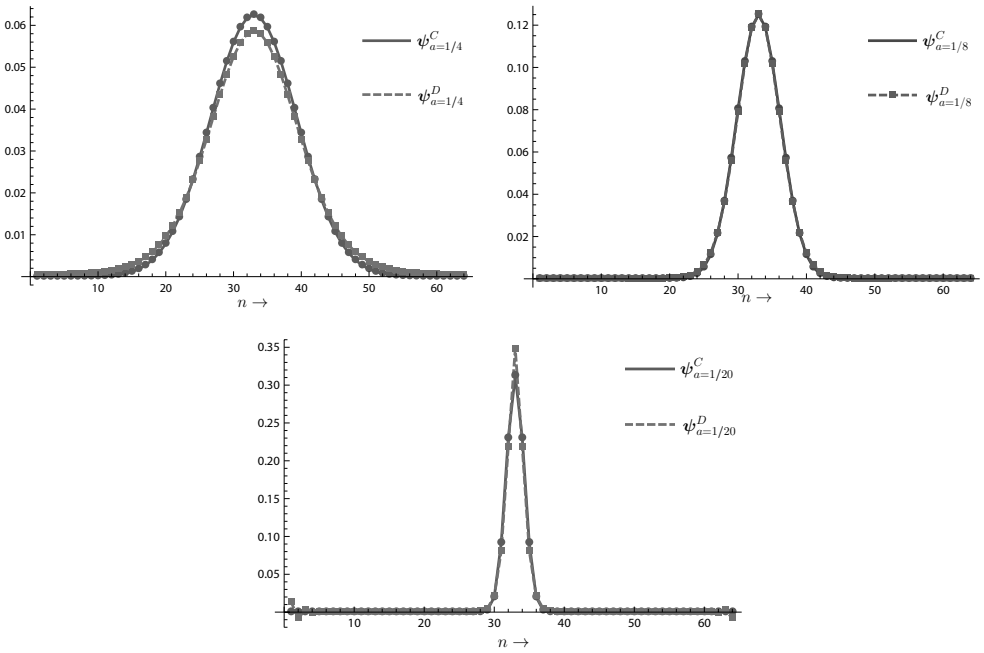

Figure C.17: A comparison between the solution $\boldsymbol{\psi}^D_a = \{\psi[n]\}^{N-1}_{n=-(N-1)}$ of the discrete Cauchy-Riemann equations (C.12), for the case $K = M = N$, $L = 1$, $P = N$ and the discrete sampling $\boldsymbol{\psi}^C_a = \{\psi_a\left(\frac{n}{N}\right)\}^{N-1}_{n=-(N-1)}$ of the continuous solution $\psi_a(\xi)$ (36), for different values of $a > 0$ with $N = 64$.

Consequently, we get the following 2-fold recursion (enumerated by l making steps of L in $\{0, \ldots, N-1\}$) for the even discrete kernel $\boldsymbol{\psi}^D_a := \{\psi[n]\}^{N-1}_{n=-(N-1)} = \{\psi[n' - lL]\}^{L-1,K-1}_{n'=0,l=0}$:

$$\begin{cases} \frac{NK}{2M} a^2 \left(\psi[n' - (l+1)L] - \psi[n' - (l-1)L]\right) + \psi[n' - l\,L] \sin\left(\frac{2\pi lL}{M}\right) = 0, \text{ for } l = 0, \ldots K-1, \\ \psi[-n] = \psi[n], \psi[N] := \psi[0], \psi[-N] := \psi[0] \text{ and } \sum\limits_{l=0}^{K-1} \psi[n' - lL] = 1 \end{cases}$$

In case of extreme oversampling $K = M = N$, $L = 1$, $P = N$ we get a unique solution. Figure C.17 shows a comparison of this discrete solution and the continuous Cauchy-Riemann window given in Eq. (36), again using the fundamental transformation $p = \frac{l}{N}$, $q = \frac{mM}{N}$ for several scaling values of $a > 0$. As $a > 0$ decreases the solution of the discrete Cauchy-Riemann window converges pointwise to the sampled continuous window. Similar behavior is obtained if we keep $a > 0$ fixed and increase the number of samples N.

References

[1] M. Akian, J. Quadrat, and M. Viot. *Bellman processes.* volume 199 of *Lecture Notes in Control and Information Science*, pages 302–311. Springer Verlag, 1994.

[2] T. Arts, F. W. Prinzen, T. Delhaas, J. R. Milles, A. C. Rossi, and P. Clarysse. Mapping displacement and deformation of the heart with local sine-wave modeling. *IEEE Trans. Med. Imag.*, 29(5):1114–1123, May 2010.

[3] F. Auger and P. Flandrin. Improving the readability of time-frequency and time-scale representations by the reassignment method. *IEEE Trans. Signal Proc.*, 43(5):1068–1089, May 1995.

[4] A. Becciu. *Feature based estimation of myocardial motion from tagged MR images.* PhD thesis, Eindhoven University of Technology, Eindhoven, The Netherlands, 2010.

[5] A. Becciu, R. Duits, B.J. Janssen, L.M.J. Florack, B.M. ter Haar Romeny, and H.C. van Assen. Cardiac motion estimation using covariant derivatives and Helmholtz decomposition. In *Statistical atlases and computational models of the heart, STACOM 2011 held in conjunction with MICCAI 2011*, pages 263–273, 2011. LNCS 7085.

[6] A. Becciu, B.J. Janssen, H.C. van Assen, L.M.J. Florack, V. Roode, and B.M. ter Haar Romeny. Extraction of cardiac motion using scale-space features points and gauged reconstruction. In *CAIP '09: Proceedings of the 13th International Conference on Computer Analysis of Images and Patterns*, pages 598–605, Berlin, Heidelberg, 2009. Springer-Verlag.

[7] B. Bellaïche. *The tangent space in sub-Riemannian geometry.* Progress in Mathematics. Birkhäuser, New York, 1996.

[8] H. Bölcskei and F. Hlawatsch. Discrete Zak transforms, polyphase transforms, and applications. *IEEE Trans. Signal Proc.*, 45(4):851–866, Apr 1997.

[9] A. Bruhn, J. Weickert, T. Kohlber, and C. Schnoerr. A multigrid platform for real-time motion computation with discontinuity-preserving variational methods. *Int. J. Comput. Vis.*, 70(3):257–277, 2006.

[10] L.C.M. Bruurmijn. Local frequency analysis and its application in biomedical imaging. Master's thesis, Department of Biomedical Engineering, Eindhoven University of Technology, The Netherlands, October 2011.

[11] R.L. Bryant, S.S. Chern, R.B. Gardner, H.L. Goldschmidt, and P.A. Griffiths. Exterior differential systems, volume 18 of *Mathematical Sciences Research Institute Publications*. Springer-Verlag, New York, 1991.

[12] A.V. Bukhvalov and Arendt W. Integral representation of resolvent and semigroups. *Pacific J. Math.*, 10:419–437, 1960.

[13] B. Burgeth and J. Weickert. An explanation for the logarithmic connection between linear and morphological systems. In *Proc. 4th Int. Conference Scale Space*, Lecture Notes in Computer Science, pages 325–339. Springer Verlag, 2003.

[14] E. Chassande-Mottin, I. Daubechies, F. Auger, and P. Flandrin. Differential reassignment. *IEEE Signal Proc. Letters*, 4(10):293–294, Oct 1997.

[15] G.S. Chirikjian. *Stochastic Models, Information Theory, and Lie groups*, volume 1 and 2 of *Applied and Numerical Harmonic Analysis*. Birkhäuser, New York, 2009–2011.

[16] G.-H. Cottet and L. Germaine. Image processing through reaction combined with nonlinear diffusion. *Math. Comp.*, 61:659–667, 1990.

[17] Michael G. Crandall and Pierre-Louis Lions. Viscosity solutions of Hamilton-Jacobi equations. *Trans. Amer. Math. Soc.*, 277(1):1–42, 1983.

[18] I. Daubechies and S. Maes. A nonlinear squeezing of the continuous wavelet transform based on auditory nerve models. In *Wavelets in Medicine and Biology*, pages 527–546. CRC Press, 1996.

[19] L. Daudet, M. Morvidone, and B. Torrésani. Time-frequency and time-scale vector fields for deforming time-frequency and time-scale representations. In *Proceedings of the SPIE Conference on Wavelet Applications in Signal and Image Processing*, pages 2–15. SPIE, 1999.

[20] J. Dieudonné. *Treatise on analysis. Vol. 5. Chapter XXI.* Academic Press [A subsidiary of Harcourt Brace Jovanovich, Publishers], New York-London, 1977. Translated by I. G. Macdonald, Pure and Applied Mathematics, Vol. 10-V.

[21] P.A.G. Dorst, B.J. Janssen, L.M.J. Florack, and B.M. ter Haar Romeny. Optic flow using multi-scale anchor points. In *Proceedings of The 13th International Conference on Computer Analysis of Images and Patterns (CAIP09)*, LNCS, Berlin, 2009. Springer Verlag.

[22] R. Duits. *Perceptual Organization in Image Analysis.* PhD thesis, Eindhoven University of Technology, 2005. A digital version is available on the web http://alexandria.tue.nl/extra2/200513647.pdf.

[23] R. Duits and B. Burgeth. Scale spaces on Lie groups. In *Proceedings,of SSVM 2007, 1st international conference on scale space and variational methods in computer vision*, Lecture Notes in Computer Science, pages 300–312. Springer Verlag, 2007.

[24] R. Duits, M. Felsberg, G. Granlund, and B.M. ter Haar Romeny. Image analysis and reconstruction using a wavelet transform constructed from a reducible representation of the Euclidean motion group. *Int. J. Comput. Vis.*, 72:79–102, 2007.

[25] R. Duits and E.M. Franken. Left invariant parabolic evolution equations on $SE(2)$ and contour enhancement via invertible orientation scores, part I: Linear left-invariant diffusion equations on $SE(2)$. *Quarterly of Appl. Math.*, 68:255–292, June 2010.

[26] R. Duits and E.M. Franken. Left invariant parabolic evolution equations on $SE(2)$ and contour enhancement via invertible orientation scores, part II: Nonlinear left-invariant diffusion equations on invertible orientation scores. *Quarterly of Appl. Math., AMS*, 68:293–331, June 2010.

[27] R. Duits and E.M. Franken. Left-invariant diffusions on the space of positions and orientations and their application to crossing-preserving smoothing of HARDI images. *Int. J. of Comput. Vis.*, 92:231–264, March 2011. Published digitally online in 2010, *http://www.springerlink.com/content/511j713042064t35/*.

[28] R. Duits, T.C.J. Dela Haije, E.J. Creusen and A. Ghosh. Morphological and linear scale spaces for fiber enhancement in DW-MRI. Accepted for publication in *Jour. of Math. Imaging and Vis.* to appear in 2012, *http://www.bmia.bmt.tue.nl/People/RDuits/JMIVDuits2011final.pdf*.

[29] R. Duits, H. Führ, and B.J. Janssen. Left invariant evolution equations on Gabor transforms. Technical report, Eindhoven University of Technology, 2009. CASA-report Department of Mathematics and Computer Science, Technische Universiteit Eindhoven. Nr. 9, February 2009. Available on the web *http://www.win.tue.nl/casa/research/casareports/2009.html*.

[30] R. Duits, B.J. Janssen, A. Becciu, and H. van Assen. A variational approach to cardiac motion estimation based on covariant derivatives and multi-scale Helmholtz decomposition. *Quarterly of Appl. Math.*, 2012. accepted for publication Octobre 2011, to appear in December 2012, url: *http://bmia.bmt.tue.nl/people/RDuits/DuitsQAM5.pdf*.

[31] R. Duits and M. van Almsick. The explicit solutions of linear left-invariant second order stochastic evolution equations on the 2D Euclidean motion group. *Quarterly of Appl. Math.*, 66(1):27–67, 2008.

[32] L.C. Evans. *Partial differential equations*, volume 19 of *Graduate Studies in Mathematics*. American Mathematical Society, 2002.

[33] H.G. Feichtinger and K. Gröchenig. Non-orthogonal wavelet and Gabor expansions, and group representations, in: *Wavelets and their applications*, pages 353–376. Jones and Bartlett, 20 Park Plaza Boston, MA 02116, USA, 1992.

[34] H.G. Feichtinger, W. Kozek, and F. Luef. Gabor analysis over finite abelian groups. *Appl. Comput. Harmon. Anal.*, 26(2):230–248, 2009.

[35] L.M.J. Florack, W. J. Niessen, and M. Nielsen. The intrinsic structure of optic flow incorporating measurement duality. *Int. J. Comput. Vis.*, 27(3):263–286, May 1998.

[36] L.M.J. Florack, H. C. van Assen, and A. Suinesiaputra. Dense multiscale motion extraction from cardiac cine MR tagging using HARP technology. *8th IEEE Computer Society Workshop on Mathematical Methods in Biomedical Image Analysis held in conjunction with the ICCV workshop*, October 2007. Digital Proceedings by Omnipress.

[37] L.M.J. Florack and H.C. van Assen. A new methodology for multiscale myocardial deformation and strain analysis based on tagging MRI. *Int. J. Biom. Imag.*, pages 1–8, 2010. Published online *http://downloads.hindawi.com/journals/ijbi/2010/341242.pdf*.

[38] E.M. Franken. *Enhancement of crossing elongated structures in images.* PhD thesis, Dep. of Biomedical Engineering, Eindhoven University of Technology, The Netherlands, Eindhoven, October 2008. URL: http://alexandria.tue.nl/extra2/200910002.pdf.

[39] E.M. Franken and R. Duits. Crossing preserving coherence-enhancing diffusion on invertible orientation scores. *Int. J. Comput. Vis.*, 85(3):253–278, 2009.

[40] D. Gabor. Theory of communication. *J. IEE (London)*, 93:429–457, 1946.

[41] B. Gaveau. Principe de moindre action, propagation de la chaleur et estimées sous elliptiques sur certains groupes nilpotents. *Acta Math.*, 139(1-2):95–153, 1977.

[42] K. Gröchenig. *Foundations of time-frequency analysis. Applied and Numerical Harmonic Analysis.* Birkhäuser Boston Inc., Boston, MA, 2001.

[43] C.W. Helstrom. An expansion of a signal in Gaussian elementary signals (corresp.). *IEEE Trans. Inform. Theory*, 12(1):81–82, Jan 1966.

[44] L. Hörmander. Hypoelliptic second order differential equations. *Acta Math.*, 119:147–171, 1967.

[45] B.K.P. Horn and B.G. Shunck. Determining optical flow. *AI*, 17:185–203, 1981.

[46] A.J.E.M. Janssen. The Zak transform: a signal transform for sampled time-continuous signals. *Philips J. Res.*, 43(1):23–69, 1988.

[47] B.J. Janssen. *Representation and manipulation of images based on linear functionals.* PhD thesis, Eindhoven University of Technology, Eindhoven, The Netherlands, 2009. URL: http://alexandria.tue.nl/extra2/200911295.pdf.

[48] B.J. Janssen, L.M.J. Florack, R. Duits, and B.M. ter Haar Romeny. Optic flow from multi-scale dynamic anchor point attributes. In *Lecture Notes in Computer Science, Vol. 4141, Proc.3rd Int. Conf. ICIAR 2006*, pages 767–779, Portugal, 2006. Springer.

[49] B.J. Janssen, L.M.J. Florack, R. Duits, and B.M. ter Haar Romeny. Optic flow from multi-scale dynamic anchor point attributes. In A. Campilho and M. Kamel, editors, *Image Analysis and Recognition, Third International Conference, ICIAR 2006*, volume 4141 of *LNCS*, pages 767–779, Berlin, September 2006. Springer Verlag.

[50] K. Kodera, C. de Villedary, and R. Gendrin. A new method for the numerical analysis of non-stationary signals. *Physics of the Earth and Planetary Interiors*, 12:142–150, 1976.

[51] P.L. Lions and E. Magenes. Non-homogeneous boundary value problems and applications, volume 1-3. Springer-Verlag, Berlin, 1972–1973.

[52] M. Loog, J.J. Duistermaat, and L.M.J. Florack. On the behavior of spatial critical points under Gaussian blurring. a folklore theorem and scale-space constraints. In Kerckhove et al., editor, *Proceedings scale space conf. 2001, LNCS*, pages 182–192, 2001.

[53] B. Lucas and T. Kanade. An iterative image registration technique with application to stereo vision. In *DARPA, Image Process*, volume 21, pages 85–117, 1981.

[54] J.J. Manfredi and B. Stroffolini. A version of the Hopf-Lax formula in the Heisenberg group. *Comm. Partial Differential Equations*, 27(5):1139–1159, 2002.

[55] M. Nitzberg and T. Shiota. Nonlinear image filtering with edge and corner enhancement. *IEEE Trans. Patt. Anal. Mach. Intell.*, 14:826–833, 1992.

[56] N.F. Osman, W.S. Kerwin, E.R. McVeigh, and J.L. Prince. Cardiac motion tracking using CINE Harmonic Phase (HARP) Magnetic Resonance Imaging. *Magnetic Resonance in Medicine*, 42(6):1048–1060, 1999.

[57] V. Prckovska, P. Rodrigues, R. Duits, A. Vilanova, and B.M. ter Haar Romeny. Extrapolating fiber crossings from DTI data. can we infer similar fiber crossings as in HARDI ? In *CDMRI'10 MICCAI 2010 workshop on computational diffusion MRI*, volume 1, pages 26–37, Beijing China, august 2010. Springer.

[58] P. Rodrigues, R. Duits, A. Vilanova, and B.M. ter Haar Romeny. Accelerated diffusion operators for enhancing DW-MRI. In *Eurographics Workshop on Visual Computing for Biology and Medicine*, ISBN 978-3-905674-28-6, pages 49–56, Leipzig Germany, 2010. Springer.

[59] H. Rund. *The Hamilton-Jacobi theory in the calculus of variations: Its role in mathematics and physics.* D. Van Nostrand Co., Ltd., London-Toronto, Ont.-New York, 1966.

[60] T. Taylor. A parametrix for step-two hypoelliptic diffusion equations. *Transactions of the American Mathematical Society.* 296(1):191–215, 1986.

[61] A.F.M. ter Elst and D.W. Robinson. Weighted subcoercive operators on Lie groups. *J. Funct. Anal.*, 157(1):88–163, 1998.

[62] H.C. van Assen, L.M.J. Florack, F.J.J. Simonis, J.J.M. Westenberg, and G.J. Strijkers. Cardiac strain and rotation analysis using multi-scale optical flow. In *MICCAI workshop on Computational Biomechanics for Medicine 5*, pages 91–103. Springer-Verlag, 2011.

[63] H.C. van Assen, L.M.J. Florack, A. Suinesiaputra, J.J.M. Westenberg, and B.M. ter Haar Romeny. Purely evidence based multiscale cardiac tracking using optic flow. In K. Miller, K.D. Paulsen, A.A. Young, and P.M.F. Nielsen, editors, *Proc. MICCAI 2007 workshop on Computational Biomechanics for Medicine II*, pages 84–93, 2007.

[64] J. Weickert. Coherence-enhancing diffusion filtering. *Int. J. Comput. Vis.*, 31(2/3):111–127, 1999.

[65] F. Weisz. Inversion of the short-time Fourier transform using Riemann sums. *J. Fourier Anal. Appl.*, 13(3):357–368, 2007.